Zeitschrift: IABSE reports of the working commissions = Rapports des commissions de travail AIPC = IVBH Berichte der Arbeitskommissionen

Band: 13 (1973)

Rubrik: Theme III: Experimental studies concerning steel structures, their elements and their connections

III

Predictable Properties of Material under Incremental Cyclic Loading

Propriétés prévisibles du matériau soumis à des charges cycliques non-constantes

Vorhersagbare Materialeigenschaften unter zunehmender zyklischer Belastung

Ben KATO, Professor
Hiroshi AKIYAMA, Associate Professor
Yasuyuki YAMANOUCHI, Graduate Student
University of Tokyo, Japan

1. INTRODUCTION

This paper deals with mechanical properties of materials for structural steels which are subjected to irregularly fluctuating external forces such as seismic forces and wind storms. The elastic response of the structure to such a loading is of harmonic oscillations. However the inelastic response may be characterized by non-steady development of plastic deformations and the number of cycles which produces large plastic strain seems to be smaller than the number discussed in the problem of fatigue. Thus the effect of accumulation of plastic strain into a critical state would be more important than the effect of fatigue as a collapse criterion of the material.

It is well-known that the inelastic stress-strain relation(σ-ε relation) of materials for structural use is mathematically expressed in exponential Ramberg-Osgood function and Masing's assumption can be applied to hysteretic relations in cyclic loading.(1),(2) Fig.1 shows the most popular relation adopted by many researchers for structural analysis.(3) According to Masing's assumption, the shape of the hysteretic branch is twice as large as that of the monotonic σ-ε relation. Fig.2 shows a typical stress-strain relation of usual carbon steels, which is characterized by yielding plateau in initial loading,

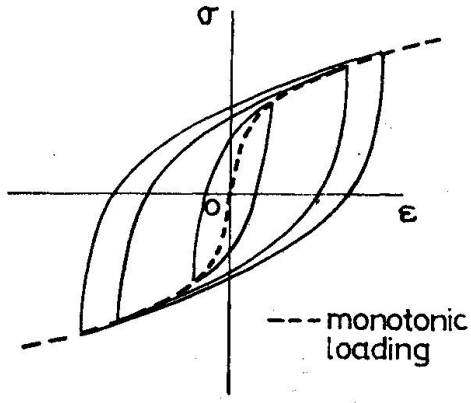

Fig.1. Ramberg-Osgood Function

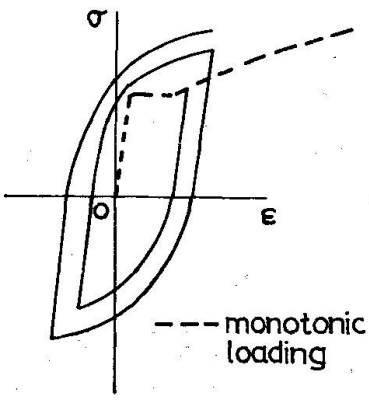

Fig.2. Realistic σ-ε Relation of Steel

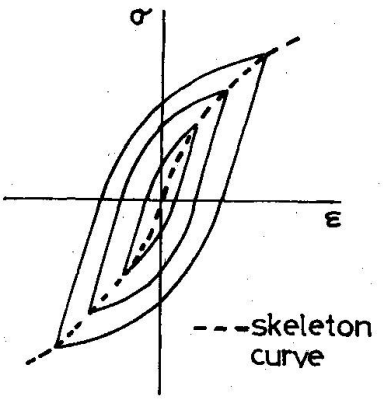

Fig.3. Halford's Expression

strain-hardening and Bauschinger effect. It is obvious that the hysteretic pattern in Fig.1 does not cover the realistic stress-strain relation of steels which allows remarkable enlargement of hysteresis loops in the direction of σ-axis due to strain-hardening.

Halford suggested a definite expression for prediction of hysteretic relation under steady-state cyclic loading as shown in Fig.3.(4) The effect of strain-hardening is well introduced in his expressions. However his pattern does not present any informations about transient paths from one stationary loop to the other.

Moreover the criterion for the fracture of the materials under incremental cyclic loading is still left unknown.

From this point of view, to extract predictable nature of the material subjected to arbitrarily changing strain history, series of material tests were carried out.

2.TESTING PROGRAM

Fig.4 shows series of test specimens. Test-series-A involves two kinds of materials and eleven specimens. In this series of testing, tensile and compressive loads were gradually increased in every loading cycles. In test-series-B two kinds of materials and 29 specimens were used. In this series of testing, loading history involves stationary loops and incremental paths. In test-series-C, also two kinds of materials and 30 specimens were used. Prior to the testing preliminary test was conducted aiming to obtain fatigue strength of materials under cyclic loading with constant stress amplitude in positive and negative direction. In this series of testing, first, stationary cyclic loading in which substantial amount of fatigue life is exhausted is applied and subsequently monotonic tensile loading is applied up to the fracture of the material. Thus the reserve of ductility after the exhaustion of fatigue life is sought after. Detailed descriptions as for the results of the tests are reported elsewhere. (5),(6),(7)

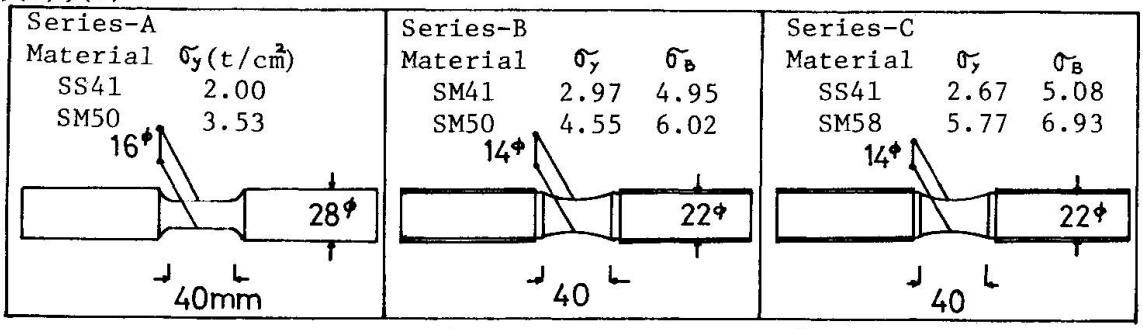

Fig.4. Test Specimens (σ_y=yielding stress, σ_B=breaking stress)

3. RESOLUTION OF $\sigma-\varepsilon$ RELATION INTO THREE COMPONENTS

Conventional Ramberg-Osgood function expresses continuously Bauschinger effect and strain-hardening. However these phenomena seem to be independent each other. Based on the results of test-series-A, realistic features are observed. Fig.5 shows a result of testing. In Fig.6, $\sigma-\varepsilon$ relation in each sign of loading is extended in one sequence. Bold line shows loading path which exceeds the stress level attained by the preceding loading in the same stress domain. Connecting these segments independently, two monotonic curves are obtained and compared with the relation obtained under monotonic loading in Fig.7. The initial loading path in compression loading is considerably softened by Bauschinger effect. Disregarding this deviation, the next remarkable fact can be confirmed.

A skeleton curve can be found independently in each loading domain and these curves coincide with the relation under monotonic loading.

This fact can be verified extensively even in the case that loading path includes large numbers of stationary loops(test-series-B,C). For the practical purpose to simplify the structural analysis, Bauschinger effect may be neglected in many cases. Advanced treatment of the skeleton curve is discussed extensively

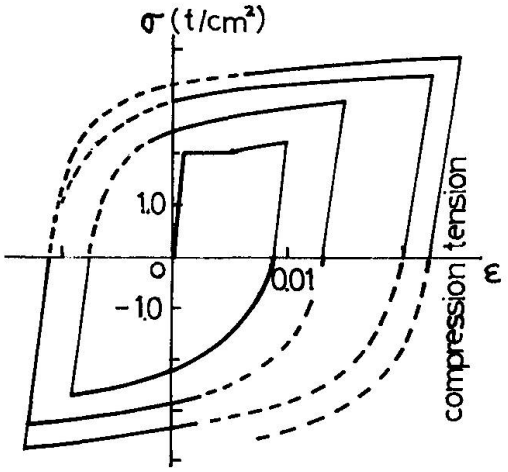

Fig.5. A Result of Test-Series-A

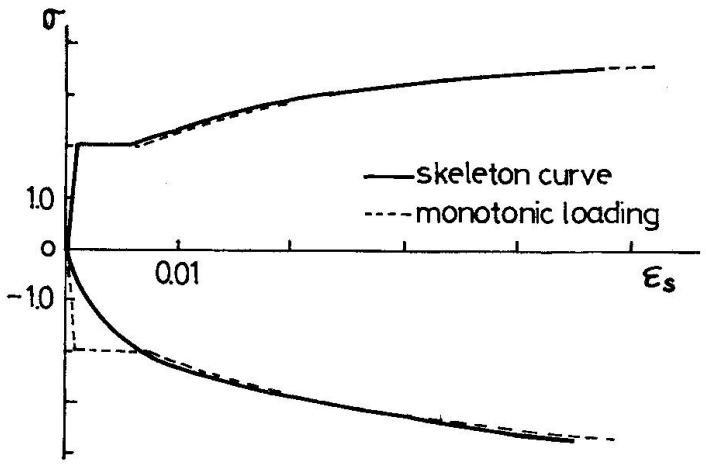

Fig.7. Skeleton Curves

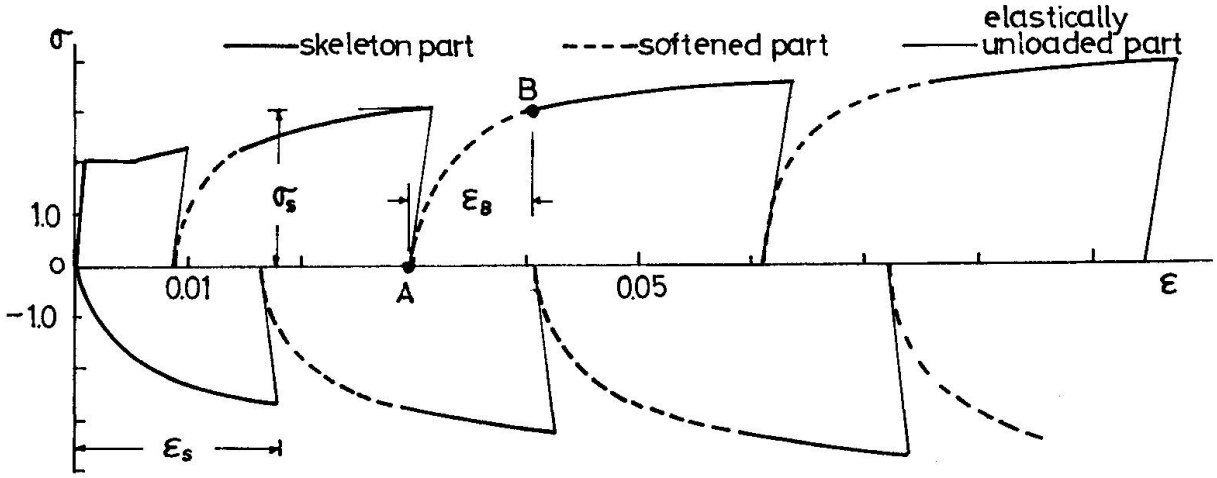

Fig.6. Stretched Figures of the Hysteretic Curve

elsewhere of this symposium.(8)

The stress-strain relation under cyclic loading can be resolved into the skeleton part and the rest. The rest of σ-ε relation is composed of the elastically unloaded part and the softened part due to Bauschinger effect. Results of test-series-A show that rigidity of the unloaded part preserves almost initial rigidity of elasticity and the onset of the softened part lies on the zero stress level. Therefore, problem is how to estimate the softened part illustrated in Fig.6 which connects from point A where stress is zero to point B where stress reaches σ_s which is the maximum stress previously attained in the same stress domain. Nondimensional expression for the softened part is obtained by taking σ/σ_s as the ordinate and $\varepsilon/\varepsilon_B$ as the abscissa where ε_B is termed as Bauschinger strain. Fig.8 shows the results of test-series-A. Bold line shows the bound of the experimental plots. Obviously the shape of the softened part is hyperbolic and expressed as

$$(y+a)(x-a-1)+a(a+1)=0. \tag{1}$$

Slope of the shape is given as

$$\frac{dy}{dx} = \frac{-(y+a)}{(x-a-1)} \tag{2}$$

Initial slope at x=0 is given by the next equation.

$$y = \left(\frac{\sigma}{\sigma_s}\right) / \left(\frac{\varepsilon}{\varepsilon_B}\right) = \frac{\sigma}{\varepsilon}\frac{\varepsilon_B}{\sigma_s} = \frac{E}{E_B} \tag{3}$$

where E=Young's modulus, $E_B = \sigma_s/\varepsilon_B$.
Therefore a is determined as

$$a = \frac{E}{(E_B - E)} \qquad (4)$$

Empirically E_B is judged to be highly affected by the inelastic deformation under the opposite sign of loading. Fig.9 shows the experimental plots of E_B versus the maximum strain on the skeleton curve attained under the opposite sign of loading, ${}_o\varepsilon_s$. Although these data scatter widely, it is distinct that E_B decreases as ${}_o\varepsilon_s$ increases. The lower bound is simply expressed under the range of ${}_o\varepsilon_s$ below o.1 as

$$E_B = \frac{-\log_{10} 10\,{}_o\varepsilon_s}{6} \times E. \qquad (5)$$

Fundamental features of the softened part may be estimated by Eq(1) and Eq(5).

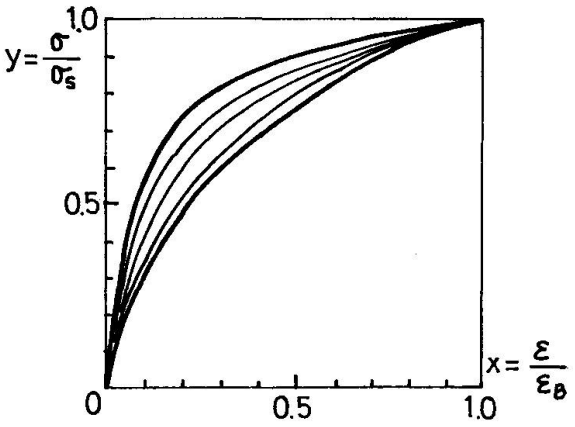

Fig.8. Shape of Softened Part

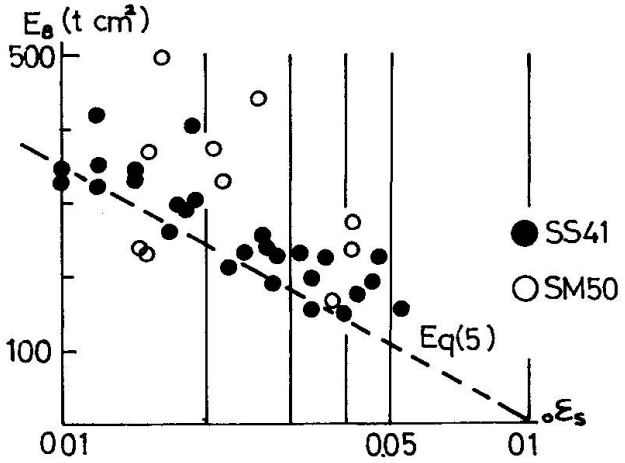

Fig.9. Secant Modulus of Softened Part

4. APPLICABILITY OF ANALYTICAL EXPRESSION

4-1. Prediction of Stationary Loops

Eq(5) was derived from the results of testing under incremental loading. If Eq(5) is extensible to such a loading as shown in Fig.10, Eq(5) may also gives the scale of the converged stationary loops. Test-series-B involves some available data suitable for comparison. Fig.11 shows the compared aspects. The prediction is almost agree with the test data. In Fig.11 broken lines show the limit of convergence above which hysteresis loops do not converge under a constant stress amplitude. It can be seen that the limit of convergence of stationary loops nearly corresponds to the limit of application of the formula.

4-2. Criterion for Ductile Fracture of Materials

Under monotonic tensile loading ductile fracture occurs immediately after the maximum stress σ_B is attained. Stress-strain relation under arbitrarily fluctuating loading is divided into skeleton part and the rest. The accumulated skeleton part in each sign of loading coincides with the monotonic σ-ε relation. Therefore the criterion for ductile fracture may be expressed as

$$\sum \Delta\varepsilon_s = \varepsilon_u. \qquad (6)$$

where $\Delta\varepsilon_s$= strain on the skeleton part under tensile loading,
ε_u= strain at the ultimate state under monotonic loading.

Stationary hysteresis loops under constant stress amplitude do not make any contribution to accumulation of strains on skeleton part. Thus it can be deduced that fatigue strength and ductile fracture are independent each other.
Fig.12 shows the loading history of test-series-C. First, considerable amount of hysteresis loops under constant amplitude are exerted, and next, tensile loading

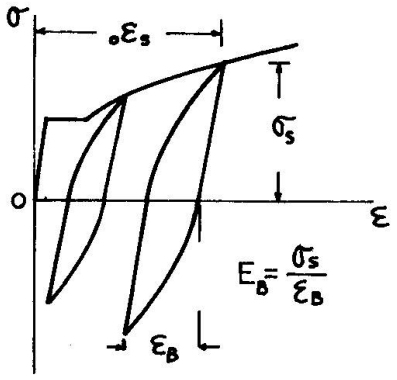

Fig.10. Loading History

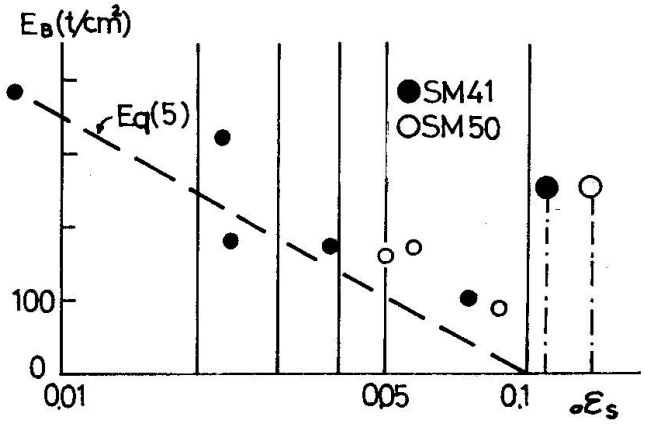

Fig.11. Secant Modulus of Stationary Loops

is applied until the ultimate state is attained. Conventionally ultimate state was assumed to reach when the stress goes down to 98% of the maximum stress. Applied stress amplitude in cyclic loading ranges between $0.6\sigma_B$ and $0.9\sigma_B$ and the number of cycles N is varied from 10% to 90% of fatigue life N_f. Fig.13 shows the reserve of ductility and strength after a certain amount of fatigue life is exhausted. In Fig.13 $\Sigma\Delta\varepsilon_s$ denotes the summation of the strain on the skeleton parts under tensile loading and σ_u means the maximum stress attained in each specimen. From the figure it can be seen that the reserve of strength and ductility is scarecely affected by the presence of large number of stationary loops.

5. CONCLUSION

Based on series of material tests, it was concluded that the basic feature of stress-strain relation of the steel under cyclic loading is predictable.

Principal findings are followings.

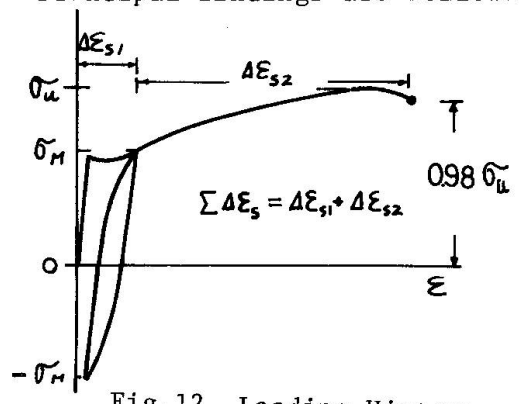

Fig.12. Loading History

1. Stress-strain relation of the steel subjected to arbitrarily changing loading history was found to be composed of three parts: skeleton part, elastically unloaded part and softened part by Bauschinger effect.
2. Skeleton part coincides with σ-ε relation under monotonic loading.
3. Softened part begins at zero stress level and terminates at the maximum stress point previously attained in the same sign of loading and is expressed by Eq(1) and Eq(5).

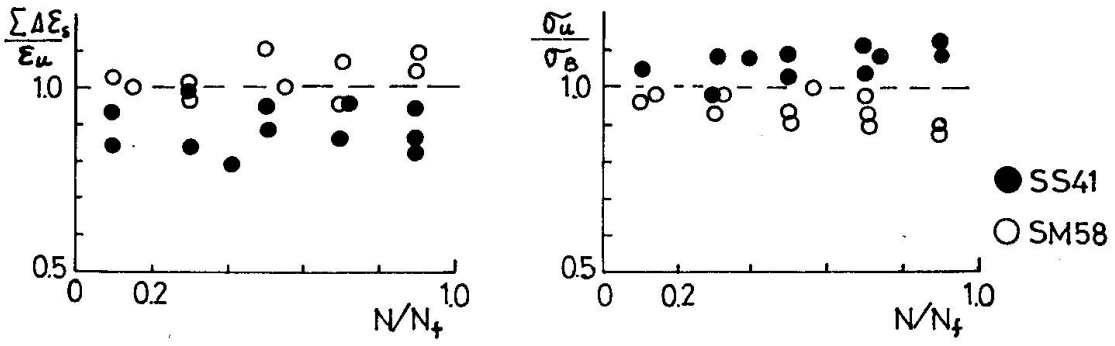

Fig.13. Reserve of Ductility and Strength

4. Scale of stationary loops involved in the loading history can be successfully predicted by Eq(5).
5. Fatigue and ductile fracture are essentially independent phenomena and the criterion for ductile fracture of the steel is given by Eq(6).

REFERENCES

1. Ramberg,W. & Osgood,W.R., Description of Stress-Strin Curves by Three Parameters, NACA TN902, July 1943.
2. Masing,G., Eigenspannungen und Verfestigung beim Messing, 2nd International Congress for applied Mechanics, Zurich 1926.
3. Jennings,P.C., Periodic Response of a General Yielding Structure, Proc. ASCE, Vol.90, EM2, Apr. 1964.
4. Halford,G.R. & Morrow,J., Low-Cycle Fatigue in Torsion, Proc. ASTM, Vol.62, 1962.
5. Kato,B., Aoki,H. & Yamanouchi,Y., Experimental Study on Structural Steels Subjected to Tensile and Compressive Cyclic Loading, Summaries of Research Reports, Annual Meeting of AIJ, Sept. 1970(in Japanese).
6. Kato,B., Yamanouchi,Y. & Inoue,K., Bauschinger Effect of Structural Steels Subjected to Tensile and Compressive Cyclic Loading, Summaries of Research Reports, Annual meeting of AIJ, Nov. 1971(in Japanese).
7. Kato,B., Akiyama,H. & Yamanouchi, Y., Tensile Strength and Ductility of Structural Steels Subjected to Tensile and Compressive Cyclic Loading, Summaries of Research Reports, Annual Meeting of AIJ, Oct. 1972(in Japanese).
8. Kato,B., Akiyama,H., Theoretical Prediction of the Load-Deflection Relationship of Steel Members and Frames, Theme I, IABSE Symposium, Lisboa 1973.

SUMMARY

Systematic expression for the stress-strain relation of the steel under arbitrarily fluctuating loading history was sought after. Stress-strain relation of the steel was found to be composed of three parts: skeleton part, elastically unloaded part and softened part due to Bauschinger effect. The softened part can be analytically expressed and only to know the stress-strain relation under monotonic loading is required to predict the stress-strain relation of the steel subjected to complex cyclic loading.

RESUME

Dans ce travail on a recherché une expression systématique pour la relation tension-déformation de l'acier soumis arbitrairement à des fluctuations de charges. On a trouvé que la relation tension-déformation de l'acier se compose de trois parties: la partie du squelette, la partie élastique non-chargée et la partie calmée due à l'effet Bauschinger. La partie calmée peut être exprimée analytiquement et la connaissance de la relation tension-déformation sous charges monotones permet de prédire la relation tension-déformation de l'acier soumis à des charges cycliques complexes.

ZUSAMMENFASSUNG

Es wurden systematische Ausdrücke für die Spannungs-Dehnungs-Beziehung von Stahl unter beliebig ändernder Last gesucht. Die Beziehung setzt sich aus drei Teilen zusammen: Skelett-Teil, Teil der elastischen Entlastung, Teil der Enthärtung infolge Bauschinger-Effekt. Der Teil der Enthärtung kann analytisch ausgedrückt werden; zur Voraussage der Spannungs-Dehnungs-Beziehung von Stahl unter einer komplexen zyklischen Belastung ist nur die Kenntnis der Spannungs-Dehnung-Beziehung unter einseitiger Belastung notwendig.

III

Experiments with Steel Members and their Connections under Repeated Loads

Essais d'éléments en acier et leurs liaisons soumis à des charges répétées

Versuche mit Stahlbauteilen und deren Verbindungen unter wiederholter Belastung

Egor P. POPOV
Professor of Civil Engineering
University of California
Berkeley, California
USA

1. INTRODUCTION

For many years rational design of civil engineering structures has been based almost entirely on the assumption of the elastic behavior of materials. This approach has not lost its validity at service loads normally encountered during the life of a structure. However, the necessity for designing more economical structures and the interest in true factors of safety led to the study of the ultimate load-carrying capacity of such structures and to the development of plastic methods of design based on the concepts of limit analysis. This newer approach is based on the assumption of applying a monotonically increasing load until failure occurs; and for ductile materials, the developed theories lead to excellent estimates of the ultimate limit state for a structure under such circumstances. On the other hand, during a strong motion earthquake, a structure such as a building is subjected to random cyclic loadings that may cause inelastic behavior in members and their joints. This necessitates a study of the behavior of members and their connections under repeated loads. In comparison with the experiments in which the applied load is monotonically applied until failure, information on the behavior of structural elements under repeated loading is rather meager.

In this paper, remarks are limited to the behavior of structural elements in moment-resistant steel frames under prescribed cyclic loading. Therefore, although the earthquake problem that motivates this study is a nondeterministic one, in the work reported here the intensities of the induced cyclic load or displacement amplitudes are prescribed a priori. Further, in this investigation mainly the extreme conditions simulating earthquake actions are considered. Interest is centered on the ultimate limit state under cyclic loading corresponding to the maximum load-carrying capacity of steel members and their connections. In many respects, the reported experiments may be characterized as "overtesting," i.e., the members are subjected to extreme actions that normally would not be expected in practice. Nevertheless, it is important to know the ultimate limit-state capabilities of the steel members under extreme repeated loads to be knowledgeable of the true safety margin.

Some phases of the work have reached the stage of development where mathematical models can be suggested. This is done for the inelastic cyclic behavior of beams, as well as for a particular type of a panel zone in a column. No recommendations as yet are given for a model to represent a plastic hinge in a column. Other important situations that may be troublesome are also pointed out, but their behavior is described only in qualitative terms. This pertains to doubler plates and possible buckling failures.

The question of low-cycle fatigue is examined, and a tentative suggestion for analyzing such situations is made. A brief discussion of the brittle failure phenomenon encountered with steel is also brought in.

2. MOMENT-RESISTANT FRAMES

2.1 THE GENERAL PROBLEM

A typical portion of a moment-resistant steel frame consisting of a series of vertical columns and horizontal beams is shown in Fig. 1(a). A good deal of information is available on the elastic and inelastic behavior of these individual members under monotonically increasing loads. Less is known under the action of repeated and reversed cyclic loading. Some information of this type for beams will be presented below.

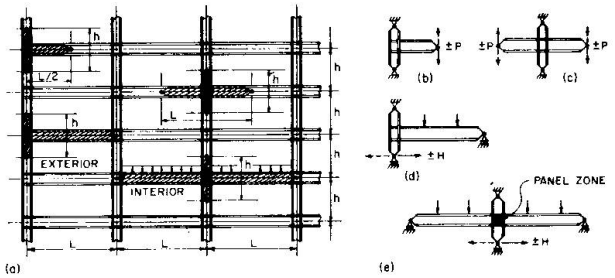

Fig. 1: Moment-Resistant Frame and Subassemblages

Moreover, since in actual construction the beam depths may be on the order of 10 per cent of the column height in a typical building and some 20 per cent or more at the lower floor levels of tall buildings designed to resist seismic forces, the highly stressed regions of the column corresponding to the beam's depth also require investigation. As experiments with complete frames are prohibitive in cost under normal circumstances, much attention by the investigators has been directed to selecting meaningful subassemblages that would provide the necessary data. Several possibilities of subassemblage designs are shown cross-hatched in Fig. 1(a) and are repeated in Figs. 1(b), (c), (d), and (e). A detailed experimental analytical study of such subassemblages can provide very useful information on the load-deformation characteristics of complete frames in elastic as well as in the inelastic range for specified cyclic loadings or displacements.

The subassemblage of the type shown in Fig. 1(b) has been used in an important study [1]. Since the horizontal displacements of the top and the bottom of the column in this type of an experiment is prevented, no $P\delta$ effect is included in such experiments. This is also true for the specimen of the type shown in Fig. 1(c) [2]. Moreover, in both of the above specimens, no provision is made to properly account for gravity loads. Further, since moment-resistant frames are statically indeterminate, correct distribution of the applied moments in the inelastic range cannot be achieved. For this reason, although the subassemblages of the above type are useful, the results obtained from such experiments must be carefully interpreted.

An indication of how a column and a panel zone act in a frame is illustrated in Fig. 2. Note that three items contribute to the story-drift: deformation of the column, rotation of the beam, and panel-zone deformation which is principally caused by shear. It is the combination of all three of these effects that contributes to the $P\delta$ effect. The subassemblage shown in Fig. 1(e) with the outer ends of the beams and the bottom of the column on rollers represents fairly realistically the actual conditions existing in a typical steel frame. By providing torsional restraint at the outer ends of the beams, the model would be improved; but this was not considered essential in the installation referred to later [3,4]. The subassemblage of Fig. 1(d) is similar to that of Fig. 1(e) and is useful for the study of outside columns.

The elastic and inelastic behavior of beams, panel zones, and columns under repeated loads is discussed below, with emphasis being placed on beams and their connections. These data should be sufficient to determine complete load-deformation histories under cyclic loadings of subassemblages as well as complete frames. Analytical formulation of this whole problem is not entirely complete at this time.

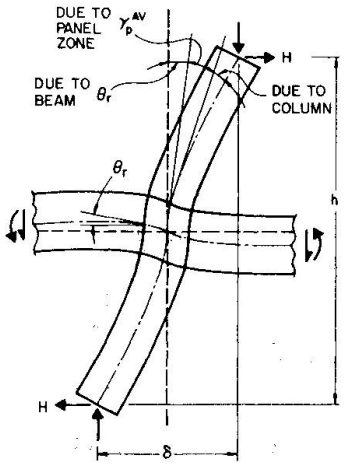

Fig. 2: Components of Story Drift

2.2 BEHAVIOR OF BEAMS

The commonly accepted approach of designing earthquake moment-resistant frames tries to avoid significant inelastic action in the columns. Further, by means of doubler plates or other types of reinforcement, the panel zone deformation is kept to a minimum. For these reasons, it is especially important to study the inelastic behavior of beams and their connections under cyclic loading.

Based on the above approach, a typical interior span with negligibly small gravity loads would have the moment diagram shown in Fig. 3(a), and the deflected shape as in Fig. 3(b). The dashed lines correspond to the moment diagram for a lateral load acting in the opposite direction. A cantilever with a cyclically applied force P at the tip, as in Fig. 3(c), provides a suitable experimental arrangement. For situations where gravity loads are also acting on the girder, the distance ℓ must be made shorter. In such cases the simulation of the actual conditions that develop in a beam is less accurate.

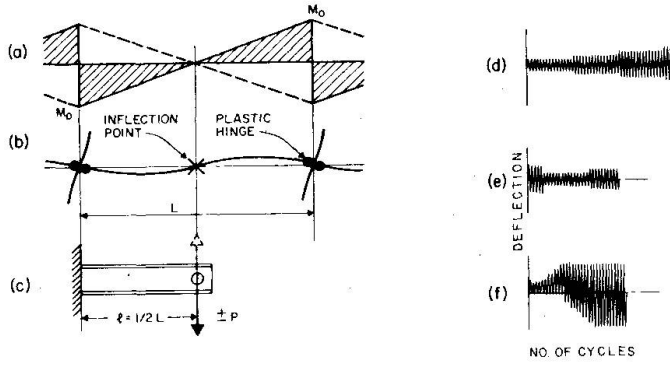

Fig. 3: Cantilever Idealization and Programs of Cycling

Experiments with many cantilevers were performed at the University of California, Berkeley [5,6] Of these, 24 were done with W 8 x 20 specimens of approximately 5 ft. in length; 5 with W 18 x 50 beams, and 3 with W 24 x 76 members. The 8 large specimens were approximately 7 ft. long. Many different types of connections were used in these investigations. These included all-welded, bolted, and hybrid types with welded flanges and bolted webs. In all cases, cyclic load applications were decided a priori and were intense enough to cause inelastic behavior in the specimens. The most frequently used scheme of loading was of the stepladder type with the induced tip deflections progressively increasing in their magnitude, Fig. 3(d). In some instances, the inelastic excursions were begun with very large amplitudes and then were returned to the stepladder type, Fig. 3(e). Displacements that randomly varied from one side to the other were used in some experiments, Fig. 3(f). These variations in the prescribed loading paths were made to determine history dependence on the results.

During the final stages of the experiments the specimens were usually severely deformed, and in all cases they either fractured or the displacements reached the capacity of the equipment. The photographs in Figs. 4, 5, and 6 show some of the specimens at the end of the experiments. The flange crack in

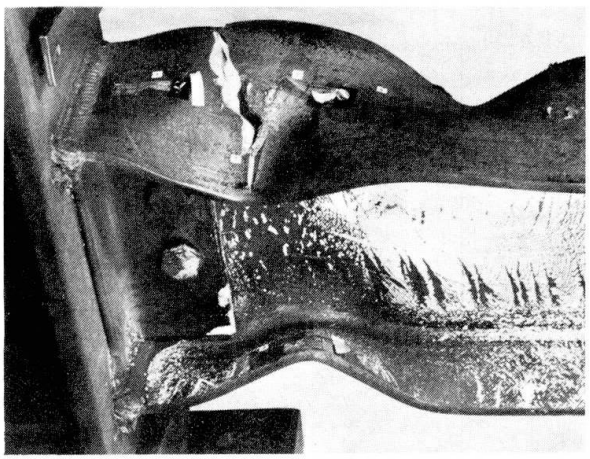

Fig. 4

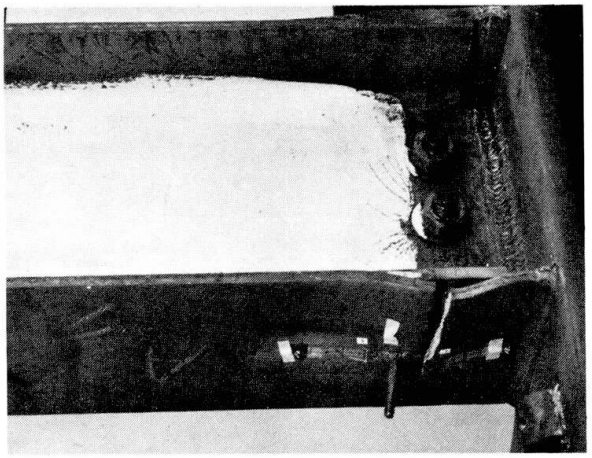

Fig. 5

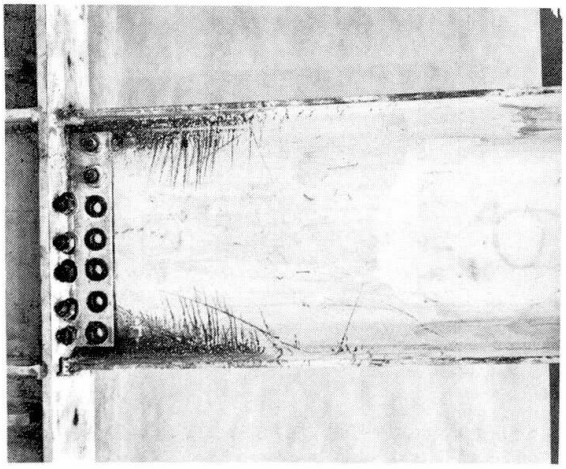

Fig. 6

a direct welded specimen, Fig. 4, began at a tackwelded stud used for instrumentation. For the specimen with connecting plates, Fig. 5, the fracture took place at the end of a fillet weld. A fractured specimen with a bolted web and welded flanges is shown in Fig. 6. Incomplete participation of the web at high loads may be noted by observing that whitewash did not flake off across the whole depth of the member.

The most important characteristic of the behavior of these cantilevers is exemplified by their load-deflection curves which, for cyclic loading, are their hysteresis loops. A good example of a series of hysteretic loops for a W 24 x 76 is shown in Fig. 7 [6]. In this experiment, the induced tip deflections were progressively increased in a manner indicated in Fig. 3(d). The similarity of the consecutive loops for the same displacement is to be noted. Since the area enclosed by the hysteretic loops indicates the amount of dissipated energy, such repetitiveness, synonymous with reliability, is an important property of structural steel members.

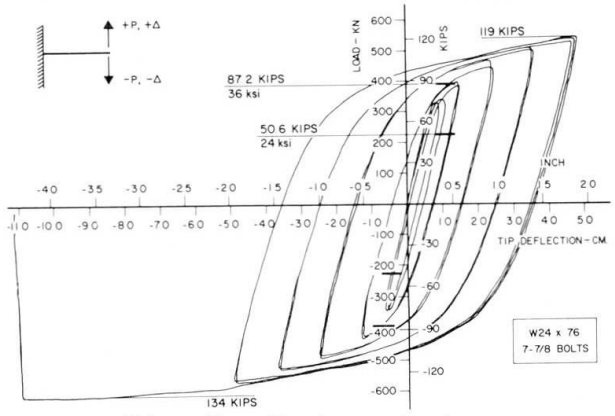

Fig. 7: Hysteresis Loops

The hysteresis loops shown in Fig. 8 [7] correspond to the cycling pattern of Fig. 3(e). The initial elastic excursions for this W 8 x 20 member were very large, and it is important to note that essentially the same shape loops are observed as in Fig. 7, although some upward drift of the loops can be observed. Nevertheless, practically speaking, a rather weak history dependence characterizes the behavior of these laterally braced steel members under cyclic loading. Load-deflection loops enlarging to the right

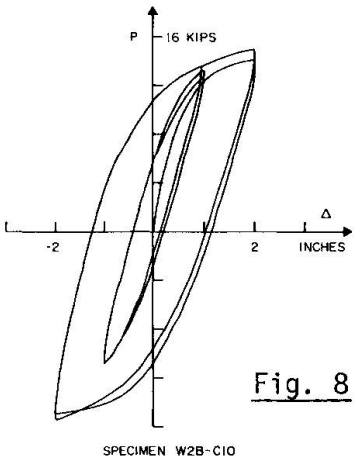

Fig. 8

generated by a W 8 x 20 cantilever specimen are shown in Fig. 9 [7]. Their shape remains quite similar to the ones of Fig. 7. This fact reinforces an assertion made earlier [8] that a moderate shift of the hysteresis loops along the deformation axis is possible. The above two observations provide some justification for mathematical idealization of the hysteresis curves.

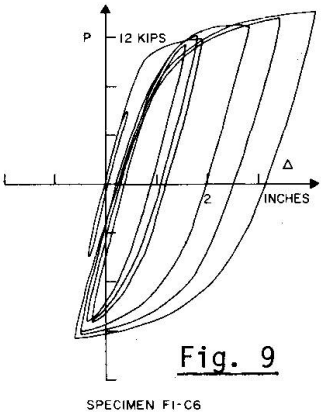

Fig. 9

2.3 IDEALIZATIONS OF CYCLIC BEHAVIOR OF BEAMS

Hysteresis loops of the type shown in Figs. 7, 8, and 9 can be very accurately represented using a Ramberg-Osgood function augmented by Masing's hypothesis [5,9,10]. This formulation has been used in analyzing some simple frames [11]. However, these functions are not always convenient to apply; and, what is more important, the load-deflection characteristics of a cantilever beam are not the fundamental quantities for a general frame analysis. If one were assured that buckling is not critical, it would seem best to begin with a stress-strain diagram obtained for cyclic loading; then to integrate this to obtain the moment-curvature relation for a given member; and, finally, using the latter information, to calculate the load-deflection response due to cyclic loading.

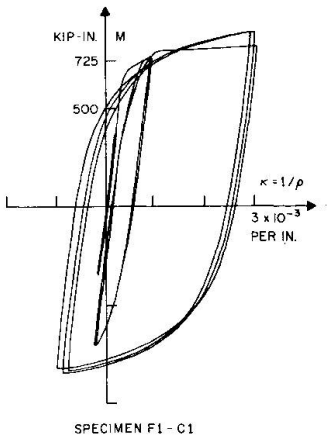

Fig. 10

It can be fully anticipated that stress-strain hysteretic curves for different steels will gradually become more generally available, and the procedure stated above could be followed. For the present, moment-curvature relationship can be easily obtained from any cantilever experiment. By measuring longitudinal strain near the support with an electric strain gage and by neglecting local buckling, the curvature of the member becomes known. Since the location of the gage is also known, the bending moment corresponding to a given curvature is established. Using this procedure the moment-curvature diagram shown in Fig. 10 was constructed. Note that except for the first new and different excursion, the curves in each group repeat themselves. Again an accurate representation using a Ramberg-Osgood function can be achieved, but this does not seem to be necessary.

For cyclically repeating loads, the skeleton curve for the moment-curvature relationship M-ϕ may be approximated with a sufficient degree of accuracy for many purposes by a simple bilinear relationship shown in Fig. 11. On this basis, the agreement between calculated and experimental results for P-Δ is quite satisfactory. If a better agreement is desired, the use of a trilinear approximation for the moment-curvature relationship improves the results, Fig. 12. (As before, the calculated results are shown with dashed lines.) Analogous conclusions were reached by another investigator [16]. To obtain accurate results for the first application of a large load, the established procedures of elastic-plastic analysis should not be abandoned.

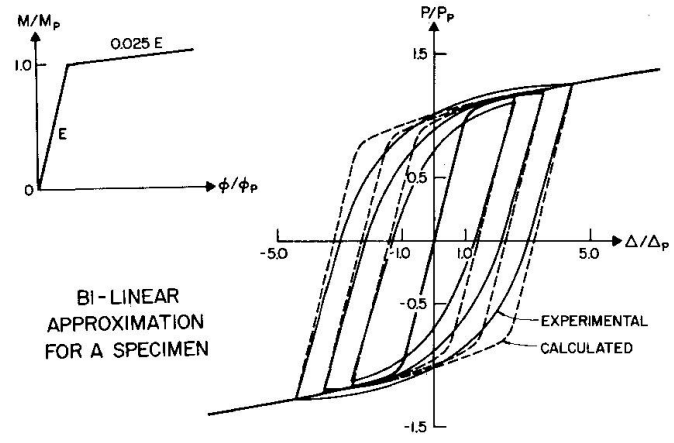

Fig. 11: Load-deflection Hysteresis Loops

deteriorated but unique hysteresis loops persist for many cycles. In these later stages of cycling one notes substantial regions of slip and of joint stiffening once the bolts become seated.

Another anomalous situation is shown in Fig. 14, where the connecting plate of the type shown in Fig. 5 buckles and thereby temporarily reduces the stiffness of the joint.

2.4 BEHAVIOR OF PANEL ZONES

The deformation of the panel zone was studied using subassemblages of the type shown in Fig. 1(c) [4,12,13]. As may be noted from Fig. 2, the horizontal force H acting with a lever arm h and the vertical force P (not shown) with an arm δ apply axial forces, moments, and shears to the column joint. This system of forces is resisted by the forces in the beams. For this connection, the differences in beam moments ΔM at the joint can be related to the average angle of shear deformation γ^{av}_{p} in the panels. This angle as well as the angular rotation θ_r of the joint due to bending of the beams are indicated in Fig. 2.

The bi- or trilinear moment-curvature relationships appear to be both simple and sufficiently accurate for most practical applications in dealing with cyclic loadings. If properly used, they should provide a good indication of hysteretic damping in steel structures; however they are not universally applicable to all steel members regardless of the connection used. For example, load-tip deflection curves for a bolted connection are shown in Fig. 13 [7,8]. These hysteresis loops do not resemble the ones discussed previously. Initially, the high-strength bolts held well--on the first load reversal their behavior is still very good--but then the

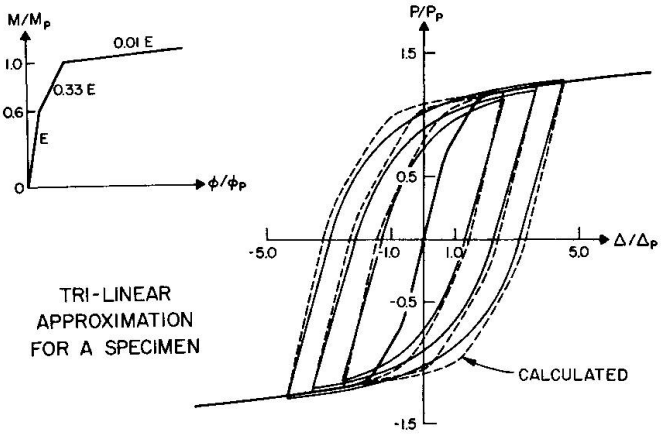

Fig. 12: Hysteresis Loops

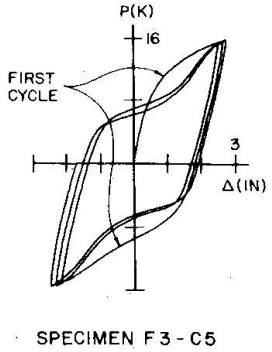

Fig. 13

The panel-zone shear deformations versus the difference in beam-end moments for a particular experiment are plotted in Fig. 15. It is important to note that these load-deformation curves for cyclic loading become the hysteresis loops. Therefore, in the inelastic range of the joint behavior, panel zones dissipate energy.

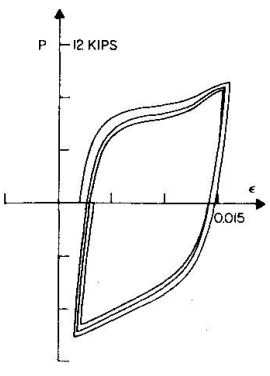

Fig. 14

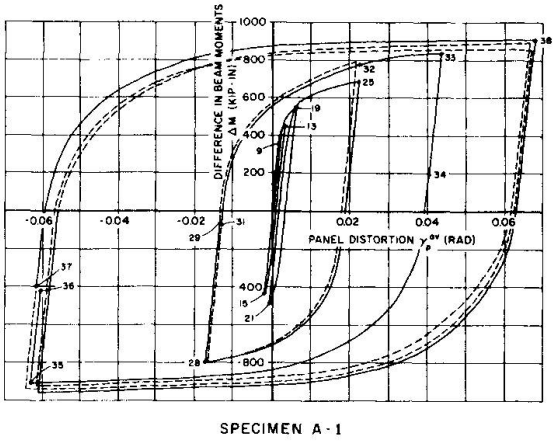

Fig. 15: Shear Hysteresis

The deformation of the panel zone contributes to story drift (see Fig. 2). This may be noted by studying Fig. 16, where the behavior of a subassemblage with a weak panel zone is shown. The experimental curve lies far below the prediction based on the conventional rigid-plastic analysis even including the Pδ effect. The experimental and theoretical results can be brought into good agreement, however, by considering panel-zone deformation. First, the experimental curve can be raised vertically by the amount Pδ/h, which is very nearly the exact equivalent of the horizontal force H caused by the Pδ effect. Then the new curve can be shifted horizontally to the left by δ_p, which is obtained by multiplying the angle of panel shear distortion γ_p^{av} by the clear column height. In this manner, excellent agreement with the calculated results is obtained. In applications, the process can be reversed leading to good estimates of story drifts. In some situations, strain hardening of the material must also be included.

The illustrated case is rather extreme, and in most practical cases the story drift caused by the panel distortion is considerably smaller. However, it is important to point out that the current procedure [14] for designing the panel zones, while providing sufficient strength to resist the difference in beam end-moments, gives inconsistent results for deformations in the inelastic range. An improved approach is suggested in Ref. [13].

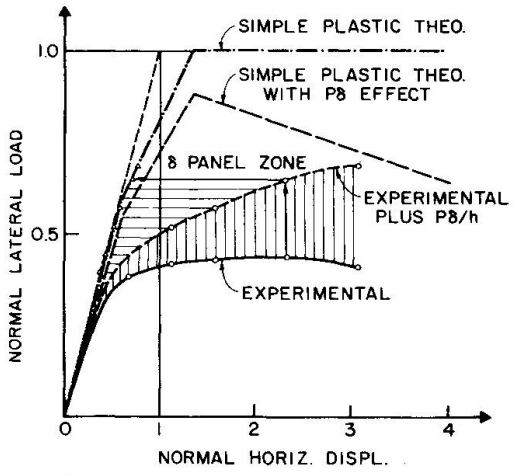

Fig. 16

In an attempt to minimize story drift due to panel-zone deformation, doubler plates are frequently used. They are quite effective, but experimental results indicate that shear is not distributed directly in relation to the plate thicknesses of the web plates. The column web takes up a substantially larger part of the shear than do the doubler plates. Thus for stiffness, the doubler plates cannot be considered to be as effective as the column web. An example of this situation is shown in Fig. 17. Similar conclusions were reached by other investigators [15].

2.5 PLASTIC HINGES IN COLUMNS

As stated in Article 2.2, the commonly accepted approach for design of earthquake moment-resistant frames tries to avoid significant inelastic action in the columns. However, considering the uncertainties of such design, some inelastic action is likely to occur in the columns during a strong-motion earthquake. Therefore, it is very important to know how axially loaded members behave under cyclic loading in the inelastic range.

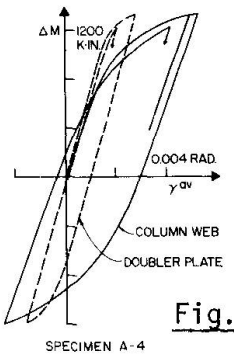

Fig. 17

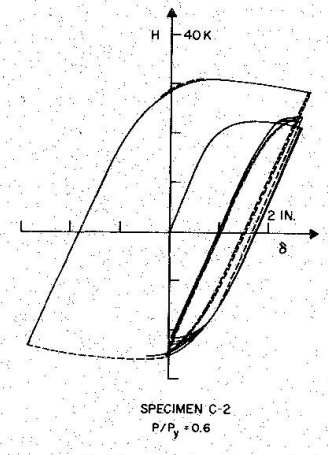

Fig. 18

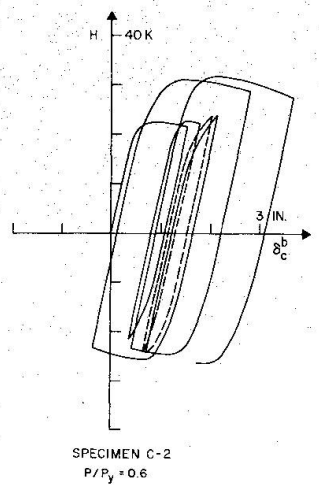

Fig. 19

With the above in mind, six experiments employing subassemblages of the type shown in Fig. 1(e) were performed. In four cases, the columns were bent around their strong axes and in two, around their weak axes. In all cases, the beams framing into the columns were selected to be sufficiently large to act elastically under the applied loadings. Therefore, the plastic hinges were forced to occur in the columns. The ratios of the axially applied loads P to the axial load P_y at yield varied from 0.8 to 0.3. When such a ratio is zero, one has the case of a cyclically loaded beam discussed previously. Thus, a very wide range of P/P_y ratios has been explored. In all of these experiments large story drifts were imposed.

The results for a typical case, corresponding to $P/P_y = 0.6$ for a W 8 x 48 column, are shown in Figs. 18 and 19. The H-δ hysteresis loops in Fig. 18 look remarkably normal and resemble the ones obtained for beams; however, this is not the complete story. Axially loaded columns when subjected to very severe cyclic loading tend to assume single curvature from top to bottom. The permanent set is such that the columns become and remain C-shaped. As inelastic strains occur, the material strain hardens and becomes stronger elastically. Therefore, on a return stroke the column does not fully straighten out, and progressively the single curvature shape becomes more and more pronounced. The displacement of the panel zone relative to both of the column ends moves in the same direction but by different amounts. The control load-displacement path is shown in Fig. 18. The resulting load-displacement path between the panel zone and the bottom of the column as seen from Fig. 19 looks quite different. As to be expected, at high lateral loads the column flanges buckle.

Essentially, the same type of behavior was observed for bending of columns around their weak axes. Some suggestions for mathematically modeling the inelastic behavior of columns under cyclic loading has already been made [16]. These results, however, were obtained on simplified small models, and further verification of the conclusions seems desirable. For the present, it seems encouraging that there are strong indications that some plastic activity in columns can be tolerated during cyclic loading.

3. LOW-CYCLE FATIGUE AND BRITTLE FAILURE

Very little, if any, evidence is available on failures of buildings due to low-cycle fatigue. Nevertheless, with ever-changing design requirements of structures, it is important to consider this problem [17]. Brittle failure of steel is also a possibility for large weldments and deserves most careful scrutiny for this reason [20,21].

To establish a damage criterion for low-cycle fatigue, the critical section of a member must be considered. The behavior of a member as a whole is not the

real issue. Fortunately, however, as indicated in Article 2.3, if buckling effects are small, the general deformational behavior of a structure may be related to its moment curvature or, if necessary, to the stresses and strains at any section. Therefore, it is possible to apply the cumulative damage criterion at the point of the maximum cyclic stress or strain.

There are three possible alternative cumulative damage criteria, which may be written in the following convenient form:

Miner's Rule
$$\sum_{i=1}^{k} \frac{n_i}{N_i} = 1 \qquad (1)$$

Manson-Coffin Hypothesis
$$\sum_{i=1}^{k} \left(\frac{\Delta\varepsilon_{pi}}{\varepsilon_p}\right)^a = 1 \qquad (2)$$

Dissipated Energy Hypothesis
$$\sum_{i=1}^{k} \left(\frac{\Delta e_i}{e}\right)^b = 1 \qquad (3)$$

In Eq. 1, n_i is the number of design cycles at a given stress, and N_i is the corresponding number of cycles causing failure. In applying this relation to randomly applied cycling, an experimentally determined stress-cycle diagram with N_i's corresponding to the number of cycles (life) at the various stress levels S must be known. Then, if in a particular case the indicated sum on the left-hand side of the equation is less than unity, it is presumed that the member will not fail in fatigue. This equation is widely used by mechanical engineers [18] for stresses at essentially elastic levels and appears to be reasonably accurate for high-cycle fatigue.

For low-cycle fatigue the criterion based on plastic strain is more appropriate (Eq. 2). In this equation ε_{pi} is the plastic amplitude range (permanent deformation per half-cycle) and ε_p and a are experimentally determined constants [19]. Good correlation with experimental results can be achieved using this equation.

Another logical possibility for a cumulative damage criterion for low-cycle fatigue is expressed by Eq. 3 where Δe_i is the dissipated energy per half-cycle (full loop can be used for completely skew-symmetric cases), and e and b are appropriate experimental constants. If a skew-symmetric bilinear skeleton curve idealization is used, this equation reverts to Eq. 2. On the other hand, it is believed that this formulation is more universal and is applicable to a larger class of problems. For example, for reinforced concrete members the hysteresis loops are quire irregular, yet this approach would seem to be appropriate. Efforts to verify the above cumulative damage criterion both for steel and reinforced concrete are now being pursued by the writer and his associates.

It is believed that for steel beams, low-cycle fatigue is not a serious problem, but it would be well to have an analytical procedure to verify this fact. Eq. 2 and/or 3 provide this possibility. However, the more pressing problem in structural steel fabrication is brittle fracture. As the thickness of the members increases, and welding is becoming the conventional manner of interconnecting the members, these difficulties increase. The necessity of being appraised on such matters as the Charpy V-notch impact values, as well as the effects of temperature, loading rate, and plate thickness must not be overlooked [20]. The question of

the lack of isotropy of rolled steels also is becoming increasingly important [21]. In all of this, fracture mechanics related to crack propagation plays the dominant role [20].

4. BUCKLING OF STEEL MEMBERS

The behavior of steel members described above can terminate abruptly if excessive buckling occurs. For monotonically applied loading, ratios of flange widths b to their thicknesses t, as well as beam depths d to their thicknesses t_w, are carefully limited [14]. This avoids, or at least minimizes, local buckling of the members. For cyclic loading, no similar provisions exist. From the experience gained from the experiments described here, it is clear that the requirements for repeated loading are more severe. As loads are cycled, the buckled regions tend to enlarge. Therefore, it is prudent to be more conservative in assigning maximum b/t and d/t_w ratios for cyclic loadings than for those that are monotonically applied.

Lateral torsional buckling of beams also needs to be very carefully guarded against. The bottom flange of a beam can be in compression over a considerable portion of a span. In contrast to the top flanges held by the floor system, often the bottom flanges are not laterally braced. Under cyclic loading, lateral deflections tend to magnify, and it is imperative to prevent this by bracing. Observations in the laboratory demonstrated that deep beams with unbraced bottom flanges are particularly vulnerable to this phenomenon which is very dangerous [22].

5. ACKNOWLEDGEMENTS

The writer is most grateful for the financial support given by the American Iron and Steel Institute which made this work possible. He also is greatly indebted to his colleague Professor V. V. Bertero for continuous collaboration on the projects described as well as to Dr. H. Krawinkler and Messrs. Roy Stephen and S. Chandramouli who gave much valuable assistance.

9. REFERENCES

1. Hason, R.D., and H. W. Connor, "Seismic Resistance of Reinforced Concrete Beam-Column Joints," Proc. ASCE, 93 (ST 5), 1967, pp. 533-560.

2. Miki, S., et al, "Some Problems of Beam-to-Column Connections in Steel Frames," Report, Kawasaki Dockyard Co., Nov. 1964.

3. Popov, E.P., V. V. Bertero, and M. Watabe, "A Test Frame for Simulating Gravity and Ground Motion on Structural Assemblages," RILEM Symposium, Bucharest, Sept. 1969.

4. Bertero, V. V. and E. P. Popov, "Testing Facility for Frame Subassemblages," Experimental Mechanics, Vol. 11, No. 8, August 1971, pp. 337-345.

5. Popov, E. P. and R. B. Pinkney, "Cyclic Yield Reversal in Steel Building Joints," Journal of the Structural Division ASCE, Vol. 95, No. ST3, Proc. Paper 6441, March 1969, pp. 327-353.

6. Popov, E. P., and R. M. Stephen, "Cyclic Loading of Full-Size Steel Connections," Report No. EERC 70-3, Earthquake Engineering Research Center, University of California, Berkeley, CA., July 1970. Republished, AISI Bulletin No. 21, February 1972.

7. Popov, E. P., and R. B. Pinkney, "Behavior of Steel Building Connections Subjected to Inelastic Strain Reversals - Experimental Data," AISI Bulletin No. 14, November 1968.

8. Popov, E. P., "Low-Cycle Fatigue of Steel Beam-to-Column Connections," RILEM Symposium, Mexico, Sept. 1966.

9. Jennings, Paul C., "Earthquake Response of a Yielding Structure," Journal of the Engineering Mechanics Division, ASCE, Vol. 91, No. EM4, Proc. Paper 4435, August 1965, pp. 41-68.

10. Kaldjian, M. J., "Moment-Curvature of Beams as Ramberg-Osgood Functions," Journal of the Structural Division, ASCE, Vol. 93, No. ST5, Proc. Paper 5488, October 1967, pp. 53-65.

11. Berg, G. V., "A Study of the Earthquake Response of Inelastic Systems," Proceedings, Structural Engineers Association of California, October 1965.

12. Bertero, V. V., E. P. Popov and H. Krawinkler, "Beam-Column Subassemblages under Repeated Loading," Journal of the Structural Division, ASCE, Vol. 98, No. ST5, May 1972, pp. 1137-1159.

13. Krawinkler, H. V. V. Bertero and E. P. Popov, "Inelastic Behavior of Steel Beam-to-Column Subassemblages," Report EERC 71-7, Earthquake Engineering Research Center, University of California, Berkeley, California, October 1971.

14. "Plastic Design in Steel," ASCE Manual No. 41, 2nd Ed., 1971.

15. Becker, E. R., "Panel Zone Effect on the Strength and Stiffness of Rigid Steel Frames," USC Structural Mechanics Laboratory, Los Angeles, California, June 1971.

16. Yamada, M., and K. Shirakawa, "Elasto-plastische Biegeformanderungen von Stahlstutzen mit I-Querschnitt," Der Stahlbau, 3, March 1971.

17. Popov, E. P., "Low-cycle Fatigue of Connection and Details," ASCE-IABSE Conference on Tall Buildings, Tech. Com. 18, SOAR #3, August 1972.

18. Jwinall, R. C., "Stress, Strain, and Strength," McGraw-Hill, 1967.

19. Yamada, M., "Effect of Cyclic Loading on Buildings," ASCE-IABSE Converence on Tall Buildings, Tech. Com. 18, SOAR #1, August 1972.

20. Rolfe, S., and G. R. Egan, "Designing to Prevent Fracture in Tall Buildings," Tech. Com. 18, SOAR #6, August 1972.

21. Naka, T., "Design Limitations for Fatigue," ASCE-IABSE Conference on Tall Buildings, Tech. Com. 18, SOAR #5, August 1972.

22. Bertero, V. V., E. P. Popov and H. Krawinkler, "Effects of Local Instabilities in Beam-Column Subassemblage Behavior," Proceedings, Int'l Symposium on Experimental Analysis of Instability Problems on Reduced and Full-Scale Models, RILEM, Buenos Aires, Argentina, September 13-15, 1971.

Leere Seite
Blank page
Page vide

III

Elasto-Plastic Behaviour of High Tensile Bolted Connections in Wide Flange Beams under Repeated Loading

Comportement élasto-plastique des liaisons par boulons à haute résistance pour poutres à aile larges soumises à des charges répétées

Elasto-plastisches Verhalten von hochfest verschraubten Verbindungen in Breitflanschträgern unter wiederholter Belastung

S. IGARASHI
Professor

K. WAKIYAMA
Associate Professor

Osaka University
Osaka, Japan

E. KAWADA
Chyoda Chemical Engineering and Construction
Kawasaki, Japan

1. Introduction

In practical design works, elastic strengths of steel members are usually designed as to be higher than those of joints which connect them. But, to clear up collapse processes of steel structures under excessive loads and to estimate reserved strengths of structures, we have to investigate plastic behaviors and ultimate strengths of individual structural elements clearly. On the other side, it may be interesting to research for proper use of high tensile bolted friction joints for seismic design of steel structures. Moreover, it is necessary to certify details of fatigue fracture by stress concentration which was mentioned in the paper by Dr. M. Yamada.[3)]

This paper reports the results of experimental research concerned in the former two problems and does not treat fatigue fracture.

2. Loading Conditions

It is not easy to study details of complicated behaviors of high tensile bolted friction joints, and it does not always necessary to analyse some effective factors upon them. We would rather consider the joint as one point in steel structures and try to have their behaviors macroscopically.

Usual buildings receive repeated loads by winds, earthquakes or machinaries like cranes. Wind loads are not cyclic reverse and accelerograms are random and individual in every cases. But, for convenience, we shall take earthquake loads as alternately repeated cyclic waves and adopt, in our experiments, alternately repeated cyclic loads controlled by large deformation with constant plus and minus amplitudes and increase the amplitudes gradually in loading processes.

3. Test Specimens

Details, dimensions and stress conditions of such joints are

differ from each other and there are many variations in practical case. But, as for friction joints, even if they are single shear or double shear types, their behaviors as a whole may be assumed from those of individual bolt. And so, we take beam joints as the specimens proper for the object of this experimental study.

The specimens are built up with two wide flange beams (H-200×150×6×9 mm) and they are connected with high tensile bolts. We classify them into group A and B.

The specimens in group A are connected at midspans as single shear type and grade of high tensile bolts used for them are F 10T (JIS B 1186). Faying surfaces of the beams and cover plates are rusted or are treated by sandblast or shotblast.

The specimens in group B are connected as double shear type using F 8T (JIS B 1186) high tensile bolts and their faying surfaces are rusted naturally.

In every specimens, diameters of bolts are 16 mm and those of bolt holes are 17 mm. High tensile bolts are fastened under torque coefficient 0.169 and tightening torque is 24.5 kg.m in group A. These values in group B are 0.190 and 27.0 kg.m respectively.

Lengths of the specimens are 260 cm and their both ends are supported by rollers.

Mechanical properties of these materials are listed in Table 1 and figures of the specimens are shown in Fig.1&2.

Compressive and tensile reverse forces are applied repeatedly on the simple beams at midspans or two symmetrical points. Deflections at midspans of the test beams and loads are traced electrically by X-Y autorecorder.

4. Experiments under simply increasing loads

These experiments are introductory ones. In Fig.3 is shown a load-deflection curve of A1,2 beam under static simple loads and Fig.4 shows that of B1,2 beam under same loading conditions. As are seen in Fig.3, elastic curves of shotblasted and sandblasted A specimens are dropped down by first major slip. After then, clearances of bolt holes decrease and bearing resistance appear gradually. In B specimen, many minor slips appear continuously with sharp metalic sounds under increasing loads. In these cases, we do not notice clearly yielding plateaus in these P- δ curves. The experimental data already presented showed various kinds of P- δ curves for similar specimens. In one case, curves like Fig.3 was presented, and in another paper a curve like Fig.4 was shown. Perhaps, this difference may be brought on by various mechanical conditions of faying surfaces. But, we should pay some attentions on the following two points.

i. After some slips, distinguished increases of strengths by bearing resistances of bolts are expected.
ii. As was shown in Fig.5, elastic tangent moduli does not reduce under repeating loads in one side.

5. Experiments under repeated cyclic loadings

After the first major slip happened, cyclic loadings with constant deflection amplitudes were repeated reversely. Each cycle having equal plus and minus deflection amplitudes was repeated four or five times and, then, these amplitudes were increased until bearing resistance zone were marked.

In Fig.6 and Fig.7, some of the relations between load P and deflections δ at midspans are shown, and the next are concluded from these figures.

i. Slip loads in each cyclic loop tend to drop slightly compared with major slip loads under simply increasing loads, but they approach gradually to some fixed values. Slip zones look like a saw-tooth but they become to be smooth by repetitions of the loading loops.
These two phenomena may be due to smoothing of the faying surfaces and due to reduction of bolt tension. On reduction of bolt tension, one of the authors had already appointed that 10~20 % of initial bolt tension disappear by slipping ultimately.

ii. Elastic tangent moduli of these hysteresis loops are reduced slightly by repeated loading but the reduction are negligible small.

iii. When the maximum deflections are limited in slip zones, the shapes of hysteresis loops are nearly bi-linear type, and, when the maximum deflections are in bearing resistance zones, hysteresis loops are composed of two parts, i.e. slip plateau and shearing resistant zone. And their whole shapes become to reversed S type. We should notice that the shapes of these hysteresis loops are very stable in every cases, although lengths of slip plateaus expand gradually with increase of deflection amplitudes.

iv. Details of slip plateaus are differ from each other by difference of treatment on faying surfaces. Shotblasted or sandblasted faying surfaces show comparatively smooth curves but naturally rusted faces show sharply jaggy plateaus. But such differences have no influences on the characters of hysteresis loops and their transitional features mentioned above.

v. Collapses of all test specimens are due to ultimate strengths of the cover plates in metal touch conditions and maximum values are extremely higher than those calculated for slip strengths of bolts. Designed strengths have very high factors of safety against real ultimate strengths.
We showed, already, dynamic responses of slip models under El-Centro earthquake input[4] and, in other paper[5], some comparative data on dynamic behaviors of non-slip and slip type structures were indicated. As be assumed from these studies, it may be possible, in near future, to control dynamic behaviors of steel structures under destructively severe earthquake by using characteristic behaviors of friction joints.

Acknowledgement

The authors wish to thank Mr. K. Nakai, assistant of Osaka University, who endeavored for execution of our experiments and for adjustment of experimental data.

References

1. S. Igarashi and E. Kawada, "Elasto-Plastic Behaviors of H Beam Joint using High-Strength Bolts", Yawata Technical Report, No. 256, Sept., 1966.
2. H. Hokugo, M. Fujimoto and A. Hashimoto, "The Cyclic Load Tests of High-Tensile-Bolted Friction Joint:, Pts.1 and 2, Architectural Institute of Japan, No.103, 1964 (in Japanese)
3. M. Yamada and I. Nakaza, "Low Cycle Fatigue of Riveted and

High Strength Bolted Joints in Steel Beams", International Symposium on the "Effects of Repeated Loading of Materials and Structures", Rilem, 1966

4. S. Igarashi, K. Inoue, M. Asano and K. Ogawa, "Restoring Force Characteristics of Steel Diagonal Bracings", 5 WCEE, 1973

5. A. S. Veletsos, "Maximum Deformations of Certain Nonlinear Systems", 4 WCEE, 1969

	σ_y t/cm^2	σ_{max} t/cm^2	E t/cm^2	Elongation %	R.C.
H.T.B. 16mm ϕ	9.9	10.4		16	17~23
H-web 6mm	3.2~3.5	4.5~5.0	2.08~2.09x10^3	25~39	
H-flange 9mm	3.2~3.6	4.6~5.0	2.03~2.07x10^3	28~38	

Table 1

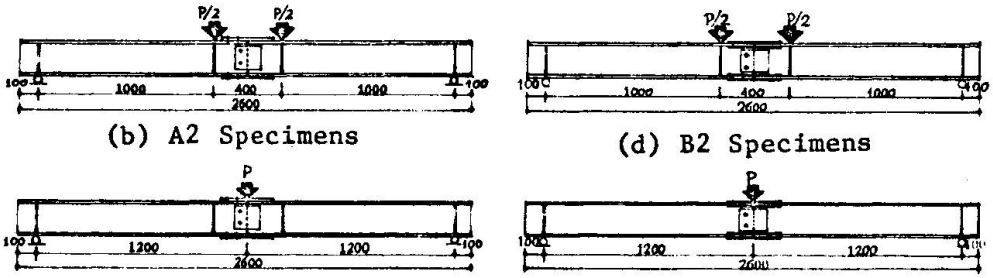

Fig.1 Specimens

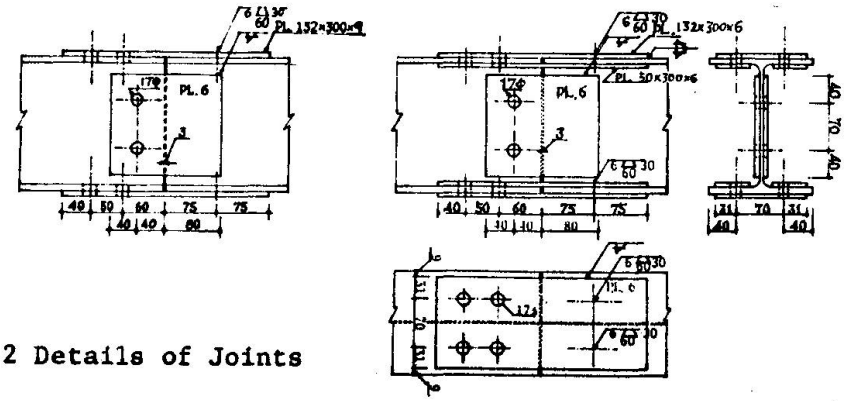

Fig.2 Details of Joints

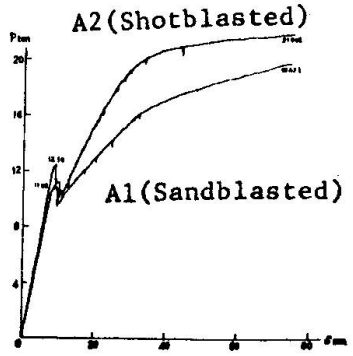

Fig.3

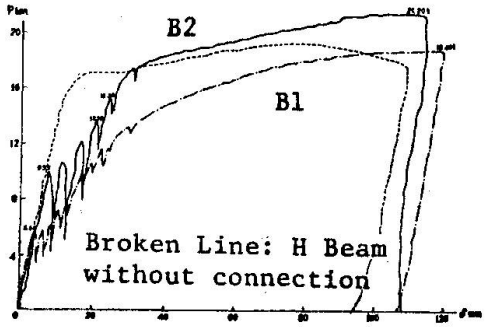

Fig.4

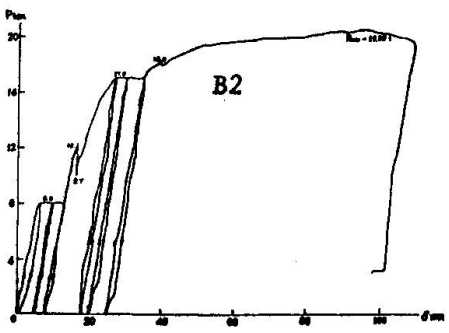

Fig.5

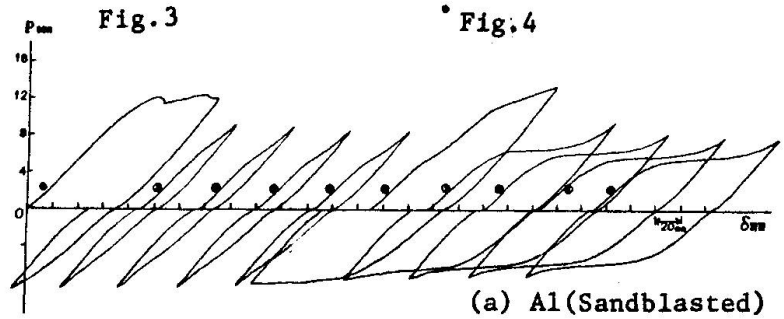

(a) A1(Sandblasted)

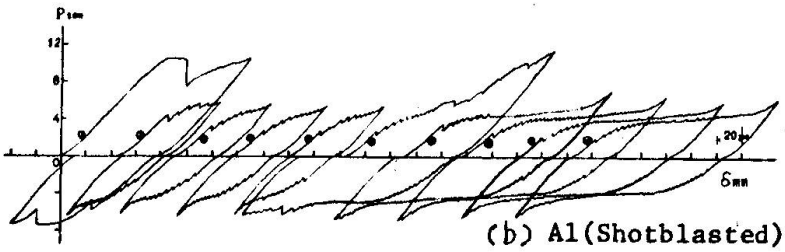

(b) A1(Shotblasted)

Fig.6 P-δ Relationships of A Specimens

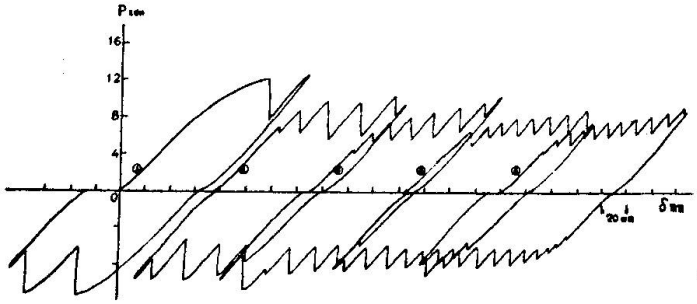

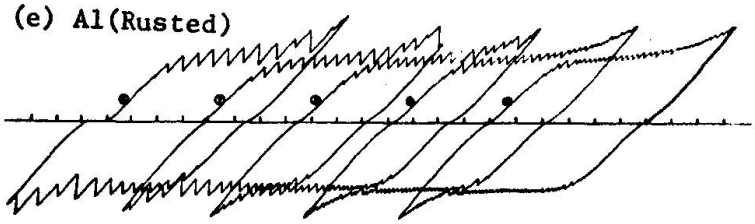

(e) A1(Rusted)

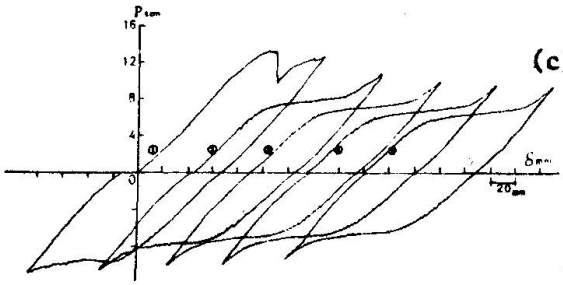

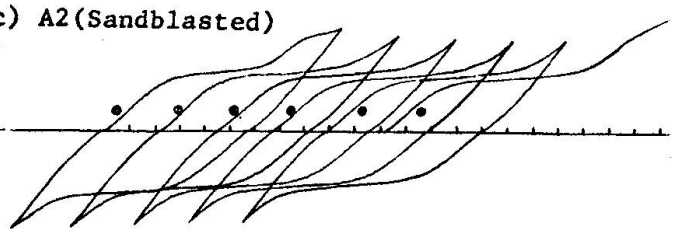

(c) A2(Sandblasted)

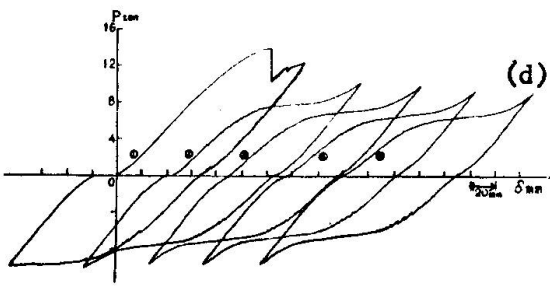

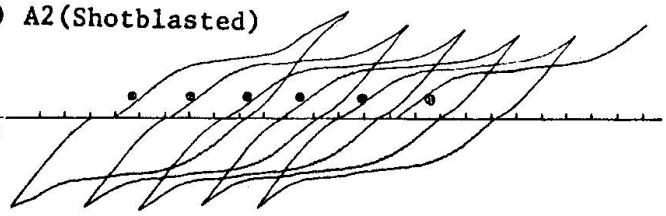

(d) A2(Shotblasted)

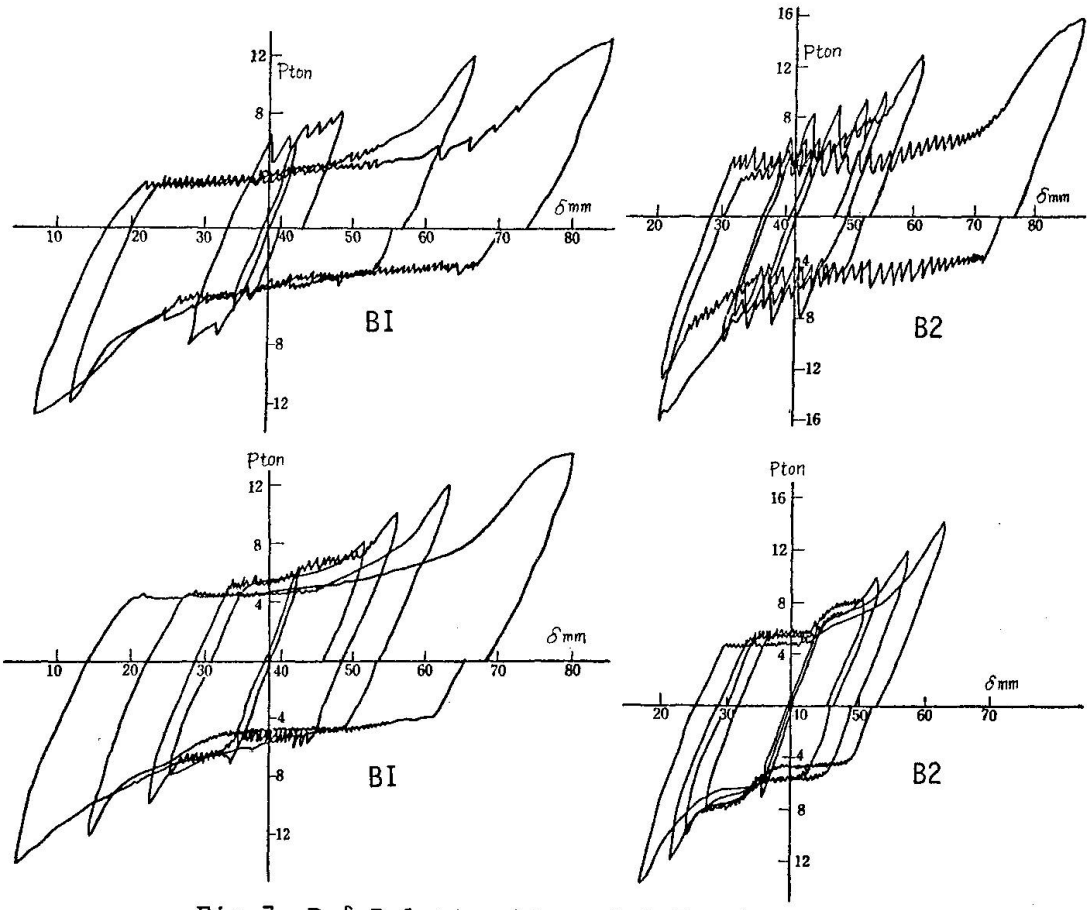

Fig.7 P-δ Relationships of B Specimens

SUMMARY

Behaviors of high tensile bolted friction joints under statically repeated cyclic loads are differ in details by minute differences of faying surfaces. But hysteresis loops distinguished by slip zone and bearing resistance zone are fairly stable under repetitions of cyclic loads with same deflection amplitudes. Their ultimate strengths are very high compared with design values. We may expect for these connections that they exhibit high resistance and absorb much seismic energy by stable slipping phenomena.

ZUSAMMENFASSUNG

Das Verhalten hochfest vorgespannter Schraubenverbindungen unter langsam ändernder zyklischen Belastung ist unterschiedlich auch bei äusserst kleinen Verschiedenheiten der aufeinanderliegenden Oberflächen. Hingegen sind die Hysteresis-Schlaufen, wo die Scherzone und die Lochleibungswiderstandszone auseinandergehalten werden, bei wiederholter zyklischer Belastung mit gleicher Verformungsamplitude ziemlich stabil. Ihre Bruchwiderstände sind sehr hoch, verglichen mit den zulässigen Werten. Man darf von solchen Verbindungen erwarten, dass sie hohen Widerstand zeigen und durch das feste Schlupfphänomen viel seismische Energie absorbieren.

RESUME

Le comportement des assemblages par boulons précontraints à haute résistance soumis à des charges cycliques répétées statiquement se distingue en détail par de petites différences dans les surfaces de contact. Mais les boucles d'hystérésis distinctes par leur zone de glissement et par leur zone de résistance sont assez stables sous des charges cycliques répétées et pour des déformations d'amplitudes constantes. Leurs résistances à la rupture sont très grandes comparées aux valeurs de dimensionnement. On peut attendre de ces assemblages qu'ils offrent une grande résistance et absorbent plus d'énergie lors de phénomènes de glissement stables.

Nonstationary Hysteretic Stress-strain Relations of Wide-Flange Steels and Moment-Curvature Relations under Presence of Axial Force

Relations hystérétiques non-stationnaires tension-déformation d'éléments en acier à ailes larges et relations moment-courbure en présence d'une force axiale

Nichtstationäre hysteretische Spannungs/Dehnungs-Beziehungen von Breitflanschstählen und Moment/Krümmungs-Beziehungen unter auftretender Axialkraft

Yoshitsura YOKOO
Prof. Dr. Eng.

Tsuneyoshi NAKAMURA
Assoc. Prof. Ph.D.Dr. Eng.

Toshiro KOMIYAMA
M. Eng.

Department of Architecture
Kyoto University
Kyoto, Japan

1. INTRODUCTION

It is apparent from the review of the Introductory Report for Theme III that, while a number of experimental results have been presented on the load-deflection behaviors of steel members and frames subjected to repeated alternating loads, almost all the corresponding results of numerical analysis have been based upon either simplified bilinear hysteretic or extended Ramberg-Osgood relations without experimental verification. To the best of the authors' knowledge and as the Introductory Report for Theme I has pointed out particularly, experimental hysteretic stress-strain curves under alternating strain and stress cycling conditions have not been obtained systematically *for the purpose of deriving the stress-strain relations applicable to arbitrary nonstationary stress-strain paths*. Although some papers presenting experimental results on low-cycle fatigue of materials have included stress-strain curves obtained under mostly constant strain or stress amplitudes and discussed their shapes and energy absorption capacities, the principal aim seems to have been at the correlations between their stationary shapes and the low-cycle fatigue properties of various metals, not particularly of structural steel.

With this understanding of the state-of-the-art [1], the senior authors (Yokoo and Nakamura) have first presented in [2], a set of hysteretic and skeleton stress-strain relations for a wide-flange steel applicable to steady-state hysteresis loops of *completely reversed* strain cycling of constant strain amplitudes and then started a series of nonstationary tension-compression tests specifying stress-strain paths [4]. In this contribution to the prepared discussion, some of the recent test results and a set of nonlinear hysteretic stress-strain relations derived from the experimental stress-strain curves are first presented.

The senior authors have also presented the experimental load-deflection curves of beam-columns subjected to dead and alternating repeated loads [5] (obtained by forced deflection). For the purpose of predicting the nonstationary inelastic behavior of beam-columns subjected to combined axial and lateral forces, Nakamura

proposed in 1966 [6] a method of analysis based upon the sandwich idealization of the cross-sectional property of a wide-flange or box section. The principal aims of the sandwich formulation are, (1) the direct analytical derivation of the axial force-bending moment-curvature relation from bilinear or nonlinear hysteretic stress-strain relations, (2) the possibility of obtaining piecewise analytical solutions for flanges obeying bilinear hysteretic stress-strain relations, and (3) to develop a rational numerical method of analysis which incorporates nonlinear hysteretic stress-strain relations and the effect of large deflection, is able to trace gradual spreading and/or diminishing of strain-hardening regions but is so simple and compact that an available computer would be able to carry out numerical integration with respect to time even for plane frames of practical size. A numerical method for the aim (3) has been described in the senior authors' prepared discussion on Theme I. In the second part of this contribution, an experimental cyclic moment-curvature relation under a constant axial force is presented and compared with the analytical prediction due to the sandwich theory.

2. NONSTATIONARY TENSION-COMPRESSION TEST

2.1 SPECIMEN Fig.1 shows the shape and size of the specimens. A specimen was manufactured by shapering from a half-flange of a commercially available SS41 wide-flange steel of the nominal size 400×400×13×21. The chemical composition of the steel due to the millsheet is c 0.25%, S_i 0.07%, M_n 0.62%, P 0.017% and S 0.013%.

2.2 TEST SETUP The senior authors devised a keyhole mechanism in [2] for gripping smaller plate specimens by modifying a commercially available gripping apparatus for cylindrical specimens. The gripping apparatus for the present plate specimens utilizes the same keyhole mechanism but is of a greater size and of a modified form suitable for an Autograph universal testing machine of capacity ±50 tons. Strain within the range of ±4% was measured by two pairs of precalibrated Π-gauges (shown in Fig.2) mounted on the four sides of a specimen symmetrically.

2.3 CONTROL CONDITION The tension-compression tests were carried out at the constant strain rate of 0.00044/sec., except the virgin paths in which the plastic flow plateaus appear. Table 1 shows the strain or stress paths prescribed for the present series of tests. A pair of amplitude limiters on the X-axis (strain axis) of the Autograph XY-recorder were moved manually in accordance with the prescribed strain cycling program.

2.4 TEST RESULT Fig.3 and 5 show two examples of experimental stress-strain curves under incompletely reversed strain cycling. Fig.4 shows a stress-strain curve in the tensile strain range, and Fig.6, in the compressive strain range.

3. NONSTATIONARY HYSTERETIC STRESS-STRAIN RELATIONS

In view of the purpose of incorporating stress-strain relations in finite element analysis of frames, it is considered appropriate to derive stress-strain relations in terms of the engineering strain ε and the nominal stress σ. It is well-known that each smooth piece of hysteresis loops can be approximately represented by a (generalized) Ramberg-Osgood equation:

$$\frac{\varepsilon-\varepsilon^{(i)}}{\varepsilon_y} = \frac{\sigma-\sigma^{(i)}}{\sigma_y}\left\{1+\left(\frac{1}{a}\right)^r\left|\frac{\sigma-\sigma^{(i)}}{\sigma_y}\right|^{r-1}\right\}, \qquad (1)$$

σ_y: the yield stress,
ε_y: the yield strain.

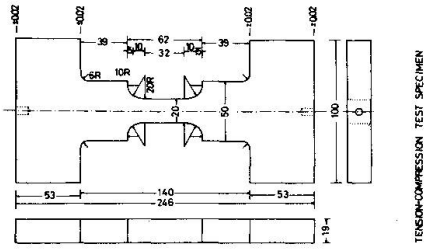

Fig. 1

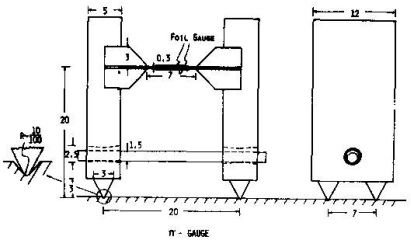

Fig. 2

Table 1 Specification of controlled strain paths and stress paths

Specimen No.	Reversal point-numbers and strains (%) or stresses														
	1	2	3	4	5	6	7	8	9	10	11	12	13	14	15
Incomplete alternating strain cycling $\varepsilon(1)\geq 0$															
SS-14ℓ	-1.0	+0.5	-1.5	+1.0	-2.0	+1.5	-0.5	+2.0	-1.0	+0.5	-2.0				
SS- 7ℓ	-1.0	+1.5	-1.5	+2.0	-2.0	+0.5	-0.5	+1.0	-1.0	+1.5	-2.0				
SS-13ℓ	-1.5	+1.0	-2.0	+1.5	-0.5	+2.0	-1.0	+0.5	-1.5	+1.0	-2.5	+2.5	-3.0	+3.0	-3.0
SS-12ℓ	-1.5	+2.0	-2.0	+0.5	-0.5	+1.0	-1.0	+1.5	-1.5	+2.0	-2.5	+2.5	-3.0	+3.0	
SS-10S	-2.0	+2.0	-3.0	+3.0	-4.0	+4.0	-1.0	+1.0	-2.0	+2.0	-4.0				
SS- 9S	-2.0	+4.0	-3.0	+1.0	-4.0	+2.0	-1.0	+3.0							
SS-15S	-3.0	+1.0	-1.0	+2.0	-2.0	+3.0	-3.0	+1.0	-1.0	+2.0	-4.0	+4.0	-4.0		
SS-16S	-3.0	+3.0	-1.0	+1.0	-2.0	+2.0	-3.0	+3.0	-1.0	+1.0	-4.0				
One-way strain cycling $\varepsilon(1)\leq 0$															
SS-11S	-1.5	0	-2.0	0	-0.5	0	-1.0	0	-1.5	0	-2.0	0			
SS- 5S	-3.0	0	-4.0	0	-1.0	0	-2.0	0	-3.0	0	-4.0	0			
SS- 3ℓ	+1.5	0	+2.0	0	+0.5	0	+1.0	0	+1.5	0	+2.0				
SS- 2ℓ	+3.0	0	+4.0	0	+1.0	0	+2.0	0	+3.0	0	+4.0	0			
SS- 4S		$+0.2\sigma_y$		$+0.4\sigma_y$		$+0.6\sigma_y$		$+0.8\sigma_y$		$+1.0\sigma_y$					
SS- 6ℓ		$-0.2\sigma_y$		$-0.4\sigma_y$		$-0.6\sigma_y$		$-0.8\sigma_y$		$-1.0\sigma_y$					

Reversal point-strain controlled

Reversal point-stress controlled

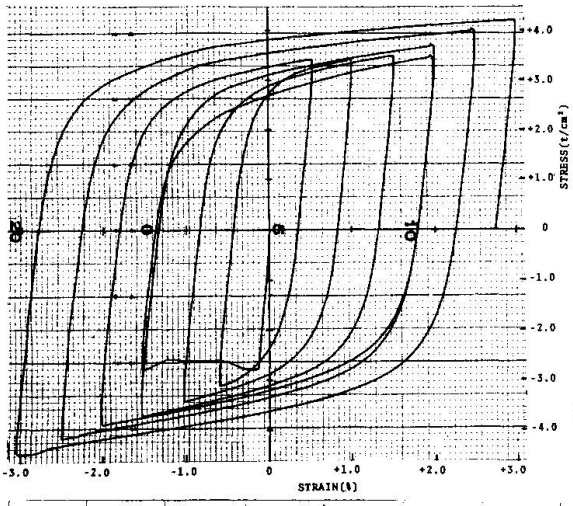

Fig. 3.

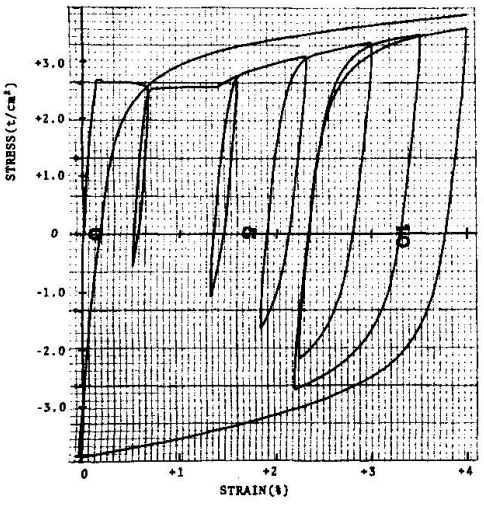

Fig. 4

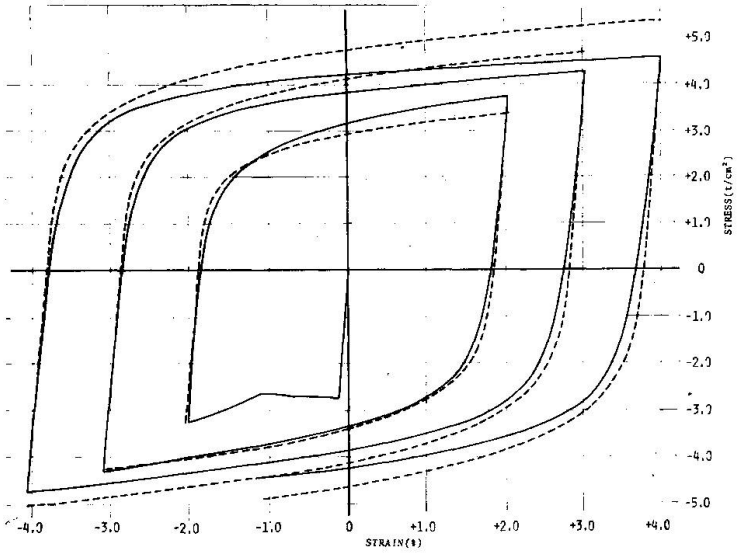

Fig. 5. COMPARISON OF EXPERIMENTAL AND APPROXIMATE STRESS-STRAIN CURVES

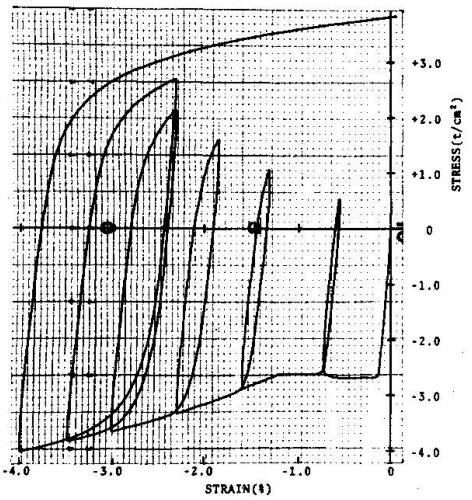

Fig. 6

where $\varepsilon^{(i)}$ and $\sigma^{(i)}$ denote the i-th reversal point strain and stress, respectively and where a and r are the parameters which may depend upon various factors discussed below. Based upon the test results on the smaller plate specimens, the authors have presented a preliminary investigation [4] concerning the dependence of a and r not only upon $\varepsilon^{(i)}$ and $\sigma^{(i)}$ but also upon other factors related to previous strain histories.

3.1 RETURN BEHAVIOR It should first be noticed that the steel has exhibited a return behavior on such a stress-strain curve as illustrated by Fig.4 or 6. It is apparently necessary to propose separate approximating equations for the virgin curve and for such loops as $\widehat{R_1R_2}$ and $\widehat{R_2R_3}$ indicated in Fig.7.

3.2 FACTORS AFFECTING r The usual log-log plot of the plastic strain component $\varepsilon-\varepsilon^{(i)}$ and stress $\sigma-\sigma^{(i)}$ for a smooth piece of a hysteresis loop would exhibit more deviation from a straight line (determined by the least square method) as the plot include those points within the range $|\varepsilon-\varepsilon^{(i)}| \lesssim 2\varepsilon_y$. While it may be necessary to determine r for several different current strain ranges piecewisely if a higher accuracy of fitting is desirable, the averages for $|\varepsilon^{tip}-\varepsilon^{(i)}| \geq 2\varepsilon_y$ without regard to the current strain ranges have been determined for the six different groups of curves mentioned in 3.3 for the convenience of their applications.

3.3 FACTORS AFFECTING a Among various factors affecting a, it has been found in [4] and in this series that the most significant factor is apparently $\sigma^{(i)}/\sigma_y$. Fig.8 shows the plot of a with respect to $\sigma^{(i)}/\sigma_y$. Fig.9 shows the same plot for the previous smaller plate specimens.

3.4 NONSTATIONARY HYSTERETIC STRESS-STRAIN RELATIONS The following six sets of a and r have been derived from the test result.

(A1) Compressive path: $\dot{\varepsilon}<0$ and $1.1<\sigma^{(i)}/\sigma_y<1.7$,
$a=1.421(\sigma^{(i)}/\sigma_y)+0.026, \quad r=8.89.$ (2.1)

(A2) Compressive path returning to the virgin curve:
$a=0.609(\sigma^{(i)}/\sigma_y)+1.358$, $r=7.80$(2.2) for $\varepsilon^{(i)}<0$, $0.6<\sigma^{(i)}/\sigma_y<1.1$.

(A3) Virgin compression path:
$a=0.483, \quad r=2.97.$ (2.3)

(B1) Tensile path: $\dot{\varepsilon}>0$ and $-1.9<\sigma^{(i)}/\sigma_y<-1.0$,
$a=-1.350(\sigma^{(i)}/\sigma_y)+0.222, \quad r=10.95.$ (2.4)

(B2) Tensile path returning to the virgin curve:
$a=-0.505(\sigma^{(i)}/\sigma_y)+1.325$, $r=7.96$(2.5) for $\varepsilon^{(i)}>0$, $-1.1<\sigma^{(i)}/\sigma_y<-0.6$.

(B3) Virgin tensile path:
$a=0.506, \quad r=3.40.$ (2.6)

In drawing an approximating curve in accordance with one of the above formulae, it has been found that the curve is very sensitive to the value of a. While the above six sets of a and r are considered to be the minimum number of formulae, a slight improvement in $a[\sigma^{(i)}/\sigma_y]$ can be attained by classifying the paths of (A1) and (B1) in accordance with Table 1 as follows:

For incompletely reversed strain cycling path;

(A11) $a=1.212(\sigma^{(i)}/\sigma_y)+0.328, \quad r=9.09$ $(\dot{\varepsilon}<0)$ (2.7)

(B11) $a=-1.464(\sigma^{(i)}/\sigma_y)+0.039, \quad r=11.04$ $(\dot{\varepsilon}>0)$ (2.8)

For one-way strain cycling path;

(A12) $a=1.894(\sigma^{(i)}/\sigma_y)-0.579, \quad r=8.52$ $(\dot{\varepsilon}<0)$ (2.9)

(B12) $a=-1.083(\sigma^{(i)}/\sigma_y)+0.618, \quad r=10.55$ $(\dot{\varepsilon}>0)$. (2.10)

Fig. 5 shows the approximating curve based upon (2.7) and (2.8). Fig.10 shows the curve drawn with (2.2), (2.3) and (2.10).

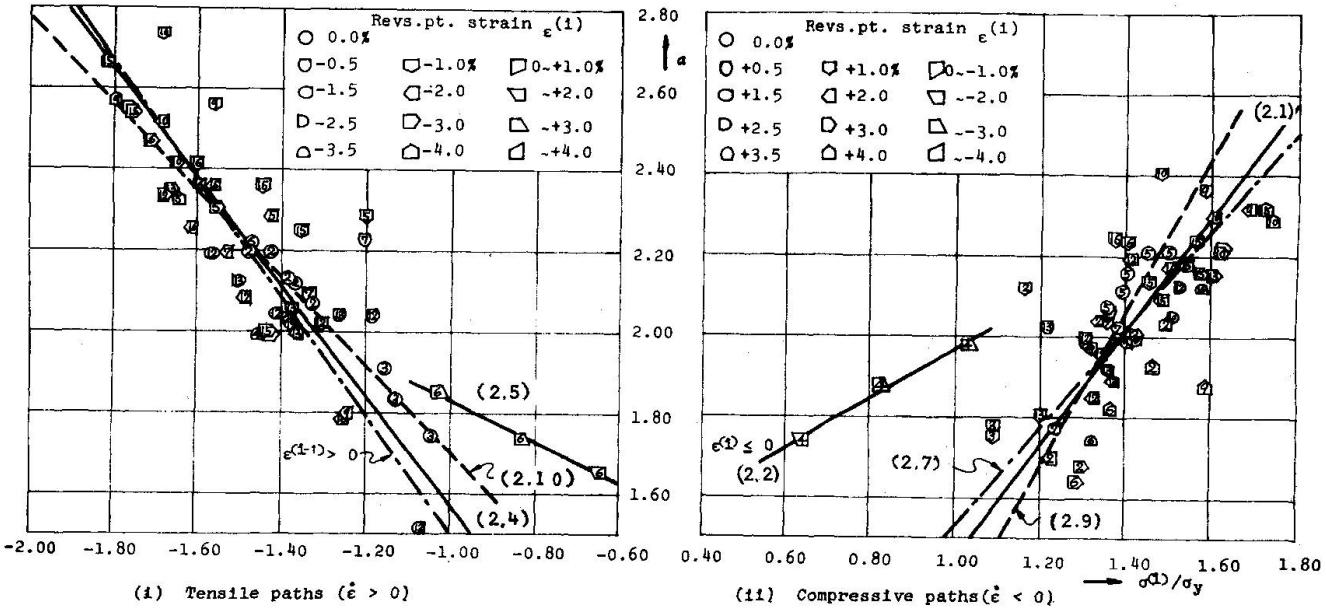

Fig. 8

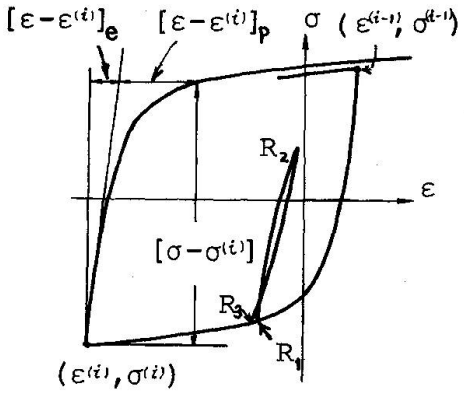

Fig. 7

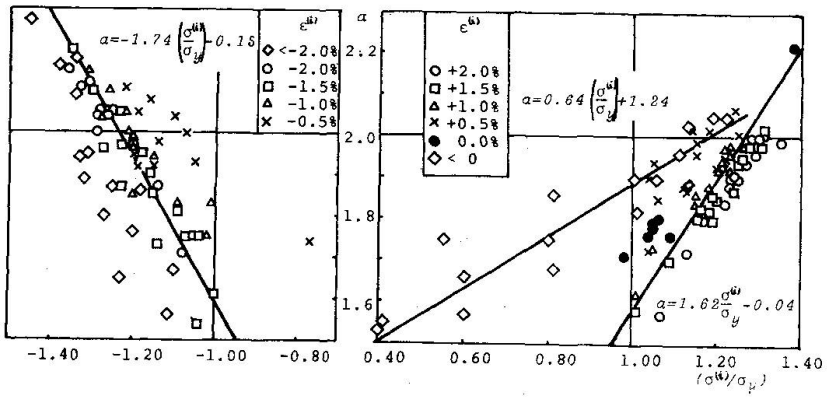

FIG. 9

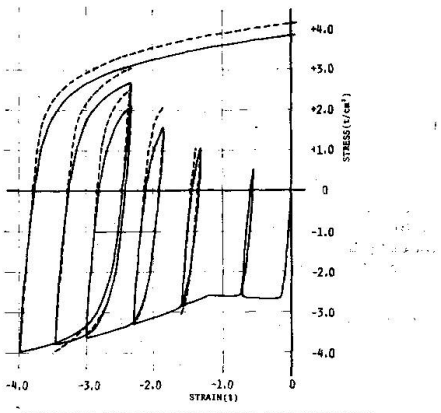

Fig. 10. COMPARISON OF EXPERIMENTAL AND APPROXIMATE STRESS-STRAIN CURVES

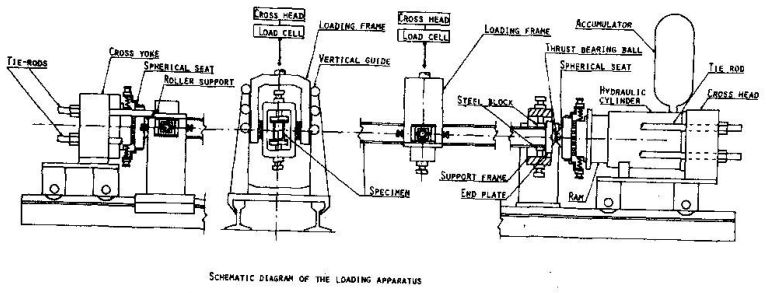

SCHEMATIC DIAGRAM OF THE LOADING APPARATUS

Fig. 13.

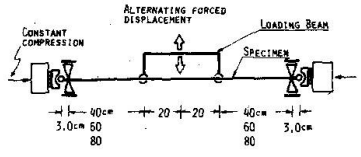

Fig. 11 SCHEMATIC DIAGRAM OF TEST CONDITIONS

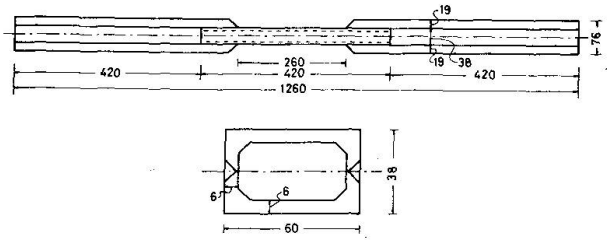

Fig. 12. TEST SPECIMEN FOR M(N)-κ RELATIONS

4. ALTERNATING PLASTIC BENDING TEST UNDER AXIAL FORCE

Fig.11 shows the schematic diagram of the test and Fig.12 the test specimen. Fig.13 shows the schematic diagram of the loading apparatus. An example of the nondimensionalized experimental moment-curvature curve under a constant axial force ratio of -0.505 is shown in Fig.14.

5. SANDWICH THEORY

The cross-sectional properties of an actual wide-flange section can be approximated by the idealized sandwich section whose two thin flanges have the half area, respectively and are located at the radius of gyration [6.7]. The nondimensionalized moment-curvature relation for the idealized sandwich section may directly be derived from Eq.(1) as follows.

$$\kappa-\kappa^{(i)} = (m-m^{(i)})\left\{1+\frac{1}{2}\left(\frac{1}{a_c}\right)^{r_c}|m-m^{(i)}|^{r_c-1}+\frac{1}{2}\left(\frac{1}{a_T}\right)^{r_T}|m-m^{(i)}|^{r_T-1}\right\} \qquad (3)$$

where (a_c, r_c) and (a_T, r_T) denote (a, r) for $\dot{\varepsilon}<0$ and $\dot{\varepsilon}>0$, respectively. A slight modification must be made for those portions after the returning points mentioned above and for initial portions corresponding to the plastic flow plateaus. The moment-curvature curve predicted by the theory is shown in Fig.14 by a dashed line and may be seen to fit the experimental curve fairly well at least during the first two cycles.

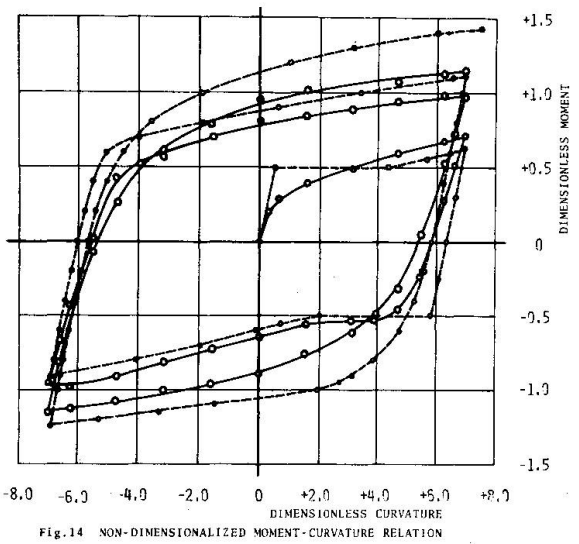

Fig.14 NON-DIMENSIONALIZED MOMENT-CURVATURE RELATION

References

[1] Ryo Tanabashi, Yoshitsura Yokoo, Minoru Wakabayashi, Tsuneyoshi Nakamura, Haruo Kunieda, Hiroyuki Matsunaga and Toshihiko Kubota, "Load-deflection Behaviors and Plastic Fatigue of Wide-flange Beams Subjected to Alternative Plastic Bending, I Experimental Investigation", Trans. A.I.J. No. 175 (Sept. 1970) pp. 17-29.

[2] Ryo Tanabashi, Yoshitsura Yokoo, Tsuneyoshi Nakamura, Toshihiko Kubota and Asao Yamamoto, "Load-deflection Behaviors and Plastic Fatigue of Wide-flange Beams Subjected to Alternating Plastic Bending, II Hysteretic and Skeleton Stress-strain Relations and Plastic Fatigues", Trans. A.I.J. No. 176 (Oct. 1970), pp. 25-36.

[3] Ryo Tanabashi, Yoshitsura Yokoo and Tsuneyoshi Nakamura, "Load-deflection Behaviors and Plastic Fatigue of Wide-flange Beams Subjected to Alternating Plastic Bending, III Steady-state Theory", Trans. A.I.J. No. 177 (Nov. 1970), pp. 35-46.

[4] Yoshitsura Yokoo, Tsuneyoshi Nakamura, Keishi Isoda and Toshiro Komiyama, "Nonstationary Hysteretic Stress-strain Relations of Wide-flange Steel," Summaries of Technical Papers presented at Annual Meeting (Kyushu) of Architectural Institute of Japan 1972, pp1299-1300.

[5] Ryo Tanabashi, Yoshitsura Yokoo, Minoru Wakabayashi, Tsuneyoshi Nakamura and Haruo Kunieda, "Deformation History Dependent Inelastic Stability of Columns Subjected to Combined Alternating Loading", Proc. 1971 RILEM International Symposium on Experimental Analysis of Instability Problems on Reduced and Full-scale Models, Buenos Aires, Sept. 1971, Vol. III, pp. 275-295.

[6] Tsuneyoshi Nakamura, "Elastic-plastic Behavior of a Linear Strain-hardening Sandwich Column Subjected to Alternating Lateral Force," Summaries of Tech. Papers presented at Annual Meeting of Archit. Inst. Japan, p285.

[7] Tsuneyoshi Nakamura, "Methods of Elastic-plastic Analysis of Structures," (Dissertation for Dr.Eng., Kyoto University), Chap.6, Dec. 1970.

SUMMARY

Nonstationary hysteretic stress-strain curves have been presented from our recent systematic experimental investigation. A set of constitutive equations have been derived from the result. An experimental moment-curvature curve under a constant axial force has been presented and shown to be predicted by a sandwich theory based upon the constitutive equations with a considerably good accuracy.

RESUME

Nous avons présenté une courbe hystérétique non-stationnaire tension-déformation qui a été dérivée de nos récentes recherches expérimentales systématiques. Une série d'équations constitutives a été dérivée du résultat. Nous avons présenté un diagramme moment-courbure sous une force axiale constante, et démontré qu'une théorie "sandwich" basée sur les équations constitutives conduisait au même résultat avec une précision considérable.

ZUSAMMENFASSUNG

Die Arbeit zeigt nicht-stationäre hysteretische Spannungs-Dehnungs-Kurven unserer kürzlichen systematischen Untersuchungen. Eine Gruppe von Grundgleichungen wurde aus dem Resultat abgeleitet. Es wird eine experimentelle Momenten-Krümmungs-Kurve unter einer konstanten Axialkraft gezeigt und ihre gute Uebereinstimmung mit den nach der Sandwich-Theorie (basiert auf den Grundgleichungen) vorausgesagten Werten dargelegt.

Leere Seite
Blank page
Page vide

Elasto-Plastic Cyclic Horizontal Sway Behaviour of Wide Flange Unit Rigid Frames Subjected to Constant Vertical Loads

Comportement élasto-plastique de cadres rigides formés de profils à ailes larges soumis à des charges verticales constantes

Elasto-plastisches zyklisch horizontales Schwingungsverhalten von Rahmen aus Breitflanschprofilen unter konstanter vertikaler Last

Minoru YAMADA Professor Dr.-Ing.
Bunzo TSUJI Ass. Prof. Dipl.-Ing.
Yasuyuki MURAZUMI Dipl.-Ing.
Department of Architecture, Faculty of Engineering
Kobe University
Kobe, Japan

1. INTRODUCTION

In order to make clear the elasto-plastic cyclic deformation behavior of steel structures, various constant deflection amplitude tests are carried out on the unit rectangular steel rigid frames as a basic element of the steel structures. Analysis are developed with the special consideration on the Bauschinger effect and compared with test results.

2. ANALYSIS

2.1. The Bauschinger Model

The Bauschinger effect plays an important role on the deformation characteristics of the steel structures under the cyclic loads. Its effect is considered here using the Bauschinger model such as shown in Fig.2. The material (steel) is assumed to be composed of three different mechanical properties such as shown in Fig.2. With this model, the cyclic stress-strain relationship obtained is tri-linear type such as shown in Fig.3. The Bauschinger effect appears when the plastic deformation occurs at the opposite direction as the original one. Therefore the bi-linear type of the stress-strain relationship as shown in Fig.1 is applied initially.

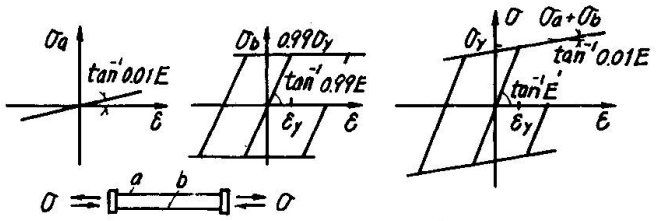

Fig.1 Bi-linear model [1)]

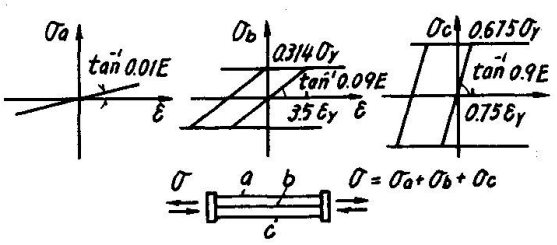

Fig.2 Bauschinger model

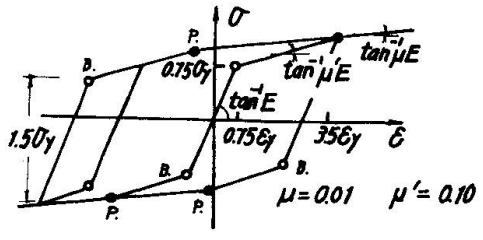

Fig.3 σ-ε relation

2.2. Deformation Analysis

The following assumptions are applied for the analysis:

(1) Wide flange section is simplified into the equivalent three points model[1] with the same cross sectional area, moment of inertia and fully plastic moment as the original one such as shown in Fig.4,

(2) Cyclic stress-strain relationships are defined intially by the bi-linear[1] model and subsequently by the Bauschinger model*,

(3) Plane section remains plane during deformation,

(4) The effect of shearing stress is not considered.

The non-dimensional stress-strain relations of each point are shown in the following equations according to the states of stress,

$q_i = e_i - e_{pi}$; elastic (1a),

$q_i = 1 + \mu(e_i - 1)$; tens. plastic (1b),

$q_i = -1 + \mu(e_i - 1)$; comp. plastic (1c),

$q_i = 1 - 0\mu(e_i - e_{pi}) + \alpha_i(1 - 10\mu)$; tens. Bauschinger (1d),

$q_i = 10\mu(e_i - e_{pi}) - (1.5 - \alpha_i)(1 - 10\mu)$; comp. Bauschinger (1e),

where $q_i = \sigma_i/\sigma_y$ and $e_i = \varepsilon_i/\varepsilon_y$, (i=1,2,3).

The equations of the equilibrium for the axial force N=nNy and the bending moment M=mMy are as follows,

$n = (q_1 + kq_2 + q_3)/(2+k)$ (2a),

$m = (q_1 - q_3)/2$ (2b).

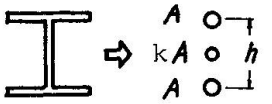

Fig.4 Three points model[1]

The stresses are composed of the elastic stress q_{ie}, that is proportional to the generalized stresses, m and n, and the residual stress q_{ir} as shown in Fig.5.

$q_{1e} = n + m$ (3a),

$q_{2e} = n$ (3b),

$q_{3e} = n - m$ (3c),

$q_{1r} = q_{3r} = \xi$ (4a),

$q_{2r} = -2\xi/k$ (4b).

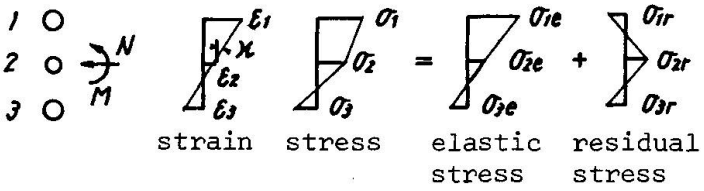

Fig.5 Strain and stress distributions

Indicating the subsequent yield stress $\bar{\sigma}_y = \alpha\,\sigma_y$ after the plastic deformation occured, the yield conditions of each point are for the bi-linear model

$\alpha_i - 2 \le q_i \le \alpha_i$ (i=1,2,3) (5),

and for the Bauschinger model

$\alpha_i - 1.5 \le q_i \le \alpha_i$ (i=1,2,3) (6).

Fig.6 shows the convex yield polygons composed of the three pairs of the parallel lines, where ξ is the parameter indicating the magnitude of the residual stress. The strain distribution of the cross section is determined by the strain of the centroidal axis $\varepsilon_2 = e_2\,\varepsilon_y$ and the curvature $\varkappa = e_\varkappa 2\,\varepsilon_y/h$ as follows:

(7a),

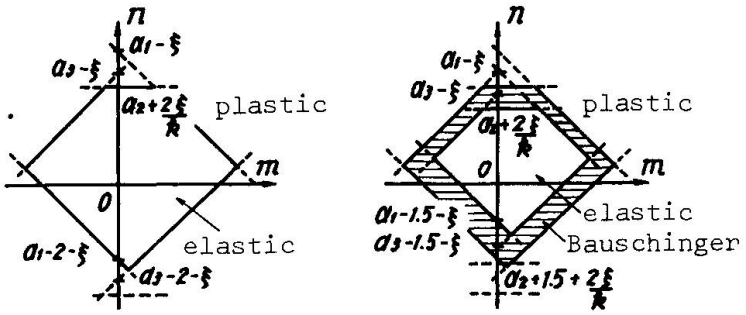

Fig.6 Yield conditions

* Recently after the completion of this analysis, a similar model was presented.[2]

$e_\gamma = e_\varepsilon - e_\kappa$ (7c).

The stress-strain relationships of each point are obtained from the yield conditions which are determined considering the strain history of the cross section. With these relations and eq.(7), the strain distribution e_ε and e_κ of the cross section corresponding to the generalized stress m and n, are able to be obtained. Deformation analysis is carried out by the numerical integration procedures, dividing the columns and beams of the model frame, as shown in Fig.7, into thirty line elements which deform parabolically and satisfying the equilibrium conditions at each nodal point. The computed load deflection relations are shown in Fig.10 by broken lines. The black and white circles, • and ○, indicate the intiation of yielding and Bauschinger effect at the column end respectively. The dotted lines show the bi-linear model analysis [1] for comparison.

3. TESTS

3.1. Test Specimens and Test Series

Test specimens are made of rolled wide flange profils with welded joints and with stiffeners in each joint (see Fig.7). Tests are carried out on the various constant relative story displacement amplitudes of ±1.0cm, ±2.0cm and ±4.0cm under the action of the various constant vertical loads of the column of 0Ny, 1/3Ny and 1/2Ny, where Ny is the yield axial load of the column.

3.2. Loading and Measuring System

The specimen is set in the loading frame through pin roller supports, consisting of the needle roller bearings in each corner such as shown in Fig.8. In order to avoid lateral buckling, the beams are supported by the roller bearings. The vertical load is applied by the testing machine through the flat cage needle roller bearings, with a friction coefficient of 1/1000, inserted between the cross head and the loading frame. The lateral force is applied diagonally by the oil jack with load cell through the steel rods. The deflections are measured by dial gages and the strain distributions by wire strain gages.

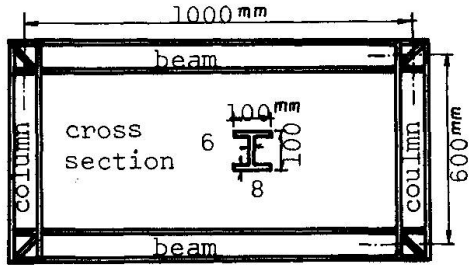

Fig.7 Specimen

Table 1 Test series

N/Ny	Displacement amplitude (cm)	Number of cycles
0	±2.0	4
1/3	±1.0	51
	±2.0	4
	±4.0	1
1/2	±1.0	10
	±2.0	4
	±4.0	1

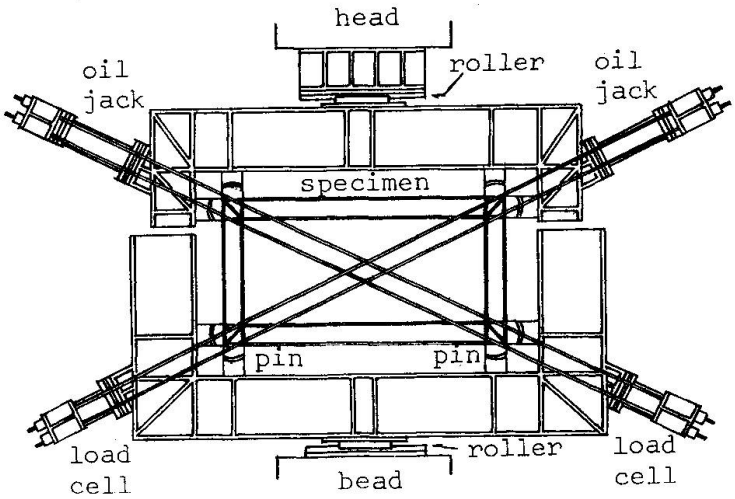

Fig.8 Loading system

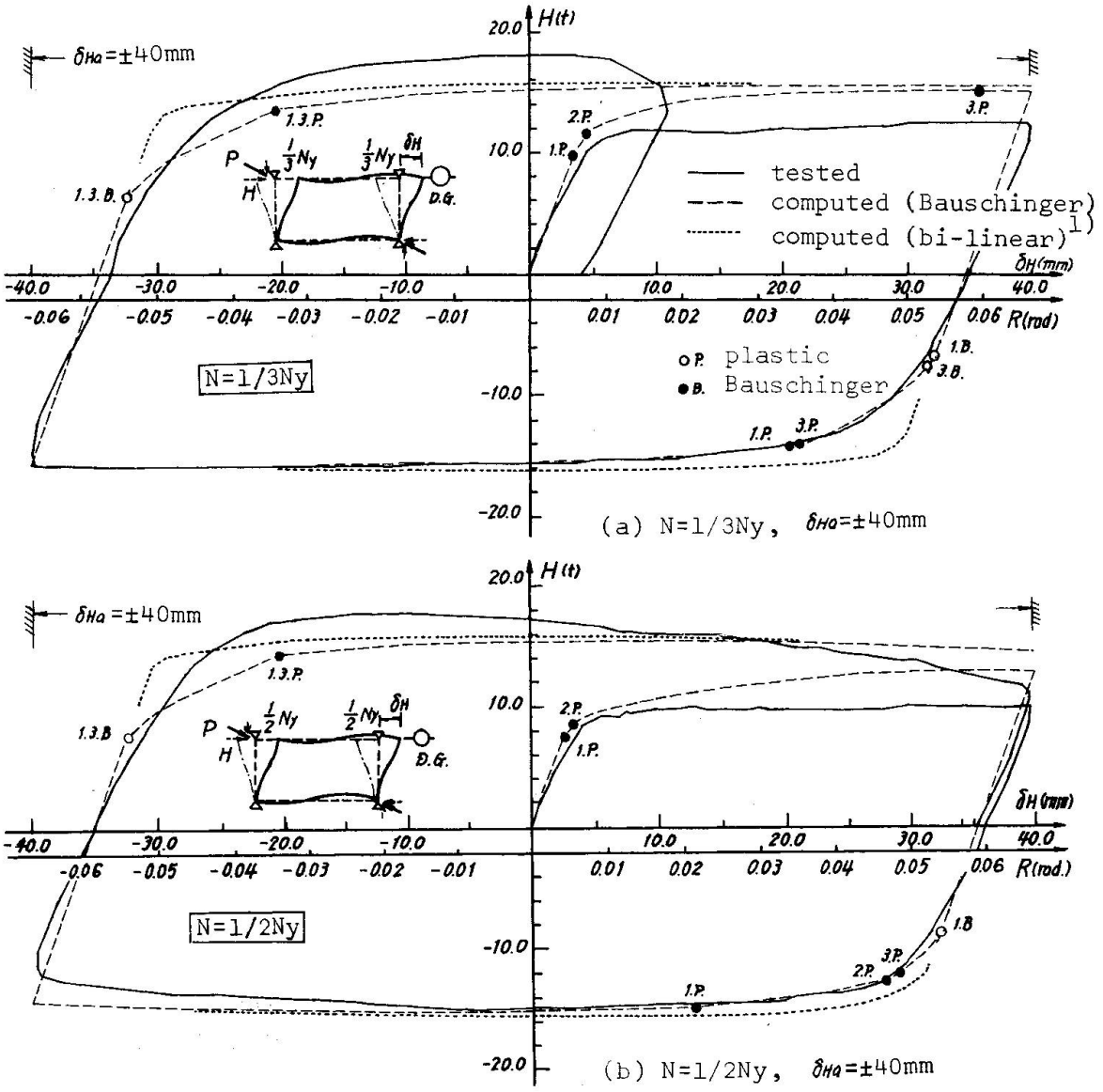

Fig.9 Load-Deflection Relationships

3.3. Test Results

The load deflection curves are shown in Fig.9 with solid lines. The relations between the sway amplitudes and the number of cycles until fracture is shown in Fig.10. The increases of the resistance with the increase of the number of cycles are shown in Fig.11.

4. DISCUSSIONS AND CONCLUDING REMARKS

4.1. Load Deflection Relationships

Fig.9 shows the load deflection relations. The maximum resictances increase at the first few cycles through the strain hardening effect. The convergence to the steady loop is rapider, the smaller the axial load or the larger the deflection amplitudes. One of the most remarkable behavior under the cyclic loading is the Bauschinger effect and it is shown clearly by these tests too. The computed results by the Bauschinger model employed here coincide very well with the tested results. At the steady state loop, the Bauschinger or the plastic stresses are reached simultaneously in both tensile and compressive flange.

4.2. Fracture Modes

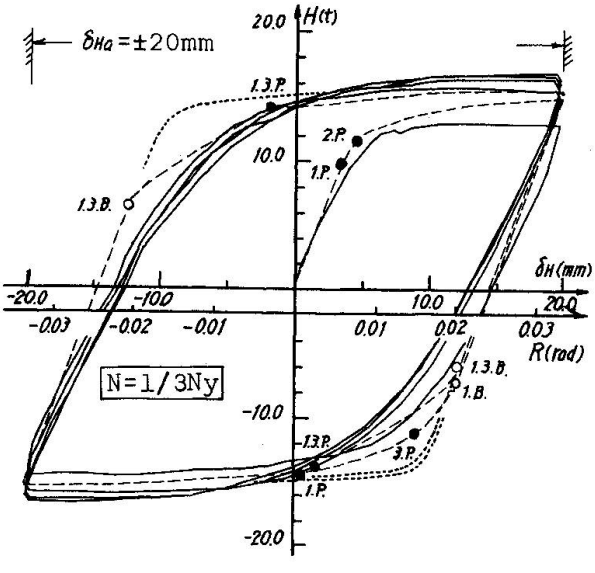

(c) N=1/3Ny, δ_{Ha}=±20mm

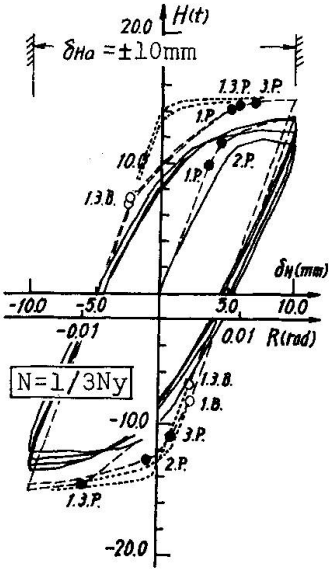

(e) N=1/3Ny, δ_{Ha}=±10mm

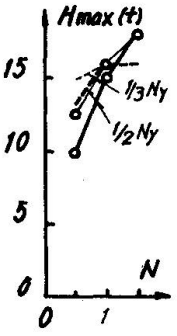

(a) δ_{Ha}=±40mm

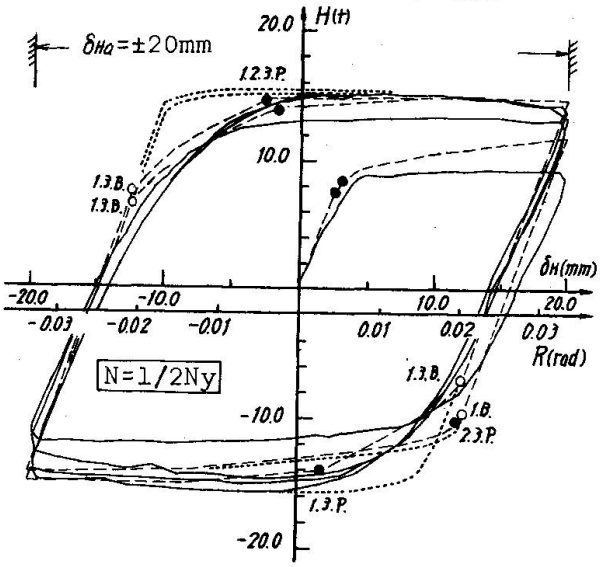

(d) N=1/2Ny, δ_{Ha}=±20mm

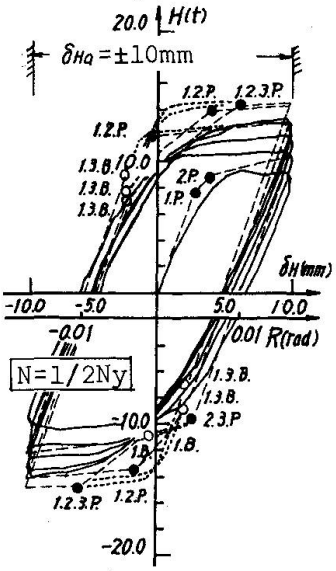

(f) N=1/2Ny, δ_{Ha}=±10mm

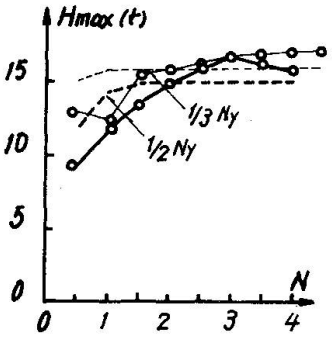

(b) δ_{Ha}=±20mm

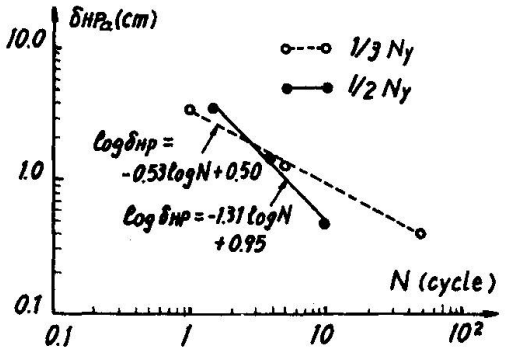

Fig.10

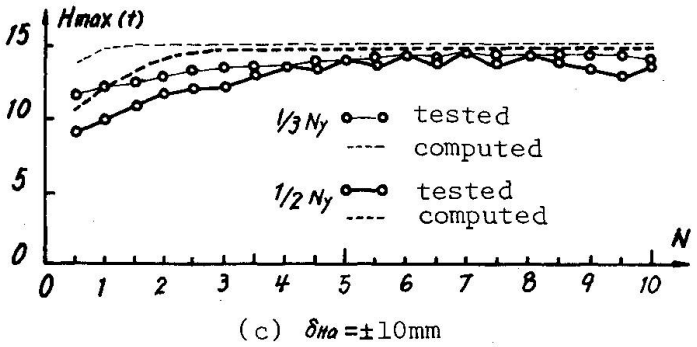

(c) δ_{Ha}=±10mm

Fig.11 Variation of Maximum Resistances

The cyclic loadings are continued until the deterioration of the lateral forces are observed. The local buckling occurs at the column flange in the case of the axial load level of 0Ny or 1/3Ny, whereas it occurs not only at the column flange but also at the column web in the case of 1/2Ny. Two

fracture modes are observed. Under the axial load level of 0Ny or 1/3Ny, the fracture occurred by the tear off of the welded joint, whereas under the axial load level of 1/2Ny, it occurred by the progress of the local buckling. The relationships between the constant plastic deformation amplitudes and the number of cycles until fracture are shown in Fig.10. They lie on the two straight lines in log-log scale corresponding to each fracture mode.

5. BIBLIOGRAPHY

(1) Yamada,M., Shirakawa,K. : Elasto-plastische Biegeformänderungen von Stahlstützen mit I-Querschnitt, Teil II : Wechselseitig wiederholte Biegung unter konstanter Normalkrafteinwirkung, Der Stahlbau, 40. Jahrg., H.3, 1971 S.65-74 u. H.5, 1971 S.143-151.

(2) Zienkiewicz,O.C., Nayak,G.C., Owen,D.R.J. : Composite and overlay models in numerical analysis of elasto-plastic continua, Internl. Symposium Preprint on Foundations of Plasticity, Edited by Sawczuck, Warsaw, 1972, Noordhoff Internl. Publ., Groningen, pp.107-123.

SUMMARY

Constant deflection amplitude tests are carried out on the unit rectangular rigid frames. The remarkable behaviors are the increase of resistances and the Bauschinger effect (Fig. 9). For analysis, the three points model for the cross section (Fig. 4) and the Bauschinger model for the material (Fig. 2) are applied here. The coincidence between tested and computed results are very well. And the both processes are clarified. The relationship between the relative story displacement amplitudes and the number of cycles until fracture are indicated (Fig. 10).

RESUME

Des essais où la grandeur de la déformation est constante sont effectués sur des cadres rectangulaires rigides. Le comportement se caractérise par l'augmentation des résistances et l'effet Bauschinger (Fig. 9). Pour l'analyse, on emploie le modèle à trois points (Fig. 4) pour la section et le modèle Bauschinger (Fig. 2) pour le matériau. Les résultats des essais coïncident très bien avec ceux du calcul. De plus, les deux processus sont expliqués. On indique aussi (Fig. 10) la relation entre la grandeur du déplacement relatif et le nombre de cycles de charge jusqu'à la rupture.

ZUSAMMENFASSUNG

Es werden Versuche mit konstant gehaltener Auslenkung an rechteckigen, steifen Einheitsrahmen gemacht. Bemerkenswert sind die Zunahme des Widerstandes und der Bauschinger-Effekt (Fig. 9). Für die Berechnung werden das Drei-Punkte-Modell für den Querschnitt (Fig. 4) und das Bauschinger-Modell für das Material (Fig. 2) angewendet. Die Uebereinstimmung zwischen den Versuchs- und Rechenresultaten ist sehr gut. Beide Verfahren werden erklärt und die Beziehung zwischen den gegenseitigen Stockwerksverschiebungen und der Anzahl Zyklen bis zum Bruch angegeben (Fig. 10).

III

Repeated Loading Tests on Continuous Beams subjected to Both Axial and Vertical Loading

Essais de chargement répété sur poutres continues soumises simultanément à des charges axiales et verticales

Wiederholte Belastungsversuche an Durchlaufträgern mit gleichzeitig wirkender axialer und vertikaler Last

J. M. DAVIES
Reader in Civil Engineering
University of Salford
England

1. Introduction

The phenomenon of incremental collapse in ductile structures subject to repeated loading has been understood for many years[1]. Incremental collapse occurs when cyclic application of alternative load combinations results in a progressive build up of deflections as restricted plastic flow takes place on each application of load. The threshold load level, above which incremental collapse can occur, is termed the shakedown load.

When designing structures using plastic theory, this effect is not usually considered. It is argued that a given structure is more likely to be rendered useless by a single overload sufficient to cause plastic collapse than by the build up of deflections as a series of somewhat smaller overloads cause incremental collapse. It is also noted that this build up of deflections is very much restricted by strain hardening.

It is necessary to reconsider this conclusion when a framed structure which exhibits frame instability is subject to loads likely to cause incremental collapse[2]. A single overload that is insufficient to cause failure can significantly weaken the resistance of a structure to subsequent cycles of repeated loading. Furthermore, at load levels above the shakedown load, successive cycles of load at a given level are accompanied by progressively increasing increments of deflection until unstable collapse takes place, often after a few cycles of load. It is clear that the probability argument used to avoid the necessity of considering variable repeated loading in plastic design breaks down in the presence of this "acceleration to collapse".

The phenomenon is convincingly demonstrated by the results of the tests described in this paper and is shown to be amenable to analysis but only when strain hardening is included.

2. Experimental Investigation

Tests were carried out using two and three-span continuous beams of 12.7mm

($^1/_2$in) square cross section. The general arrangement for these tests is shown in Figs 1 and 2. Repeated application of these loading patterns leads to the incremental collapse mechanisms indicated by plastic hinge positions in the figures.

As well as cyclic loading tests carried out using a frequency of 20 minutes per complete cycle, static loading tests were also carried out using the most severe of the two load cases which is shown in each case as that for the first half cycle.

Similar apparatus was used for both series of tests and is shown in Figs 3 and 4. It was mounted on a large lathe bed and loading was applied through chain and lever system. Vertical load was applied to the test beams through knife edges at the level of the centre line of the beams so that no secondary moments could be induced as the beams deflected.

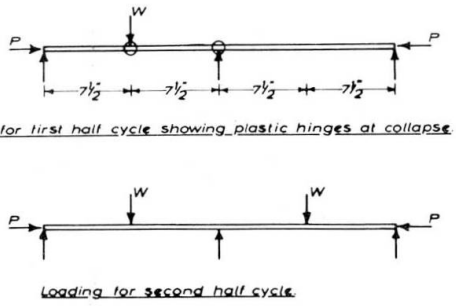

Fig 1. Loading cycle for two-span beams

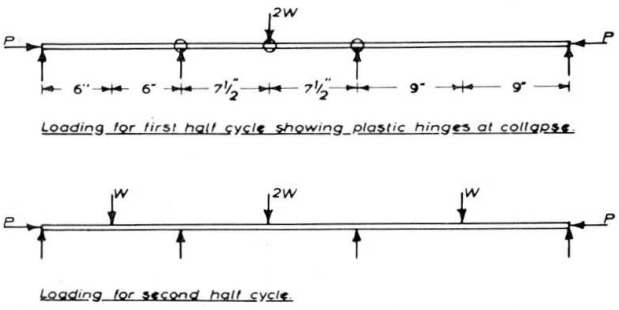

Fig 2. Loading cycle for three-span beams

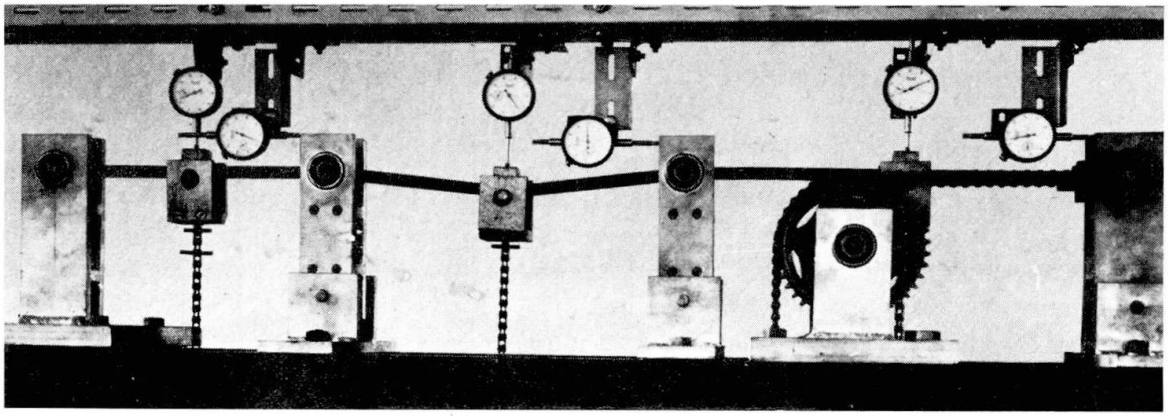

Fig 3. Apparatus for three-span tests

One of the end supports was firmly bolted to the rigid base and was capable of supplying both horizontal and vertical reactions to the beams. This support had a pair of 12mm diameter ball journals at the level of the centre line of the beams. The remaining supports allowed horizontal movement at beam level, having soft metal bushes for an axle at the lower end and ball journals at the level of the test beams. At the internal supports, the beams were lightly clamped between half-round pieces of steel in a specially designed clamp with stub axles which fitted into the journals on the supports. This arrangement provided a simple support capable of resisting vertical movement up and down without interference to the axial loads in the beams.

Steel blocks were welded to the ends of the test beams and accurately drilled to accommodate spindles which provided the end supports. One end of each beam was thus provided with a pinned connection to the rigid support, the other end with a pinned connection to a support free to move in the axial direction. It was through the spindle providing this latter connection that the axial thrust was applied.

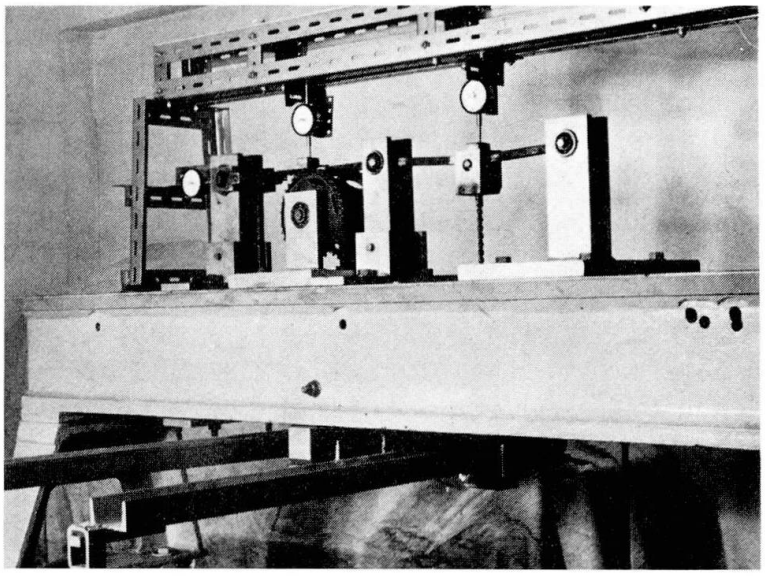

Fig 4. Apparatus for two-span tests

The ends of this 25mm dia spindle were shaped to form knife edges on the centre line of the spindle. Axial load was applied through two chains, linked to these knife edges, and passing over large chain wheels before being connected to the loading lever.

For the two-span tests, cyclic loading was achieved automatically by means of a hydraulically operated jack acting under one of the loading levers. This jack, which is not shown in Fig 4, was driven by a pulsator unit the frequency being controlled by a clock and the range by two micro-switches. When the jack was extended, the loading lever was disconnected from the structure which was therefore subjected to the single load from the second lever. When the jack returned to its lower position, the load was automatically replaced and both spans were loaded.

For the tests on three-span beams, the pulsator operated two jacks in parallel which simultaneously removed and replaced the loads on the outer spans of the beams.

3. Control Tests

The material properties of the steel were determined by means of tests on simply supported beams of 300mm span subjected to a central point load. These tests were carried well into the strain hardening range so that the flexural rigidity, full plastic moment and coefficient of strain hardening[3] were obtained for five specimens cut from each 3m length of material.

4. Experimental Results - Two-Span Beams

Both static loading and repeated loading tests were carried out by first applying an axial load, which was thereafter maintained at a constant level, and then applying increasing vertical load until collapse occurred or the deflections became excessive. Four levels of axial load were considered, namely zero, 0.974kN (219lb), 1.962kN (441lb) and 2.976kN (661lb).

For the static collapse tests, each load level was maintained until the creep rate had fallen to an acceptably low value. Failure was defined in the case of unstable behaviour as the load actually causing failure and in the case of stable behaviour as the load at which the last plastic hinge formed obtained from the load-deflection curve.

For the repeated loading tests, it was desired to investigate both the value of the shakedown load and the response to cycles of load above the shakedown load. For each test, the structure was subject to several cycles of load at a given level as the load on one span was taken on and off at regular intervals. If the deflection stabilisied, the load level was increased and further cycles of load were applied, if not, cyclic loading was continued until unstable collapse took place.

A most critical factor in the response to cycles of load is the "stability balance" value of the axial load[3]. This is the axial load at which strain hardening exactly equalises the 'PΔ' effect and the curve of deflection versus cycles of load is theoretically linear. Here strain hardening and axial load effects were predicted to balance at an axial load of 1.000kN (225lb). Figs 5, 6 and 7 show both experimental (full lines) and theoretical (broken lines) loading curves for axial loads of zero, 0.974kN (219lb) and 1.962kN(441lb).

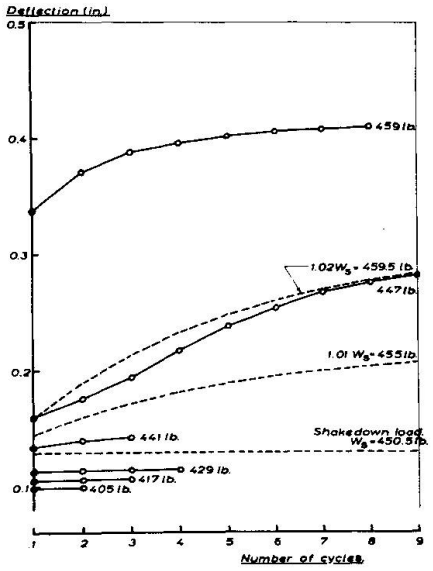

Fig 5. Two-Span Beam. Axial Load zero

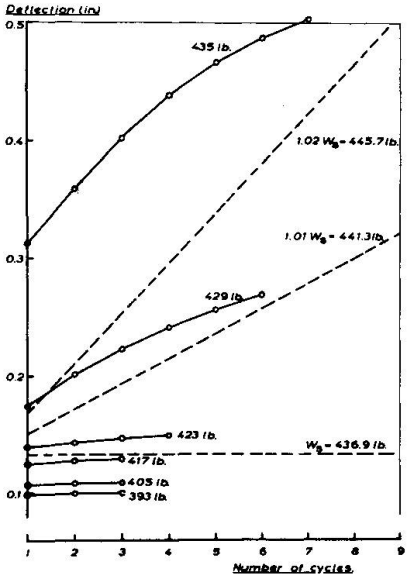

Fig 6. Two-Span Beam. Axial Load 219lb

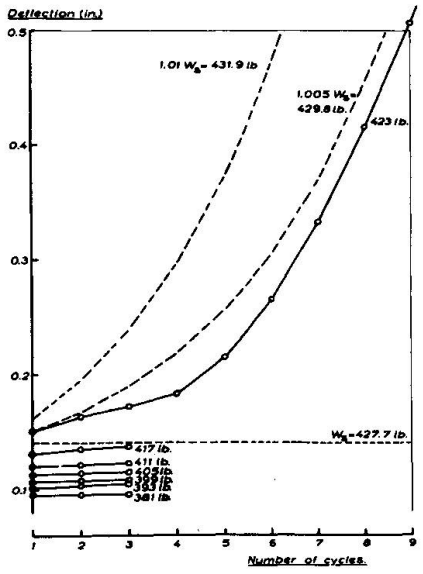

Fig 7. Two-Span Beam. Axial Load 441lb

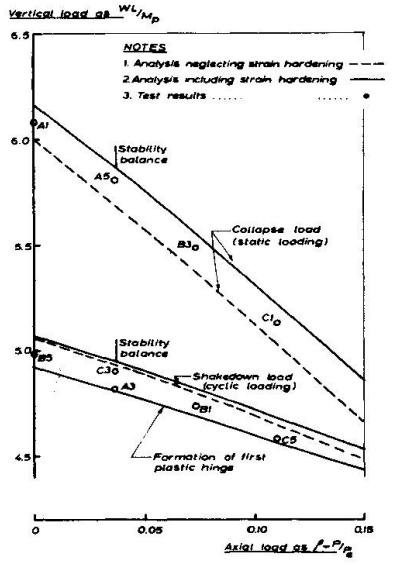

Fig 8. Two-Span Beams - Failure Loads

The derivation of the theoretical curves follows the method given previously [2]. The transition from stable to unstable behaviour is very clear and closely follows the theoretical predictions. At an axial load of 2.976kN (661lb) the acceleration to collapse was even more rapid than in the curves shown and failure took place on the 6th cycle of load which was precisely what was predicted for a load 1% in excess of the shakedown load.

The failure loads obtained are summarised in Fig 8 where they are plotted against the Euler ratio P/P_e. The slightly low values of the shakedown load are probably due to a certain amount of dynamic loading as the load was automatically taken on and off. This was, to a large extent, cured for the three-span tests.

5. Experimental Results - Three-Span Beams

The procedures and general pattern of results were similar to those for the two-span tests though, with three plastic hinges participating in the collapse mechanism, the influence of strain hardening was found to have increased. Figs 9 and 10 show representative curves of deflection versus number of cycles of load and Fig 11 summarises the experimental and theoretical failure loads.

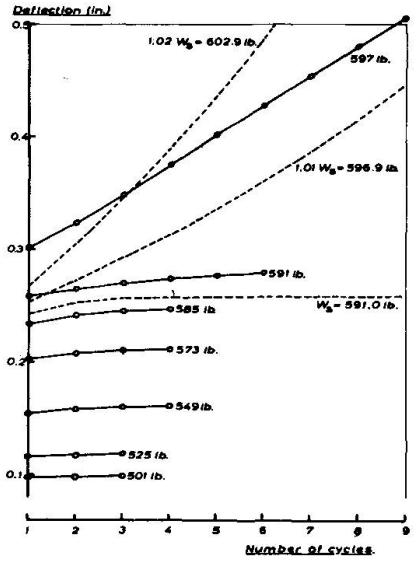

Fig 9. Three-Span Beam. Axial Load 441lb

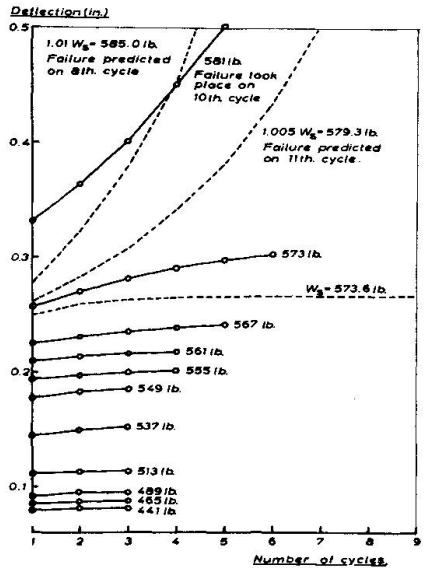

Fig 10. Three-Span Beam. Axial Load 669lb

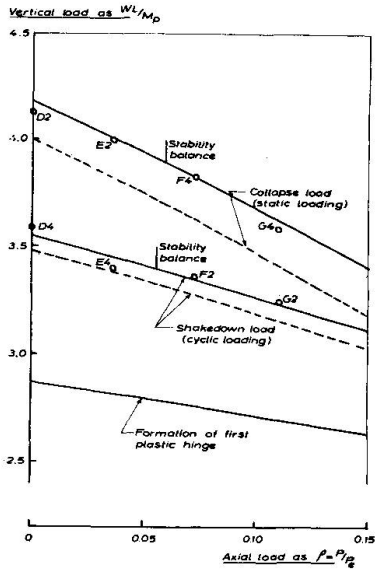

Fig 11. Three-Span Beams. Failure Loads

6. Conclusion

It has been demonstrated by tests on axially loaded continuous beams subjected to repeated cycles of vertical load that there is a transition from a stable to unstable pattern of deflection response at quite low values of axial load. A valid theoretical comparison is also demonstrated. A similar pattern of behaviour has been shown, by theoretical analysis only,[2] to exist in frames. It follows that incremental collapse is a much more serious problem in structures subject to frame instability and variable repeated loading effects cannot be readily dismissed by arguments based on probability.

7. Bibliography

1. B G Neal "The plastic methods of structural analysis. Chapman and Hall, London 1956.

2. J M Davies "Variable repeated loading and the plastic design of structures". Struct. Engr. Vol 48, May 1970.

3. J M Davies "Frame instability and strain hardening in plastic theory". Proc. A.S.C.E., J.Struct.Div. ST 3 June 1966.

SUMMARY

Tests are described in which axially loaded continuous beams were subjected to both static and cyclic loading. When the effect of the axial compressive load predominated over strain hardening, the static failure was unstable and repeated loading eventually led to "acceleration to collapse". At load levels above the shakedown load each cycle of load resulted in an increased increment of deflection until failure took place after a few cycles of load. A valid theoretically comparison is demonstrated.

RESUME

On décrit des essais au cours desquelles des poutres continues ont été soumises à des charges axiales statiques et dynamiques. Lorsque l'effet de la charge de compression axiale l'emportait sur celui de l'écrouissage, la rupture statique était instable, et une charge répétée précipitait éventuellement la rupture. A des niveaux de charges supérieurs à la charge ultime, chaque cycle de charge provoquait une augmentation toujours plus grande de la courbure, jusqu'à la rupture qui se produisait après quelques cycles de charges. On démontre une comparaison théorique valable.

ZUSAMMENFASSUNG

Es werden Versuche beschrieben, bei denen axial belastete Durchlaufträger statischer und zyklischer Belastung ausgesetzt sind. Wenn der Effekt des axialen Druckes die Verfestigung überwog, war das statische Versagen unstabil und die wiederholte Belastung führte schliesslich zum "beschleunigten" Kollaps. Bei Belastungsstufen über der "Shakedown"-Last resultierte aus jedem Lastzyklus eine Zunahme des Auslenkung, bis der Bruch nach einigen Zyklen eintrat. Ein brauchbarer theoretischer Vergleich wird angeführt.

III

Failure of Steel Beams due to Lateral Buckling under Repeated Loads

Rupture de poutres en acier due au renversement sous charges répétées

Versagen von Stahlbalken infolge horizontaler Beulung unter wiederholter Belastung

Koichi TAKANASHI Associate Professor
Kuniaki UDAGAWA Research Associate
Hisashi TANAKA Professor
Institute of Industrial Science, University of Tokyo, Japan

1. INTRODUCTION

As pointed out by the authors of the introductory report, very few researches on the lateral buckling problems of steel members under cyclically repeated loadings can be found in the literatures. This is a report of lateral buckling tests under cyclically repeated loadings which were conducted on the steel beams with H-shaped section. These tests showed the quite different behaviors of lateral buckling as compared with the behaviors for monotonic loading tests which have been carried out by many investigators for the establishment of " plastic design " of steel structures.

Many tall buildings are recently designed on the criterion that frame structures behave inelastically during severe earthquake. Hence, a nonlinear dynamic analysis is usually performed on the assumption that structural members are expected to show stable hysteresis loops in force-deformation relationships, but the failure due to buckling and deterioration of hysteresis curves are not taken into account. In inelastic or plastic range, steel structures often fail due to buckling because of the sudden reduction of rigidity and hence the studies on the lateral buckling of members under repeated loads must be required as well as other buckling problems.

To obtain the sufficient ductility of structures, the proportions of sections and spacings of lateral supports of members must be determined to possess much plastic deformation capacity. When a tall building, which has stronger and more rigid columns than beams, is subjected to severe earthquake, " plastic hinges " develope in the ends of beams and rotate repeatedly and reversedly. Popov and Pinkney have carried out the cyclic bending tests on the cantilever steel beams and concluded that the load-deflection hysteresis loops keep remarkably stable shapes and the onset of local flange buckling does not imply an immediate loss of load carrying capacity, when closedly braced compact members are used(1,2). The beams in the real structures, however, cannot be always braced closedly even though the attached slabs provide additional and uncertain restraints, so that this series of experiments is mainly intended to examine the shapes of load-deflection hysteresis loops and to obtain the critical end rotations of beams beyond which beams will fail due to lateral buckling.

2. SPECIMENS AND EXPERIMENTS

Test specimens were fabricated from rolled steel beams which have H-shaped sections with depth of 200 mm and width of 100 mm. The thicknesses of flange and web are 8 mm and 5.5 mm, respectively. The slenderness ratio with respect to weak axis, ℓ / r_y , for each specimen is shown in Table 1, where ℓ and r_y indicate unsupported length and radius of gyration with respect to weak axis, respectively. The unsupported lengths were determined so that the slenderness ratios vary from 50 to 80, because the specifications(3,4) recommend 65 as the critical slenderness ratio. The specimens of DG series and DGH series were made of JIS SS41 steel (σ_y =2.9t/cm^2) and JIS SM50 steel (σ_y =4.5t/cm^2), respectively. The average yield stresses, σ_y , were evaluated by tension coupon tests. The full-plastic moment, Mp, of each beam was calculated for these values.

The rig employed to subject the beam specimens for reversed loadings is illustrated in Fig. 1. Reversed loads were repeatedly applied by the hydraulic actuator at the center of the span, where a guide was provided to prevent lateral displacement and rotation with respect to beam axis. At the both supported ends only lateral displacement and rotation with respect to beam axis were also prevented. This loading arrangement was intented to simulate the beam behaviors of a structure under lateral loads. The motion of the top of actuator was controlled by the servo controller.

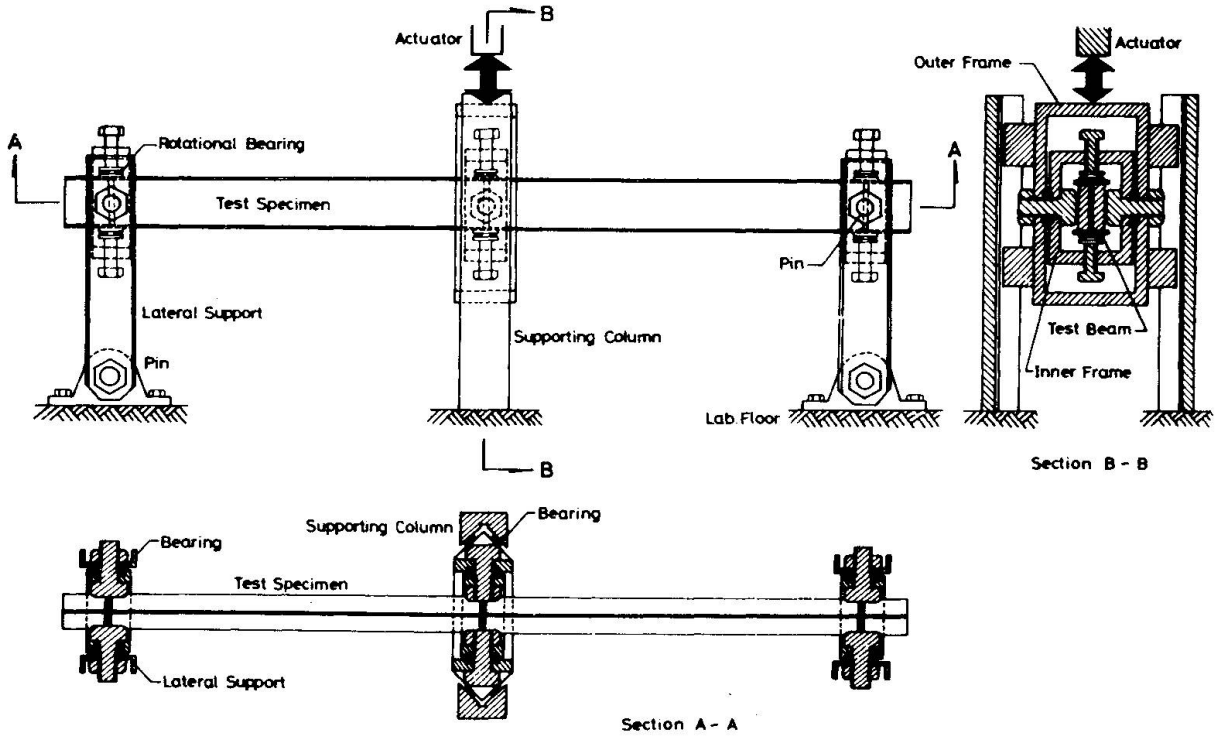

Fig. 1 General View of Test Setup

The specimens denoted by "monotonic" in Table 1 were loaded statically and monotonically. These static test results and the results previously obtained by the authors are compared to the results of reversed loading tests. The specimens denoted by "cyclic" in the Table were repeatedly loaded at constant deflection amplitudes and loading sequences were summarized in Table 1. The amplitudes were increased to the next step in each 10 cycles in general. The cycle number of 10 in each step was considered to be sufficient to exclude the transient property of material after sudden change of loading.

In order to examine the influence of the number of cycles in each amplitude on the critical amplitude, DG-130-7 and DG-130-8 were loaded each 5 and 15 cycle at each amplitude, respectively.

Table 1 Summary of Test Results

Specimen	l/r_y	Loading Condition	Frequency (Hz)	Cyclic Program Amplitude θ/θp (Number of Cycles)	Rotation Capacity (R)
DG-110-1	51.2	Cyclic	0.03	1.0(10)—2.0(〃)—2.5(〃)—3.0(〃)—3.5(15)	2.5
DG-110-2	51.3	〃	〃	1.0(10)—1.5(〃)—2.0(〃)—2.5(〃)—3.0(〃)—3.5(〃)—4.0(〃)—4.5(5)	2.0
DG-130-1	60.9	Monotonic	——		5.4
DG-130-4	62.5	Cyclic	0.03	1.0(10)—2.0(〃)—2.5(〃)—3.0(〃)—3.5(〃)	2.0
DG-130-5	62.5	Earthquake Response[1]	0.067[2]	1.0(1)—2.0(〃)—2.5(〃)—3.0(〃)—3.5(2)—4.0(〃)—3.5(1)—3.0[3](1)	
DG-130-7	62.4	Cyclic	0.05	1.0(5)—2.0(〃)—2.5(〃)—3.0(〃)—3.5(〃)—2.0(〃)—2.5(〃)—3.0(〃)—3.5(5)—2.0(〃)—2.5(〃)—3.0(〃)	2.0
DG-130-8	62.6	〃	〃	1.0(15)—2.0(〃)—2.5(〃)—3.0(〃)—3.5(5)—2.0(15)—2.5(〃)—3.0(〃)—3.5(5)—2.0(15)—2.5(〃)	2.0
DG-130-9	62.6	Random[4]	0.06[2]	1.0(1)—2.0(〃)—2.5(〃)—3.0(〃)—3.5(〃)—4.0(〃)—4.5(〃)—2.0(〃)—2.5(1)—3.0(〃)—3.5(〃)—4.0(〃)—4.5(〃)—2.5(〃)—3.0[3](1)	
DG-130-10	62.6	〃	〃	1.0(1)—2.0(2)—2.5(〃)—3.0(〃)—3.5(〃)—3.83(〃)—4.5(〃)—2.0(〃)—2.5(2)—3.0(〃)—3.5(〃)—3.83[3](〃)	
DG-150-2	70.0	Cyclic	0.05	1.0(10)—1.5(〃)—2.0(〃)—2.5(〃)—3.0(〃)—3.5(5)	1.7
DG-170-1	79.4	Monotonic	——		3.9
DG-170-3	81.7	Cyclic	0.03	1.0(10)—1.5(〃)—2.0(〃)—2.5(40)—2.75(10)—3.0(5)	1.0
DGH-110-1	52.2	Monotonic	——		3.5
DGH-110-2	52.3	Cyclic	0.03	1.0(10)—1.5(〃)—2.0(〃)	1.3
DGH-130-1	62.2	Monotonic	——		3.3
DGH-130-2	61.9	Cyclic	0.05	1.0(10)—1.5(〃)—2.0(〃)—2.5(〃)—3.0(6)	1.1
DGH-150-1	72.0	Monotonic	——		2.4
DGH-150-2	71.6	Cyclic	0.05	1.0(10)—1.5(〃)—2.0(〃)—2.5(〃)	1.0
DGH-170-1	80.7	Monotonic	——		1.5
DGH-170-2	80.9	Cyclic	0.03	1.0(10)—1.5(〃)—2.0(〃)—2.5(3)	0.5

1) Response of deflection calculated with acceleration of ground motion recorded at Hachinohe 1968 earthquake

2) Mean frequency of response waves or random waves

3) Ratio of maximum rotation to θp

4) Random deflection generated on a digital computer

The deflection was controlled so as to be a sinusoidal function of time, t, in the "cyclic" tests. As the displacements of real structures do not show the simple harmonic response during earthquake, DG-130-5, DG-130-9 and DG-130-10 were loaded by controlling the central deflection to coincide with the calculated deflection response and the random deflection generated on a digital computer.

The frequency of cyclic deflection was determined to be 0.03 or 0.05 Hz due

to the capacity of the power supply, but these low frequencies were convenient to measure force and deflection and moreover, the validity of predicting dynamic behaviors by low frequency tests was already established by Hanson(5,6) and Rea et al.(7).

3. EXPERIMENTAL RESULTS

The end rotation, θ, and the end moment, M, defined by Fig. 2 were calculated from the central deflection and the applied force in each test. In order to compare the results in the same scale, θ and M are divided by θp and Mp, respectively.

θp is given by the expression

$$\theta p = MpL/3EI_x \qquad (1)$$

where Mp is full-plastic moment and I_x is moment of inertia with respect to strong axis.

According to the traditional way to express the rotation capacity often appeared in the papers on the plastic design, the rotation capacity, R, was calculated by

$$R = (\theta/\theta p)_m - 1 \qquad (2)$$

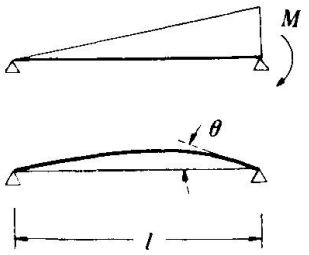

Fig.2 Definitions of Moment and Rotation

In the monotonic loading tests, $(\theta/\theta p)$ of the above expression was defined as the value of rotation, $\theta/\theta p$, at the maximum moment. The results are summarized in Table 1 and plotted in Fig. 3.

In the case of cyclic bending tests the moment-rotation hysteresis curves were obtained as shown in Fig. 4 where inserted numerals beside loops denote the numbers of cycles. As recognized by the figure, the hysteresis loops could keep their very stable shapes as long as the amplitude was controlled within some critical bound. Once the amplitude exceeded the critical bound, lateral buckling was accelerated, the hysteresis loops became unstable and the magnitude of M/Mp decreased in each cycle.

The failure due to lateral buckling is defined in this series of experiments as follows: After a few cycles at the same amplitude the moment reduces and moreover the rate of reduction does not vanish asymptotically and diverges.

The critical amplitude is defined as the amplitude, beyond which beam fails, and denoted by $(\theta/\theta p)_m$ to compare with results of the monotonic loading tests. R is defined by Eq.(2). The rotation capacity, R, obtained for specimens in the cyclic tests are summarized in Table 1 and plotted in Fig. 3. The solid curve in the figure is a regression curve which was made to be fitted to the data of the monotonic tests. It can be seen that R for the cyclic loads are considerably lower than for the monotonic loads.

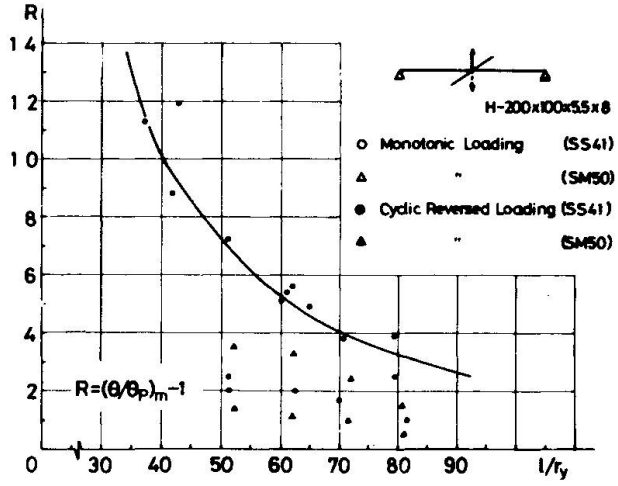

Fig. 3 Rotation Capacity-Slenderness Ratio

For specimens DG-130-7 and DG-130-8, the cyclic tests were done again at the smaller amplitudes than the critical amplitude, $3\theta/\theta p$, after the excessive buckling deformations took place at the larger amplitudes than the critical. In this loading program the stable hysteresis loops were obtained at the small amplitudes, but the reduction of the values of recorded bending moments was remarkable and it was influenced by the amount of residual buckling deformations.

To know what kinds of hysteresis loops and what behaviors of lateral

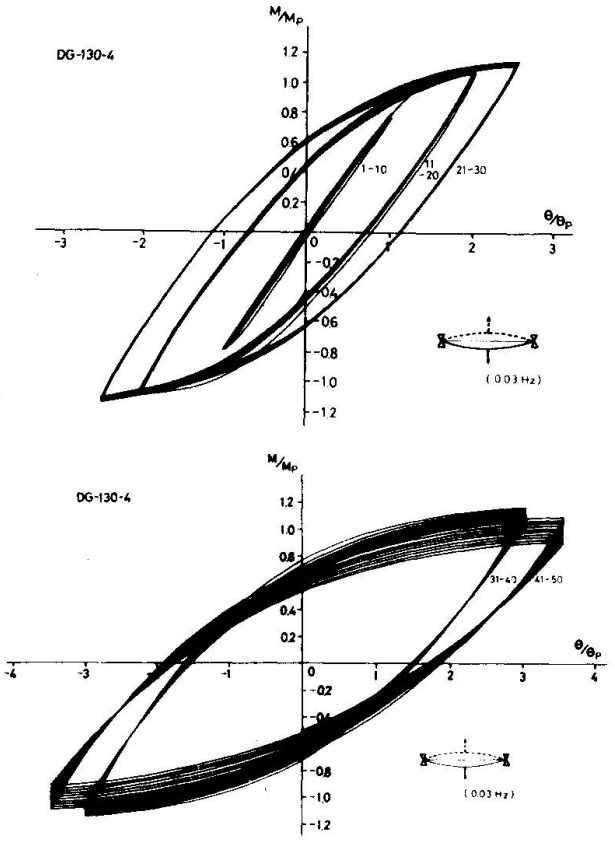

Fig. 4 Hysteresis Loops

buckling of real members show when structures are sujected to severe earthquakes, the reversed loading tests were done by controlling the deflection of DG-130-5, DG-130-9 and DG-130-10 to follow the calculated deflection response of a simple model and the random motion generated on the computer. Fig. 5 shows the recorded deflection of the center of span, δ , and the applied force, P, in DG-130-9, where the maximum value of the deflection was set to $3.5\theta/\theta p$. For comparison, the recorded deflection and force of DG-130-4 are also shown in the same figure. Figs. 6 and 7 show the hysteresis loops for DG-130-9. In Fig. 6 the maximum deflection was controlled to be equal to the critical amplitude, namely, $3\theta/\theta p$. In this case the load carrying capacity is considered to be enough because the amplitudes except the maximum are smaller than the $3\theta/\theta p$. And even though the maximum was set to $4\theta/\theta p$, the reduction of the moment at each peak is not so much. When the maximum became $4.5\theta/\theta p$, however, the remarkable reduction was observed at the maximum peak and the second maximum peaks which were also beyond the critical, $3\theta/\theta p$.

4. CONCLUSIONS

1) There exists the critical amplitude of deflection, within which the hysteresis loops are stable under cyclically repeated loads and beyond which the load carrying capacity of the beam reduces in each cycle. The same critical amplitudes are obtained for the different numbers of cycles in each amplitude if the geometric and material properties are same.
2) These critical amplitudes are considerably low in comparison with the deflections at the maximum loads in the monotonic loading tests. It is worth to be noted that the critical values for cyclically reversed loadings are lower

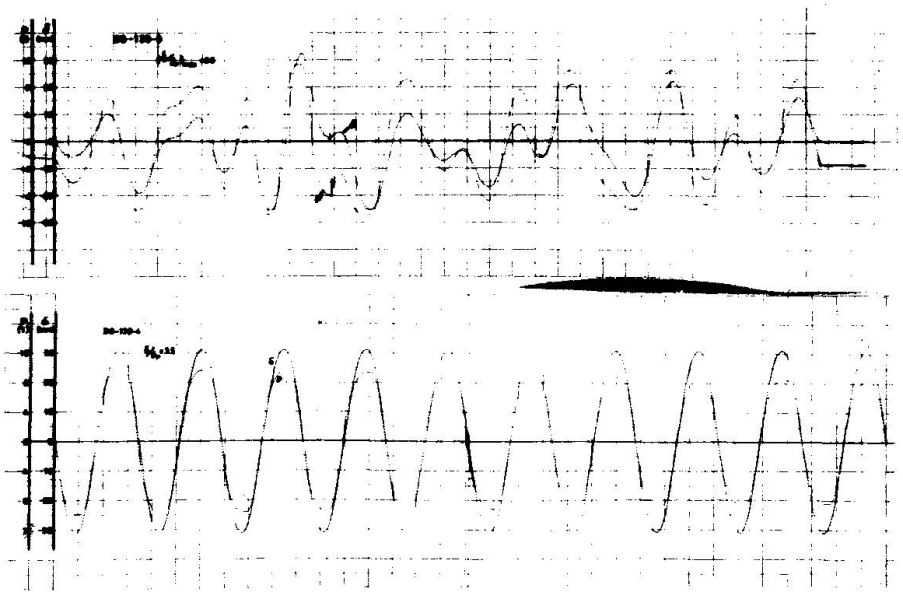

Fig. 5 Deflection and Load Recorded

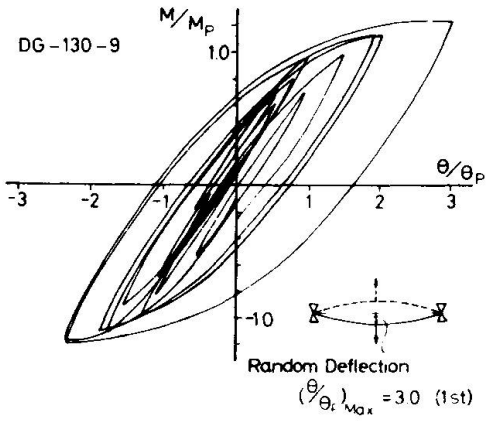

Fig. 6 Hysteresis Curves

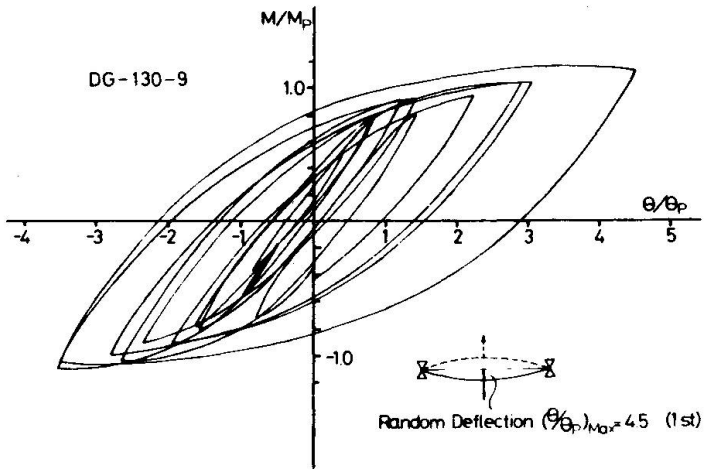

Fig. 7 Hysteresis Curves

than a half of the critical values for monotonic loadings.

3) Even though the beams were subjected to excessive deflections beyond the critical amplitude in the past, the stable hysteresis loops can be obtained if the deflection is within the critical . However, the load carrying capacity at that stages reduces depending on the amount of deflections over the critical amplitude and its number of experiences hitherto.
4) The critical amplitudes obtained by the cyclic tests are significant for analyzing the buckling failure due to random loads. For random loads only one excursion of hysteresis curve beyond the critical amplitude does not imply an immediate failure.
5) For SM50 steel, more severe bracing requirements than for SS41 steel for lateral buckling must be provided to beams of structures subjected to both monotonic and cyclically repeated loads.

REFERENCES

1) V.V. Bertero and E.P. Popov, " Effect of Large Alternating Strains Steel Beams ", Proc. ASCE, ST 1, Feb. 1965
2) E.P. Popov and R.B. Pinkney, " Cyclic Yield Reversal in Steel Building Connections ", Proc. ASCE, ST 3, March 1969
3) " AIJ Specifications for Plastic Design of Steel Structures (Draft) ", Architectural Institute of Japan, 1971
4) " AISC Specification for the Design, Fabrication and Erection of Structural Steel for Buildings ", Feb. 1969, American Institute of Steel Construction
5) R.D. Hanson, " Comparison of Static and Dynamic Hysteresis Curves ", Proc. ASCE, EM 5, Oct. 1966
6) R.D. Hanson, A.M. AlMuti and J.G. Hoad, " Post-Elastic Response of Mild Steel Structures ", Proc. 3rd. Japan Earthquake Eng. Symp. 1970
7) D. Rea, R.W. Clough, J.G. Bouwkamp and U. Vogel, " Damping Capacity of a Model Structure ", Proc. 4th World Conf. Earthq. 1969

SUMMARY

Cyclically repeated loading tests at constant deflection amplitudes were conducted on the steel beams with H-shaped section. These tests showed the quite different behaviors of lateral buckling as compared with the behaviors under monotonically increasing loads. The rotation capacities for cyclic tests are considerably smaller than for monotonic tests. Reversed loading tests due to random deflections were also conducted.

RESUME

Des essais de charges répétées avec grandeurs de déformation constantes ont été effectués sur des poutres en acier à section en double T. Ces essais ont montré que le flambement latéral se produit d'une façon tout-à-fait différente du cas où la charge augmente lentement. Les possibilités de rotation pour les essais de fatigue sont beaucoup plus petites que pour les essais statiques. Des essais de charges alternées à la suite de déformations quelconques ont aussi été effectués.

ZUSAMMENFASSUNG

Zyklische Belastungsversuche mit konstant gehaltener Ausbiegung wurden an Stahlbalken mit H-Querschnitten durchgeführt. Diese Versuche zeigten das ziemlich verschiedenartige Verhalten des Kippens, verglichen mit dem Verhalten unter ständig zunehmender gleichgerichteter Belastung. Die Rotationskapazitäten für zyklische Versuche sind bedeutend kleiner als bei gleichgerichteten Versuchen. Versuche mit Wechselbelastung aufgrund von stochastischen Ausbiegungen wurden ebenfalls ausgeführt.

Leere Seite
Blank page
Page vide

III

Experimental Study on Steel Beam-Columns under Repeated Bending

Etudes expérimentales de colonnes en acier soumises à flexion répétée

Experimentelle Studie an Stahlträger-Stützen unter wiederholter Biegung

S. IGARASHI
Professor
Osaka University
Osaka, Japan

C. MATSUI
Associate Professor
Kyushu University

K. YOSHIMURA
Lecturer
Fukuoka, Japan

1. Introduction. There have been a large number of experimental and theoretical studies that deal with steel structures subjected to alternating loads. The most significant aspect of these tests on steel frames or subassemblages whose columns are under constant high axial compression are that the maximum horizontal loads which could be carried by the frames or subassemblages are increased gradually with repetition of loading cycles. To predict rationally behaviors of such frames or structural subassemblages, which exhibit characteristics of multi-story frames, realistic relation of alternating moment-curvature of the cross section of members under constant axial compressive load is needed basically. Herein, experimental studies on steel beam-columns which are subjected to constant axial compressive load and alternately repeated bending are carried out. To determine the alternating moment-curvature relation of the members under constant axial compression, these experimental results are compared with theoretical ones by a simple method of analysis on the basis of bi-linear and curved stress-strain relations.

2. Description of Tests. Five specimens with 240mm length and with rectangular cross section (40mm × 19mm) were taken from 19mm thickness plate. Material is a structural steel, SS41, with lower yield stress, $\sigma_y = 3.17\ t/cm^2$ and ultimate tensile stress, $\sigma_u = 4.56\ t/cm^2$, which are the average of three measurements obtained from monotonic tension tests on three tensile coupons. Values of

constant axial compression to which specimens are loaded are summarized in Table 1.

Fig. 1 shows the loading arrangement. The upper and lower ends of a specimen are clamped rigidly into the arm plates by high strength bolts. Constant axial compression, P, was loaded vertically to the specimen by hydraulic testing machine with 50 ton capacity through the knife-edged pin supports. Alternately repeated bending was applied statically to the specimen by a high strength bolt, which was attached through the pin supports in perpendicular direction to the arm plates. Bending was applied to the specimen about the weak axis of the cross section. Axial tensile force applied to the high strength bolt with turn-of-nut was measured by means of a load cell connected to the high strength bolt through the universal joints. Horizontal deflection at a mid span of the specimen was measured by the displacement meter with 50mm stroke capacity. Curvature of the cross section was measured by the post yield electric wire strain gages located at the mid span of the specimen.

3. Experimental Results. Solid curves in Fig. 2 (a-e) show the moment-curvature curves obtained from the experiments. In these figures, moment, M, and curvature, ϕ, are nondimensionalyzed by initial yielding moment, $M_y (= \sigma_y Z_e$, σ_y = yield stress, Z_e = section modulus), and corresponding curvature, $\phi_y (= M_y/EI$, EI = flexural rigidity), respectively. In Fig. 4 (a-e), maximum absolute values of the resisting moment of all specimens are plotted against number of repetition of loading reversals by solid curves. It is seen from these figures that; (1) The size and shape of a virgin curve are considerably different from those of separate hysteresis loops. (2) Influence of axial compression ratio, $n (= P/P_y)$, in increasing the maximum resisting moment of the cross section is quite evident from the figures. (3) Rate of increase of the maximum resisting moment to the number of cycles becomes remarkable as the axial compression ratio, n, becomes high. (4) Such increment of maximum resisting moment becomes gradually small with repetition of bending. (5) Elastic modulus of the moment-curvature hysteresis loops does not almost vary with cycles.

In Fig. 5 (a-e), average strain in the cross section, $\varepsilon_{\bar{o}}$, defined as the strain at the centroid axis of the cross section, is plotted against number of loading reversals by solid curves.

As is seen from the figures, when the specimen is subjected

to constant axial compressive load, average strain in the cross section is increased gradually and is always accumulated to the compressive direction with repetition of bending. Under higher axial compressive load and curvature amplitude, accumulation of the average strain becomes progressively larger with each additional cycle. Therefore, it is seen from the experimental results that accumulation of the average strain in the cross section is closely related to the increase of the maximum resisting moment of the cross section due to repetition of cycles (Ref. 1).

4. Theoretical Analysis and Discussion. In Refs. 1 and 2, a simple analytical method to determine the moment-curvature relations for double symmetrical cross sections under constant axial compression and alternately repeated bending was proposed. Although this analytical method is based on trial and error technique, for a given hysteresis law between stress and strain, moment-curvature relation under any loading situation can be easily determined without simplification of the geometrical shape of the member section.

Experimental results were compared with theoretical ones obtained from the method of analysis proposed in Refs. 1 and 2, which were based on bi-linear and curved stress-strain relations, respectively. These stress-strain relations are shown in Fig. 3. In the analysis, values of strain hardening factor, μ, for bi-linear stress-strain relations are assumed as $\mu = 0.01$ and $\mu = 0.02$ (see Fig. 3), and values of the Ramberg-Osgood parameters for curved stress-strain relation shown in Fig. 3 are choosen as $\alpha = 1.5$, $\gamma = 9$ and $\alpha = 2.5$ $\gamma = 7$, which describe the stable region of the moment-curvature hysteresis loops under repeated pure bending (Ref. 3).

In Fig. 4 (a-e), relation between maximum resisting moment of the cross section at each cycle and number of loading reversals are compared with analytical results for all specimens. Analytical results based on bi-linear stress-strain relations with strain hardening factors, $\mu = 0.01$, and $\mu = 0.02$, are designated by open triangle, Δ, and solid triangle, $\blacktriangle$, respectively, and those based on curved stress-strain relations with Ramberg-Osgood parameters, $\alpha = 2.5$, $\gamma = 7$, and $\alpha = 1.5$, $\gamma = 9$, are designated by open square, $\square$, and solid square, $\blacksquare$, respectively. It may be concluded from these figures that increase of maximum resisting moment due to repetition of loading cycles for some specimens can be explained

approximately by the analysis based on curved stress-strain relations with parameters, $\alpha = 2.5$, and $\gamma = 7$ and based on the relation with strain hardening factor, $\mu = 0.01$, although all experimental results do not agree well with the theoretical results. Moment-curvature curves based on bi-linear relation with strain hardening factor, $\mu = 0.01$, are shown in Fig. 2 (a-e) by dashed curves. Althqugh analytical results based on curved hysteretic stress-strain relation is seemed to be somewhat better than those based on bi-linear one to explain the experimental results, the bi-linear relation with strain hardening factor, $\mu = 0.01$, may be quite reasonable model for inelastic analysis of steel members from the engineering points of view.

In Fig. 5 (a-e), average strain in the cross section at each of reversal points for all specimens are plotted against number of loading reversals. Symbols used in the figure are the same as those in Fig. 4. It is note-worthy that cyclic change of the average strain in the cross section for all specimens can be explained quite well by the analytical results based on bi-linear stress-strain relation with strain hardening factor, $\mu = 0.01$.

From the facts described above, it is concluded that bi-linear stress-strain relation with strain hardening factor, $\mu = 0.01$, is sufficiently reasonable relation to simulate the inelastic behavior of steel members under constant axial compression and alternately repeated bending.

References

1. S. Igarashi, C. Matsui, K. Yoshimura and K. Matsumura, "Inelastic Behavior of Structural Sections under Alternating Loadings", Pts. 1 and 2, Trans. of Architectural Institute of Japan (AIJ), No. 169 and 170, Mar., and Apr., 1970.
2. M. Hanai, K. Yoshimura and M. Kaku, "Inelastic Behavior of Steel Sections under Constant Axial Compression and Alternating Bending - Based on Curved Stress-Strain Relation", Trans. of AIJ, Extra, Nov., 1971, in Japanese.
3. K. Yoshimura, "Experimental Study on Steel Rectangular Members under Alternating Bending", Trans. of AIJ, Extra, Oct., 1972, in Japanese.

SUMMARY

Experimental Studies on steel beam-columns which were subjected to constant axial compressive load and alternately repeated bending were performed. Experimental results were analyzed by a simple method of analysis to determine the cyclic moment-curvature relation of the members under constant axial compression on the basis of bi-linear and curved stress-strain relations.

Specimen Number	Axial Compression Ratio ($n=P/Py$, $Py=A\sigma y$)
WO	0.198
WP	0.406
WQ	0.402
WS	0.606
WT	0.604

Table 1

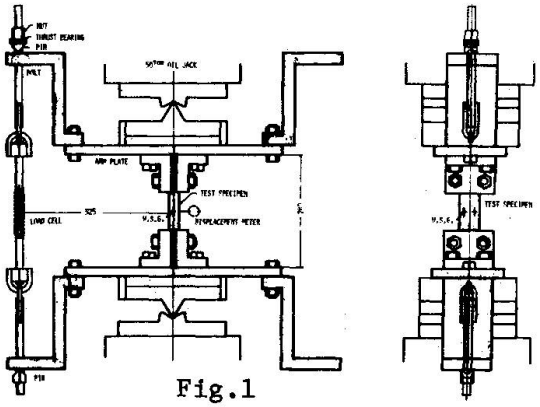

Fig.1

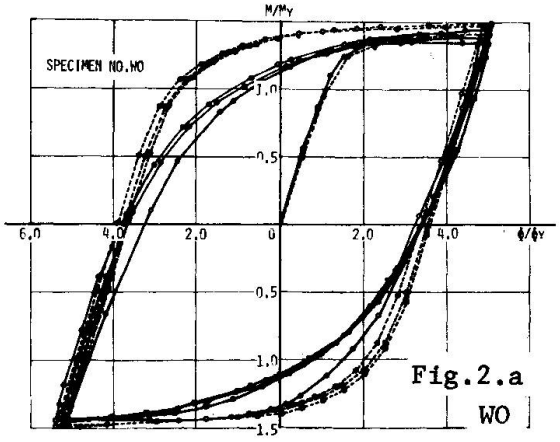

Fig.2.a WO

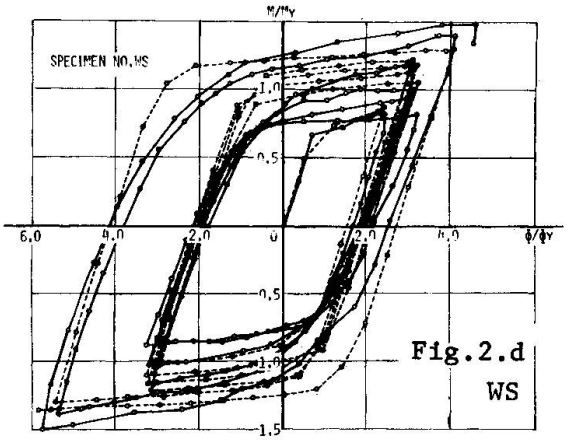

Fig.2.d WS

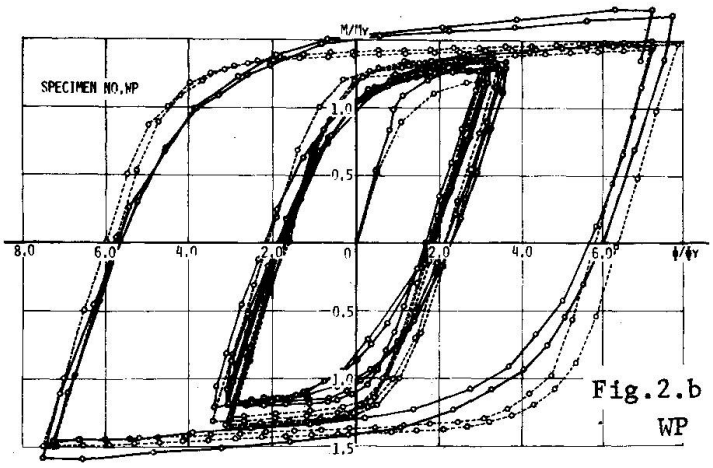

Fig.2.b WP

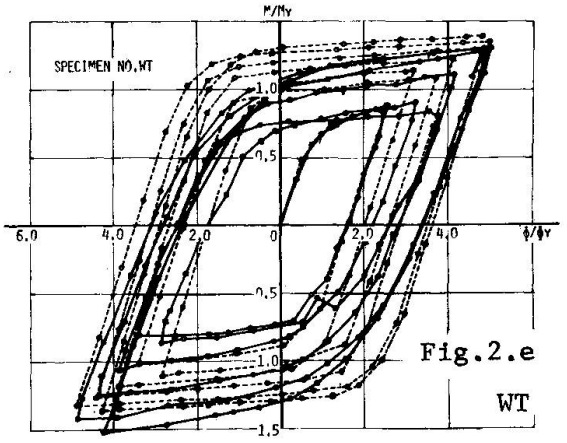

Fig.2.e WT

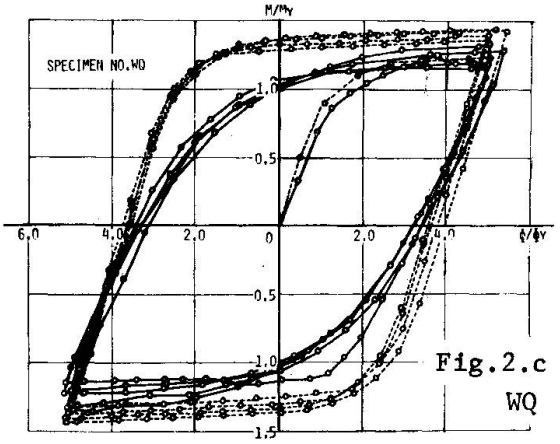

Fig.2.c WQ

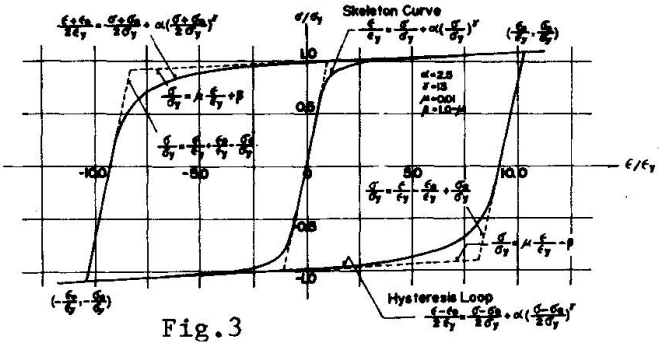

Fig.3

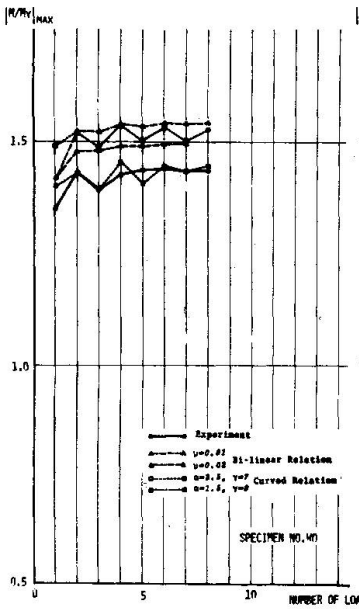

Fig.4.a WO

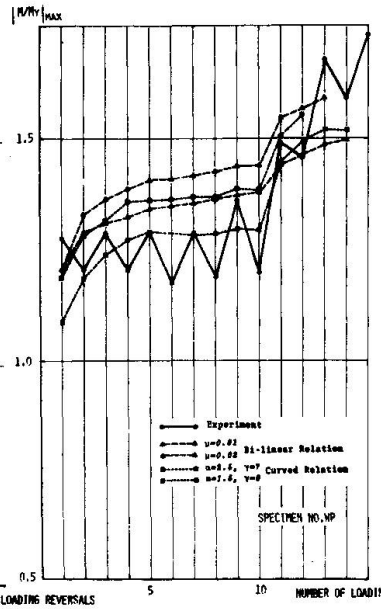

Fig.4.b WP

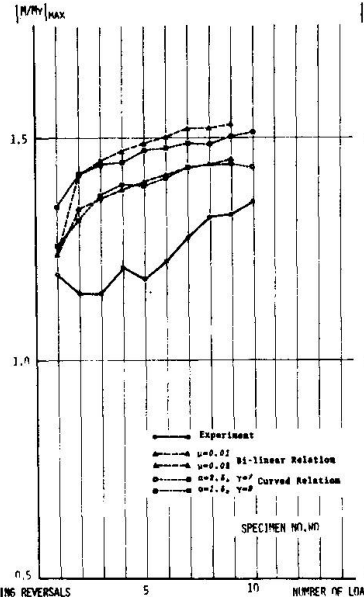

Fig.4.c WQ

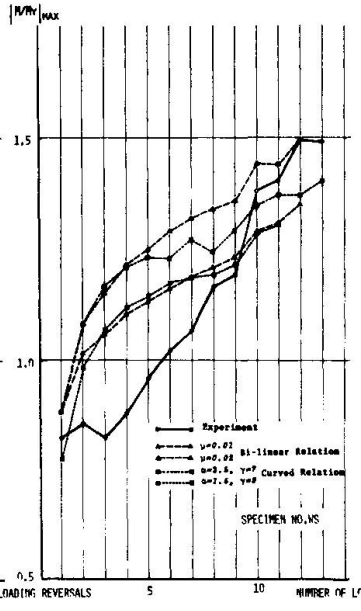

Fig.4.d WS

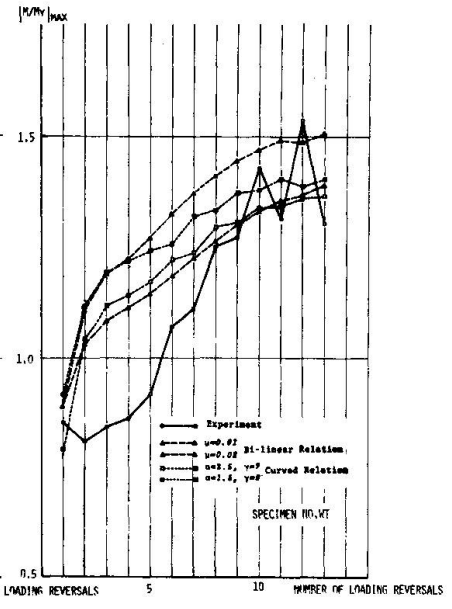

Fig.4.e WT

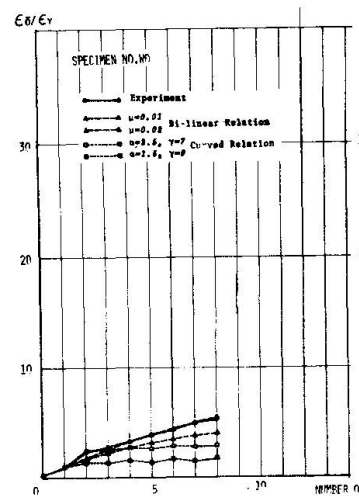

Fig.5.a WO

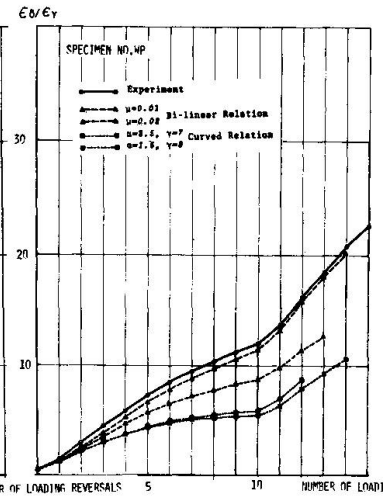

Fig.5.b WP

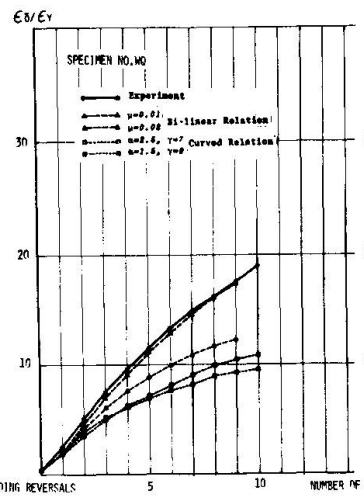

Fig.5.c WQ

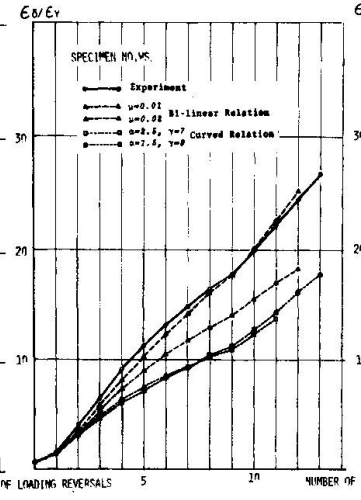

Fig.5.d WS

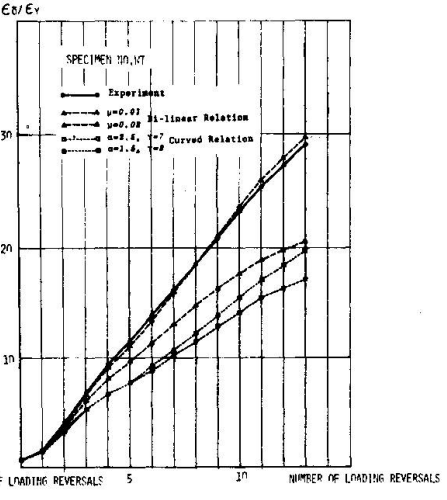

Fig.5.e WT

RESUME

On a effectué des études expérimentales sur des colonnes en acier soumises à une compression axiale constante et à un moment de flexion alterné. On a traité les résultats par une méthode d'analyse simple afin de déterminer la relation moment cyclique-courbure des éléments soumis à une compression axiale constante, sur la base de relations tension-déformation bi-linéaires et courbes.

ZUSAMMENFASSUNG

Es wurden experimentelle Studien an Stahlstützen unter konstanter axialer Druckkraft und wechselseitiger wiederholter Biegung ausgeführt. Experimentell gewonnene Resultate wurden mittels einer einfachen Rechenmethode untersucht, um die zyklische Momenten-Krümmungs-Beziehung der Stützen unter konstanter Druckspannung auf der Basis der bi-linearen und der gekrümmten Spannungs-Dehnungs-Beziehung zu bestimmen.

Leere Seite
Blank page
Page vide

Incremental Collapse of Thin Webs subjected to Cyclic Concentrated Loads

Rupture progressive des âmes minces soumises à des charges cycliques concentrées

Stufenweiser Kollaps von dünnen Stegen unter zyklischer Belastung durch Einzellasten

Pavel NOVÁK
Assoc. Prof., Ph.D., Ing.
at the Structural Institute
Prague, CSSR

Miroslav ŠKALOUD
Assoc. Prof., D.Sc., Ing.
Head of the Department "Stability"
at the Institute of Theoretical
and Applied Mechanics of the
Czechoslovak Academy of Sciences
Prague, CSSR

1. Introductory Remarks

As various elements in steel structures are subjected to variable repeated loads, it was decided to investigate the deflection stability and incremental collapse of thin webs. The first study of this kind dealt with the behaviour of webs subjected to a cyclic concentrated load, this problem being encountered frequently in the design of certain types of bridge girders, crane run-way girders and similar structures. The investigation was carried out by a research team consisting of a)both authors, b) Ing.Bohdanecký, Ing.Stárek, Ing.Studničková (all three from the Structural Institute in Prague) and c) Ing.Drdácký, Ing.Kratěna and Ing.Zörnerová (from the Institute of Theoretical and Applied Mechanics in Prague).

The investigation is a continuation to another study /1/ conducted by the same research team and dealing with the post-buckled behaviour of webs subjected to static concentrated loads.

2. Test Girders and Test Set-Up

Three series of test girders were tested; their general details are given in Fig. 1 and geometrical characteristics in Table 1. An inspection of the figure and table shows that the test girders varied in a) the aspect ratio α of the web, b) the width-to-thickness ratio λ of the web, and c) the dimensions (and, consequently, in the stiffness parameter $I_f/a^3 t - I_f$ de-

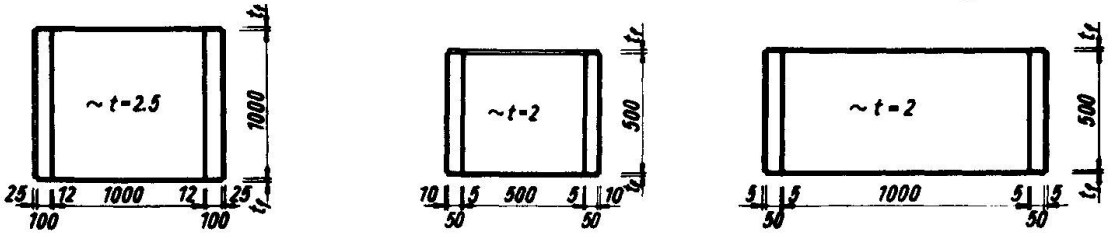

Fig. 1

Table 1

Girder	α	λ	I_f/a^3t Units of 8	P_{cr} (T)
TG 1	1	400	0.887	6.5
TG 1'			0.849	5.5
TG 2			0.85	7.0
TG 3			28.56	9.2
TG 4			54.70	8.8
TG 5			245.38	18.0
TG 5'			238.44	18.0
PTG 1		250	2.17	5.0
PTG 2			2.16	4.6
PTG 3			64.25	5.5
PTG 4			63.48	5.6
PTG 5			237.68	7.2
PTG 6			248.33	7.0
ITG 7			2.08	4.0
ITG 8			2.08	3.7
ITG 9			2.08	3.5
ITG 10			266.96	7.4
ITG 11			297.74	7.0
PTG 12	2		0.260	3.5
PTG 13			7.51	5.6
PTG 14			7.51	4.8
PTG 15			38.13	5.9
ITG 16			0.257	3.5
ITG 17			0.254	3.5
ITG 18			0.260	4.0
ITG 19			7.51	5.0
ITG 20			7.51	4.7
ITG 21			38.13	6.5
ITG 22			38.13	6.0

Table 2

Girder	α	λ	I_f/a^3t Units of 8	P_{cr} (T)
TG 1	1	400	0.887	5.0
TG 1'			0.849	5.5
TG 2			0.85	6.5
TG 3			28.55	7.0
TG 4			54.70	9.0
TG 5			245.38	18.0
TG 5'			238.44	18.5
STG 1		250	3.48	3.6
STG 2			3.50	4.0
STG 3			63.89	5.5
STG 4			64.36	5.5
STG 5			254.22	7.5
STG 6			242.71	6.0
STG 7	2		0.257	3.75
STG 8			0.254	3.5
STG 9			7.51	4.8
STG 10			7.51	5.25
STG 11			38.13	6.0
STG 12			38.13	5.5

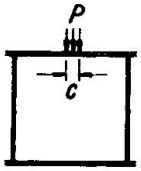

Fig. 2

noting the flange inertia, a the width of the web panel and t the web thickness) of the flanges. So it was possible to study the influence of the geometrical characteristics of the web and flanges upon the incremental collapse. In all tests the web was subjected to a narrow partial edge load (Fig.2), applied on to the upper flange at the mid-distance of the vertical stiffeners. The width of the load c=a/10, a denoting the width of the web panel.

One part of the experiments (those related to girders TG and PTG) were conducted in a pulsator, the frequency n of the cyclic load amounting to 3.3 Hz. For each loading step, 1000 loading cycles were applied. The load cycled between 0.5 T and P_i, P_i denoting various loading steps. These tests will below be referred to as "fast" cyclic tests.

As it could be argued that, in such "fast" cyclic tests, the web did not have, in individual cycles, enough time to plastify, it was decided to carry out also another group of tests with slowly cycling loads. These experiments were carried out in an Instron testing machine. The velocity of the movement of the loading beam was of 0.6 cm/min., which was about 100 times slower than the aforesaid "fast" cyclic tests. 50 loading cycles were applied for each successive loading step.

With the "fast" cyclic tests and the "slow" cyclic ones conducted, the authors were able to look also into the effect of the velocity of cycling upon the "breathing" and incremental collapse of thin webs. The reader will understand that the above adjectives "fast" and "slow" have merely a relative sense, enabling us to compare both groups of experiments with each other.

Apart from the 29 cyclic tests, the authors and their coworkers carried out 19 static experiments on test girders subjected to a static partial edge load. The geometrical characteristics of the static test girders and the experimental results are listed in Table 2. These results will be compared below to the behaviour of the girders acted on by variable repeated loads.

The authors also took the view that it was of some interest to look into two other phenomena which might play a role in the "breathing" tests. First of all it was of some importance to determine the relation of the frequency of the cyclic loads to the natural frequencies n of the test girder webs. The natural frequencies were obtained experimentally. It was found that they depended not only on the test girder dimensions, but also on the shape and magnitude of the initial curvature of the web. In all cases the values of n were greater than 20; consequently,

much higher than the frequency of the applied cyclic load. The experiments were, therefore, safely in the non-resonance range.

The writers also estimated the magnitude of the dynamic inertia forces occuring as a result of the "breathing" of the web. It was concluded that these forces were small enough not to play any pronounced part in the behaviour of the webs.

3. Experimental Apparatus

The buckled pattern of the web was measured by means of a stereophotogrammetric method, which enabled the authors to take all readings in a very short time moment (0.001 sec.). The application of such a method was indispensable in our tests, in which the web and flanges were "breathing".

The stereophotogrammetric method was combined with a special device, which made it possible to take deflection readings at a given moment of a loading cycle; in particular, when, in a "breathing" cycle, the web deflection attained its maximum value. Moreover, the stereophotogrammetric method enabled us to measure not only the deflection perpendicular to the web, but also the in-plane distortion of the mesh that was marked on the web, and the deformation of the boundary frame of the web panel.

A set of strain gauges was attached to both sides of the web and of the upper flange in order the stress pattern in the girder could be studied. The strain gauges, as well as two deflection pick-ups, were linked to an automatic recorder "Ultralette". Thus it was possible to study, in terms of time, the deflection (and strain) stability when the web was breathing.

4. Deflection Stability and Incremental Collapse

As far as deflection stability is concerned, two questions needed replying:

(i) When a girder, subjected to a cyclic load, operates in the plastic range, does an increase in web deflection occur during a certain number of loading cycles?

(ii) If it is so, do these deflection increments cease after a limited number of cycles of load applications?

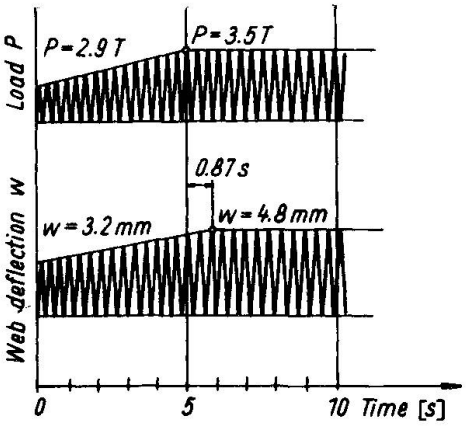

Fig. 3

Thanks to deflections and strains being measured carefully on an automatic recorder Ultralette, it was possible to give answers to the abovementioned questions.

An increase in web deflection and strain under a cyclic load was observed frequently in the plastic range of the tests. This is demonstrated in Fig. 3, in which the maximum web deflection recorded in one of the pulsator (i.e. "fast" cyclic) tests is plotted; and in Fig. 4, giving the buckled patterns of the web measured after a) the first and b) the last cycles in one loading step of an Instron (i.e. "slow" cyclic)

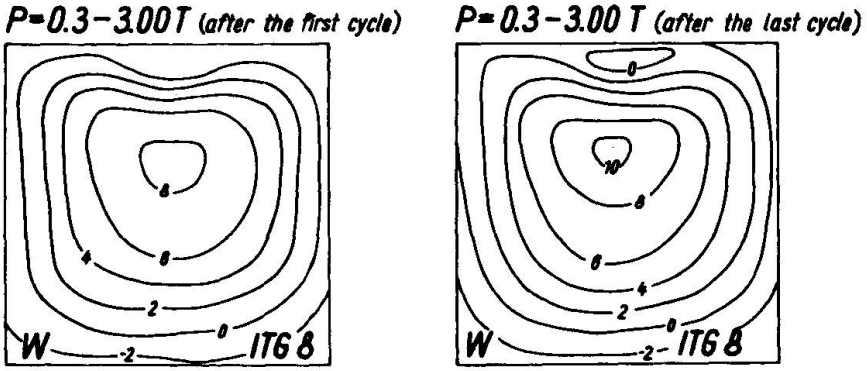

Fig. 4

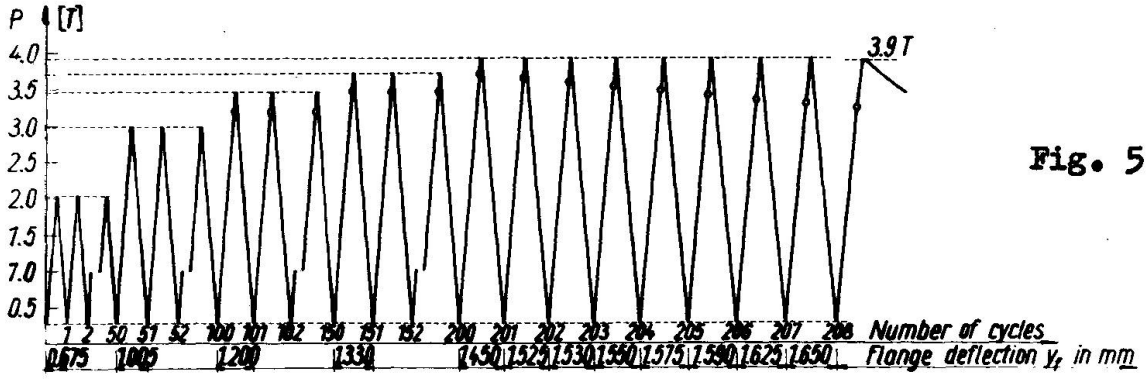

Fig. 5

experiment. The phenomenon "shook down", however, after a few (usually 3 - 5) cycles, the deflection stabilized, and the girder was able to sustain a higher load (Fig. 3). This happened for several successive loading steps; and only then the girder failed by deflection instability. This kind of failure, usually called incremental collapse, is shown in Fig. 5, presenting the load-deflection relationship measured in one of the Instron tests. The circles indicate the onset of plastification in each loading cycle.

5. Ultimate Load

The ultimate loads P_{ult} resulting from the variable repeated load tests are listed in Table 1. Some of them, the load-carrying capacities of TG-girders and α = 1-PTG-girders, are plotted (in terms of the depth-to-thickness ratio λ and the flange stiffness parameter I_f/a^3t, and in comparison with the static critical load P_{cr}) in Fig.6. An analysis of the table and figure indicates that thin webs subjected to a cyclic concentrated load manifest (see Table 2) a considerable post-buckled reserve of strength. This post-critical strength grows with the depth-to-thickness ratio of the web and with the moment of inertia of the flange.

Of particular importance was it to compare the results of the cyclic tests (Table 1) with those of the static ones (Table 2), and so give a reply to the question

(i) Whether the deflection instability and incremental collapse, discussed in par. 4, led to a reduction in ultimate strength.

Then it was of interest

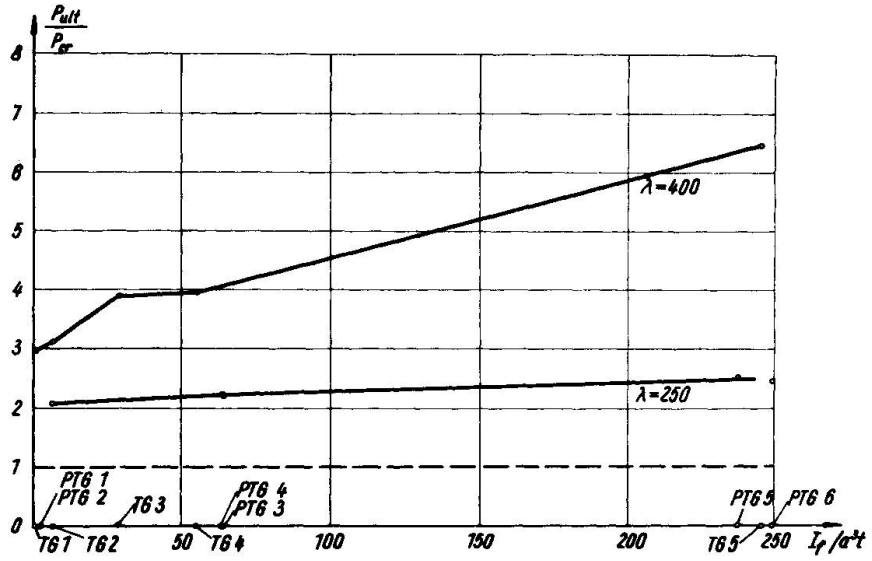

Fig. 6

(ii) To evaluate the effect of the cycling velocity upon the limiting load of the test girders.

An analysis of all results shows that

(i) In most "fast" cyclic tests, the ultimate loads were not lower than the load-carrying capacities resulting from the corresponding static experiments; and, in several cases, they were even higher.

(ii) The conclusions of the "slow" cyclic tests were similar to (i); only the number of the tests, in which the experimental load-carrying capacities were lower than the static ultimate loads, was a little greater. The corresponding reduction in ultimate load was, however, again small.

It can, therefore, be concluded that the cyclic loading and the incremental collapse did not lead to any significant reduction in ultimate strength; and, consequently, to any premature failure of the girder.

Bibliography

/1/ Škaloud M., Novák P.: Post-buckled behaviour of webs subjected to concentrated loads. Rapport Préliminaire du 9me Congrès de l'AIPC, Amsterdam, 1972.

SUMMARY

The paper deals with the deflection stability and incremental collapse of thin webs subjected to a variable repeated narrow partial edge load. An analysis of the results shows that the aforesaid phenomena did not lead to any significant reduction in ultimate strength. The ultimate loads of the test girders were also very considerably affected by the flexural rigidity of the flanges.

RESUME

Ce travail traite de la résistance à la déformation et de la ruine des âmes minces soumises à une charge variable répétée juste limitée au bord. Une analyse des résultats montre que ledit phénomène n'a pas entrainé une réduction notable de la résistance ultime. Les charges ultimes de la poutre testée ont aussi été considérablement influencées par la résistance à la flexion des semelles.

ZUSAMMENFASSUNG

Der Bericht behandelt die Deformations-Stabilität und den stufenweisen Kollaps dünner Stege unter einer veränderlichen, wiederholten linienförmigen Randlast. Eine Untersuchung der Resultate zeigt, dass das oben erwähnte Phänomen zu keiner bedeutenden Reduktion des Bruchwiderstandes führte. Die Bruchlasten der Versuchsträger wurden auch sehr stark durch die Biegesteifigkeit der Flansche beeinflusst.

Experimental Study on Thin Steel Shear Walls and Particular Steel Bracings under Alternative Horizontal Load

Etude expérimentale de parois de cisaillement minces en acier et d'entretoisements particuliers soumis à des forces horizontales alternées

Experimentelle Studie über dünne Stahlblech-Schubwände und spezielle Stahlaussteifungen unter alternierender horizontaler Last

Yasuhiko TAKAHASHI Toshikazu TAKEDA
Yasushi TAKEMOTO Masatoshi TAKAGI
Researchers of Structural Engineering Laboratory
Technical Research Institute
Ohbayashi-Gumi Ltd.
Tokyo, Japan

In seismic countries as well as in Japan, structures are designed against earthquakes and reinforced concrete shear walls or steel bracings are usually used as aseismic resistant element. However, their hysteretic characteristics in plastic region, ductility and capacity of energy absorption are not always good. Besides, their stiffness is so rigid that structure designed by static analysis is occasionally disadvantageous, when dynamically analized. The authors devised the thin steel plate shear wall and the particular steel bracing system with stable behavior and investigated their behavior through the tests whether they can be actually practised.

1. Thin Steel Plate Shear Wall

The steel plates are so strong and ductile, and their weight is so light that they are suitable as a material of shear wall. However, they have defect of buckling under low stress level. To improve this characteristic, the method of welding rib plates on one or both sides of steel plate was adopted.

First, the basic test was done, the object of which was to obtain the design principles of rib plates to be provided with consideration of calculated results. Changing the spacing between rib plates and their stiffness, the strength, hysteresis loop and post buckling behavior of steel shear wall were investigated.

Next, based on the design principles obtained through the basic test, the steel plate shear walls of the 32-storied building were designed for actual use and two full-size models of them were examined through the tests.

1.1 Basic Test

Outline of test---Twelve specimens with 2.3, 3.2 or 4.5 mm in plate thickness were made. They were reinforced with various sectional rib plates whose forms of arrangement were G, M1, and M2 type shown in Fig.1. The name of specimens, for example PR-3.2-M2-15, means the abbreviation of steel plate with rib plates, plate thickness, form of arrangement and height of rib plate in order (Table 1).

A very stiff rectangular rigid frame connected with pin joints,

was attached with high tensile bolts arround the specimen. To apply the shear force to the specimen, compressive force was subjected in one diagonal direction of the frame (Fig.2). When deflection was reached some decided values, the specimen was turned arround to be subjected to the force in another diagonal direction.

Calculation---The rigidity and yielding stress (τ_{sy}) on shear theory were calculated by eq.1 and 2. The rigidity, yielding stress (τ_{ty}) and maximum stress (τ_{tmax}) on tension field theory were calculated by eq.3,4 and 5.

$$\tau = G\cdot\gamma \quad \cdots (1) \qquad \tau_{sy} = \sigma_y/\sqrt{3} \quad \cdots (2)$$

$$\tau = E\cdot\cos^2\alpha\cdot\sin^2\alpha \quad \cdots (3) \qquad \tau_{ty} = \sigma_y\cdot\cos\alpha\cdot\sin\alpha \quad \cdots (4) \qquad \tau_{tmax} = \sigma_{max}\cdot\cos\alpha\cdot\sin\alpha \quad \cdots (5)$$

Where E,G, γ and α denote Young's modulus, shear modulus, shear strain and angle of buckling wrinkle respectively. σ_y and σ_{max} are yielding stress and maximum stress of the material.

The stress (τ_{cr}) at partial buckling (buckling of steel plate enclosed with vertical and horizontal rib plates) was calculated by eq.6 and the stress at entire buckling of the wall by eq.7. It was assumed that steel plate was connected to the surrounding frame with pin joints.

$$\tau_{cr} = \pi^2\cdot k\cdot E\cdot t^2/12\cdot(1-\nu^2)\cdot b^2 \quad \cdots (6)$$

$$\left.\begin{aligned} &U + V_p + V_r = const. \\ &U = -\tau\cdot t\int_0^a\int_0^b \frac{\partial w}{\partial x}\cdot\frac{\partial w}{\partial y}\,dx\,dy \qquad V_p = \frac{D}{2}\int_0^a\int_0^b\left(\frac{\partial^2 w}{\partial x^2}+\frac{\partial^2 w}{\partial y^2}\right)^2 dx\,dy \\ &V_r = \sum_i \frac{B_{xi}}{2}\int_0^a\left(\frac{\partial^2 w}{\partial x^2}\right)^2_{y=y_i} dx + \sum_j \frac{B_{yj}}{2}\int_0^b\left(\frac{\partial^2 w}{\partial y^2}\right)^2_{x=x_j} dy \\ &w = \sum_m\sum_n a_{mn}\cdot\sin\frac{m\pi x}{a}\cdot\sin\frac{n\pi y}{b} \end{aligned}\right\} \quad \cdots (7)$$

where t, a and b denote plate thickness, width and length, and U, Vp, Vr and potential energy of force, strain energy in plate and in rib plates.

Test result and discussion---Fig.3 showed that the initial rigidity agreed well with eq.1. Then in the steel plates of P-2.3, PR-3.2-M2-15, PR-4.5-M1-15, and PR-4.5-G-10, the rib plates of them were so small that entire buckling occurred in elastic region. In the specimen PR-2.3-M2-60, partial buckling occurred because the spacing of rib plates was so large and buckling wrinkles began to appear at the stress nearly equal to the calculated. After that the rigidity gradually decreased as the plates transferred to tension field. Accordingly their yielding stress was obtained by eq.4 and the hysteresis loop was S-shape for the load reversals at small amplitude of deflection.

The rigidity of PR-4.5-M1-35 and PR-4.5-M1-55, buckled at the stress of about proportional limit, and of the other specimens in which plastic buckling occurred, began to decrease at $0.7\tau_{sy}$. Their yielding stress could be obtained by eq.2. The hysteretic characteristics of the former was spindle shape when the deflection was small, but S-shape once the deflection got large. One of the latter was spindle shape which could be modified simple bi-linear relation.

In final stage, large buckling wrincles appeared in all specimens (Fig.4) and maximum stresses obtained with tests was from 0.74 to 0.9 τ_{tmax}. The theoretical maximum stress would be regarded as τ_{tmax} at which tensile break occurred. All specimens had very large ductility and some of them deformed to the extent of γ = 0.1 radian.

The test results showed that the steel plate with rib plates on the both sides had more stable behavior than one reinforced on one side only, and there was no difference of hysteresis loop because

of the forms of arrangement of rib plates.

Design principles for rib plates---In order to get the steel shear wall with stable spindle-shaped hysteretic characteristics and with deformability of O.Ol radian to shear stress, next two design principles were recommended through the test results.

i) Shear wall shall not buckle in elastic region.

ii) At final stage partial buckling rather than entire buckling shall occur.

For item i), spacing and stiffness of rib plates shall meet eq.6 and eq.7. For item ii), stiffness of rib plates shall have somewhat two times larger stiffness than the value requested by eq.7.

1.2 Full Size Test

Outline of test---Fig.5 shows two specimens of one bay-two storied steel plate wall, F-1, the specimen without openings in the wall and F-2, the specimen with two openings. F-1 was provided with 4.5 mm steel plate in thickness. In order to give same shear rigidity and strength as that of F-1, F-2 was provided with 6 mm steel plate in thickness. These specimens, the basis of which were fixed, were tested under the alternative horizontal load. Fig.6 shows the view at test.

Analysis---The theoretical analysis was done by elasto-plastic finite element method (F.E.M) under the following assumption: The steel plate wall never buckles, and material has bi-linear stress-strain relationship under Von Mises' criterion of yielding. Otherwise the rigidity and the yielding load were calculated by eq.1 and 2.

Test results---F-1--Horizontal load(P)-deflection(δ) curve, shown in Fig.7, was linear before P reached 250 tons and agreed with the results by eq.1 and F.E.M. Then the rigidity gradually decreased because of local yielding and subsequent yielding by shear force. As the load increased, the yielding zone spreaded and meanwhile partial buckling phenomena were observed at several points. There was indication of entire buckling in the two-storied wall at 350 tons, due to the poor lateral constraint to the beam at second floor. If the constraint of the floor slab was considered, it wouldn't supposedly occur and the calculated results by F.E.M. would agree better with the test results.

F-2--The initial rigidity could be calculated by eq.1 or F.E.M. as in F-1. The behavior was very much influenced by the exsistence of openings and the first yielding appeared in the web of beam between openings. The next yielding appeared both in the corner of wall and in frame member arround them. Before the yielding spreaded wide into steel plate, the plate buckled partially arround the openings. The influence of this buckling on the rigidity, however, was so small that the results by F.E.M. was in good agreement with the test results even in plastic region.

Judging from the test results of both F-1 and F-2, it would be satisfactory to regard the shear stress obtained by eq.2 as the yielding stress of the wall and to consider that both specimens had stable hysteresis loop and large ductility. In these test, break of the welding at the bottom of the column made the continuation of loading stop.

1.3 Conclusion

The steel plate shear wall with rib plates designed on the basis of the principles obtained by the basic test, had very good behavior and both its rigidity and strength could be calculated by shear theory. The rigidity and strength of the steel plate with an openning was supplied well with increase of plate thickness and adequate reinforcement arround it.

2. Particular Steel Bracing System

In braced frames, once the bracings buckle, the load comes down. Accordingly the ductility and capacity of energy absorption decrease to the successive load reversals. Therefore the authors tried to keep bracing system stable to the horizontal load on the basis of the two principles: Never make the bracing buckle and make only the part of the system yield. This report describes the particular bracing systems, namely tension-yield type bracing, beam yielding type, or partial yielding type of bracing in which yielding was intended to occur much earlier than the attainment of buckling of bracing.

Specimens---Fig.8 shows four specimens. SK type has standard bracings. As bracings of STK type are reinforced with 10 cm x 10 cm sectional reinforced concrete, the tensioned bracing yields first. Large eccentricity is purposely given to the bracings of BBK and SPK, and the beam or additional member that connects bracings to beam, is intented to yield before the bracings buckle.

Calculation---The specimens were analized to horizontal load in elasto-plastic region, considering such property as in Fig.9 to each member.

Test Results---Load-deflection curve in Fig.10 showed that the post buckling behavior of SK type was not good, as written in Introductory Report. The decrease of load appeared in the calculated results too.

As the reinforced concrete prevented the bracing from buckling and increased the compressive strength, the rigidity and strength of STK could be larger than ones of SK and the hysteretic characteristics was more stable. However, the concrete collapsed finally and load came down. The calculated results traced well the sequence of yield occurrence of members.

In SPK type, the first yielding was observed in the additional member at 15.2 tons and the rigidity decreased abruptly. The hysteresis loop was as stable as the steel plate shear wall. The calculated results agreed well with the tested before γ reached 1/125, where shear buckling appeared in the web of additional member. Though, by analysis, yield hinges were formed at the top and the bottom of columns, they had little influence on the deformation of the frame.

The strength of BBK was determined by the yielding of beam. The test proved that the first yielding of beam caused the decrease of the rigidity. Concerning of hysteretic characteristics and ductility, BBK was as good as SPK, however attention might have to be paid in the vertical deflection of beam. Fig.11 shows the specimens after testing.

The results showed that the behavior of these three new bracings was quite different from the standard one. Concretely speaking, the rigidity was freely changable in elastic and plastic region, the hystersis loop was spindle one and the deflection capacity was large. The behavior could be predicted well by the calculation under the assumption that each member had bi-linear stress-strain relation.

3. Conclusion

Finally both the thin steel plate shear wall and the particular steel bracing systems had large capacity of energy absorption and stable hysteresis loop which could be defined by the simple model. With use of these systems in the structure, the inelastic dynamic response of it can be easily obtained and the safe structure against earthquakes can be designed.

Table 1 Results of Test and Calculation

NAME OF SPECIMEN	STEEL PLATE THICKNESS	RIB PLATE			MATERIAL PROPERTY		CALCULATED RESULTS				MEASURED MAXIMUM STRESS
		SECTION	FORM OF ARRANGEMENT	STIFFENESS	YIELDING STRESS	MAXIMUM STRESS	BUCKLING STRESS	TENSILE YIELDING STRESS	SHEAR YIELDING STRESS	BREAK STRESS	
	cm	cm × cm		cm^4	ton/cm^2	ton/cm^2	ton/cm^2	ton/cm^2	ton/cm^2	ton/cm^2	ton/cm^2
P-2.3	0.23	——	——	——	3.10	5.04	0.08	1.55	1.78	2.52	1.86
PR-2.3-M2-60	0.23	0.45 × 6.0	BOTH SIDES, M2	8.10	3.10	5.04	1.05	1.55	1.78	2.52	2.14
PR-3.2-M2-15	0.32	0.32 × 1.5	ONE SIDE, M2	0.36	2.80	4.51	0.50	1.40	1.62	2.26	1.72
PR-3.2-M2-25	0.32	0.32 × 2.5	ONE SIDE, M2	1.67	2.80	4.51	>1.3	1.40	1.62	2.26	1.75
PR-3.2-M2-40	0.32	0.32 × 4.0	BOTH SIDES, M2	1.71	2.80	4.51	>1.3	1.40	1.62	2.26	1.83
PR-3.2-M2-60	0.32	0.45 × 6.0	BOTH SIDES, M2	8.10	2.32	3.80	>1.3	1.16	1.34	1.90	1.71
PR-4.5-M1-15	0.45	0.45 × 1.5	ONE SIDE, M1	0.51	2.37	3.54	0.41	1.19	1.37	1.77	1.42
PR-4.5-M1-35	0.45	0.45 × 3.5	ONE SIDE, M1	6.43	2.37	3.54	1.05	1.19	1.37	1.77	1.42
PR-4.5-M1-55	0.45	0.45 × 5.5	BOTH SIDES, M1	6.24	2.37	3.54	1.04	1.19	1.37	1.77	1.48
PR-4.5-G-10	0.45	0.45 × 1.0	ONE SIDE, G	0.15	2.37	3.54	0.37	1.19	1.37	1.77	1.39
PR-4.5-G-30	0.45	0.45 × 3.0	ONE SIDE, G	4.05	2.37	3.54	>1.3	1.19	1.37	1.77	1.47
PR-4.5-G-50	0.45	0.45 × 5.0	BOTH SIDES, G	4.67	2.37	3.54	>1.3	1.19	1.37	1.77	1.51

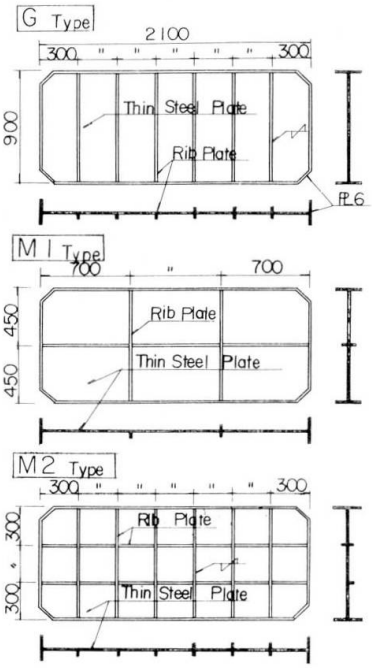

Fig.1 Test Specimens

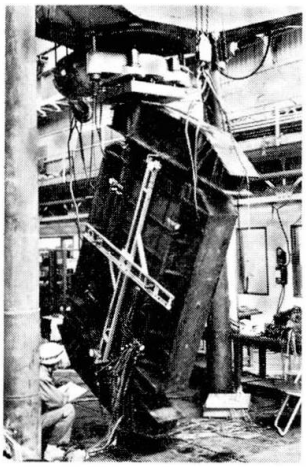

Fig.2 View at Test

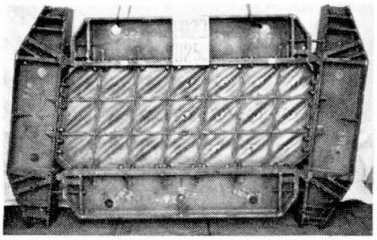

PR-2.3-M2-60

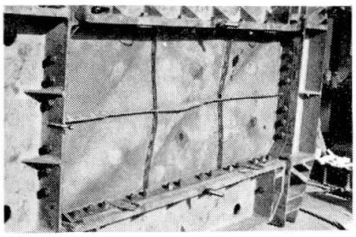

PR-4.5-M1-35

Fig.4 Failure of Specimens

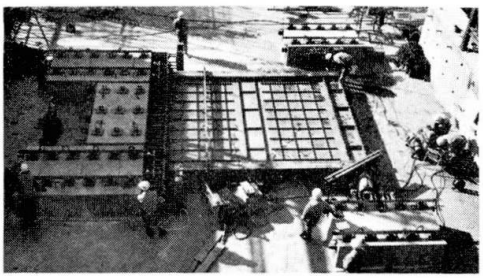

Fig.6 View at Test

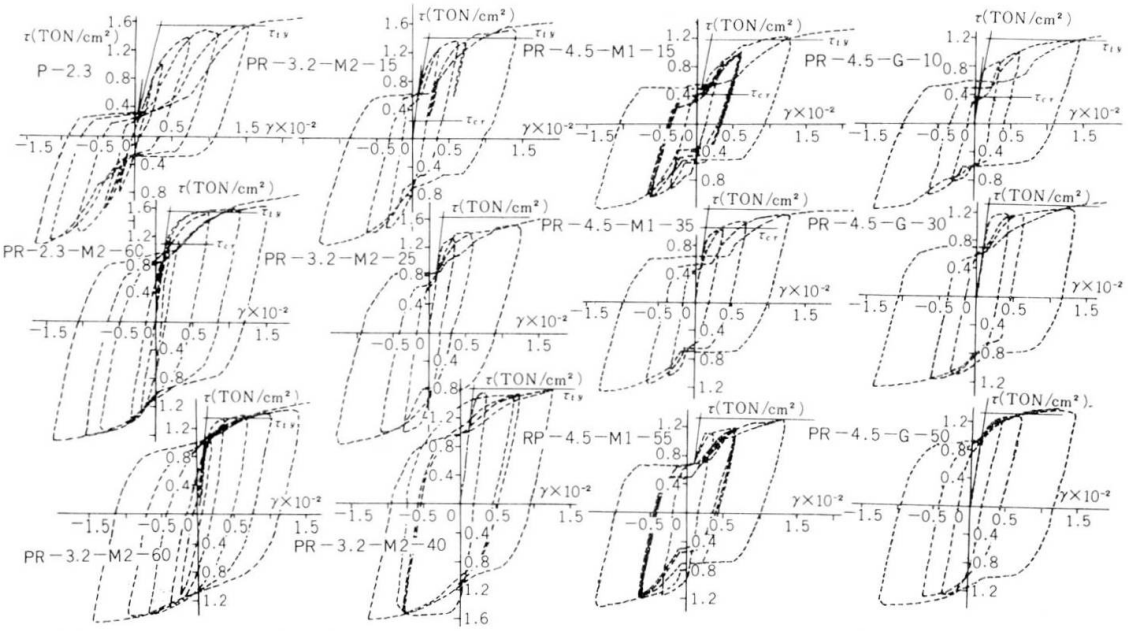

Fig.3 Shear Stress-Shear Strain Curves

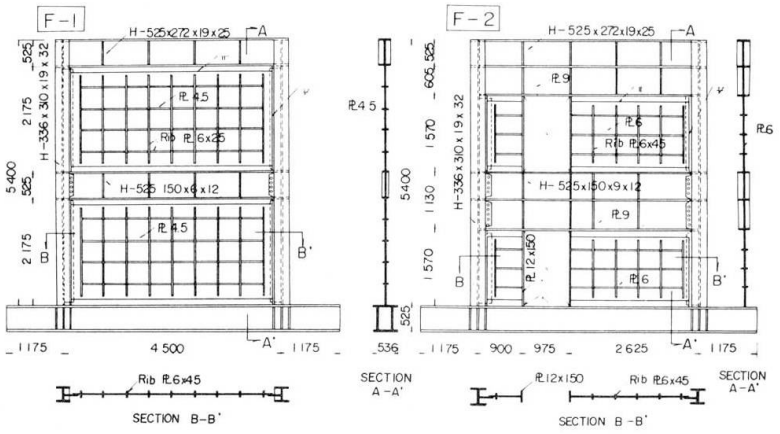

Fig.5 Specimens

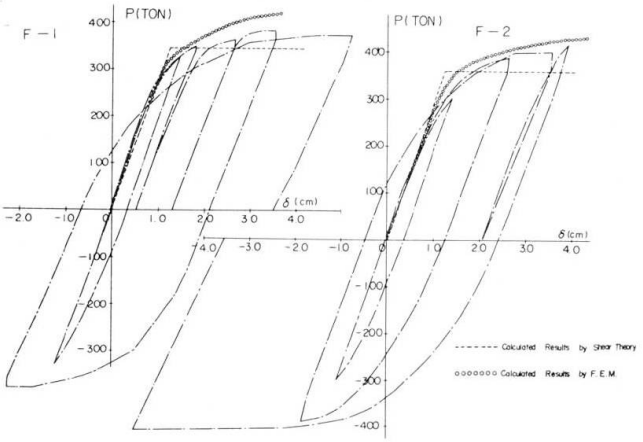

Fig.7 Load-Deflection Curves

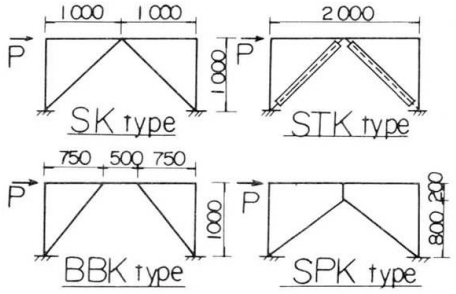

	SPECIMEN	MEMBER
COLUMN	ALL SPECIMENS	H-100×100×6×8
BEAM	"	H-150×75×4.5×13
BRACING	SK, STK	2C-65×26×4.5×4.5
	BBK, SPK	2C-75×32×4.5×4.5
STRUT	SPK	H-250×150×4.5×13

Fig.8 Specimens

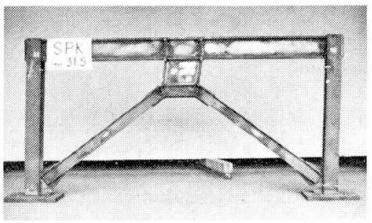

SPK type

BBK type

Fig.11 Failure of Specimens

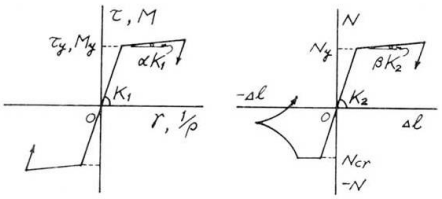

Fig.9 Property of Member

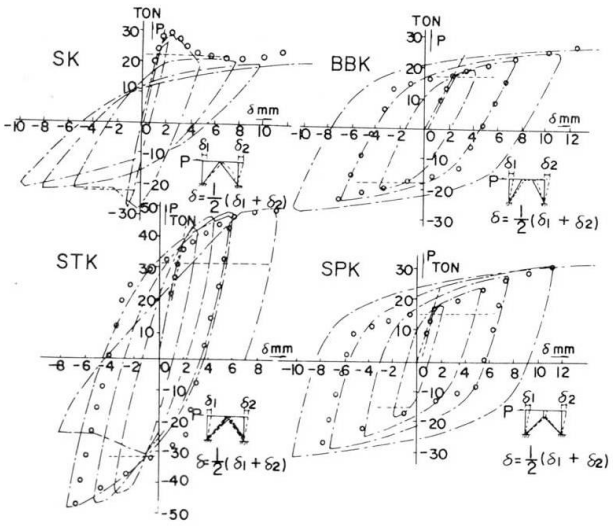

Fig.10 Load-Deflection Curves

SUMMARY

This report describes the general characteristics of the thin steel plate shear wall and the particular steel bracing systems in elasto-plastic region and the design principles to make their behavior stable, obtained through the test under alternative horizontal load and the calculated results.

RESUME

On décrit les caractéristiques générales des entretoises métalliques formées d'une plaque mince et les autres systèmes d'entretoises métalliques dans le domaine élasto-plastique, ainsi que les principes de dimensionnement permettant d'obtenir un comportement stable. On se base sur des essais de charge horizontale alternée et sur des résultats calculés.

ZUSAMMENFASSUNG

Der Bericht beschreibt die allgemeinen Charakteristiken einer dünnen Stahlscheibe und der speziellen aussteifenden Systeme im elasto-plastischen Bereich sowie die Bemessungsgrundsätze für ihr stabiles Verhalten, die sich durch Versuche unter wechselnder horizontalen Belastung ergaben, nebst den berechneten Resultaten.

Leere Seite
Blank page
Page vide